

Palaeoceanographic development in Leirdjupet Trough, western Barents Sea, during the Holocene: evidence from foraminiferal, isotopic and sedimentological records

—

Boriss Kovalenko

Master thesis in Marine Geology and Geophysics (GEO 3900)
December 2015



Abstract

The aim of this master thesis is to investigate the paleoenvironment and paleoceanography in Leierdjupet, a small north-south stretching trough in the west-southwestern Barents Sea during the Holocene interglacial.

The gravity core HH14-012GC from Leirdjupet Trough has been investigated to detect changes in sedimentation and the variations in distribution patterns of marine microorganisms (Planktic and Benthic Foraminifera) and stable isotope values of their shells to reconstruct the variability of the inflow of Atlantic water to the study area. The results are compared to published paleodata records to investigate regional paleoceanographic processes in western Barents Sea and Svalbard region.

Analyses of sediment core HH14-012GC show that Atlantic water has continuously been present in the study area during the last 11,000 years. The dominant benthic species during the Holocene transition indicate glaciomarine environmental conditions and strong influence of Polar water. During the early Holocene a significant increase of Atlantic Water inflow into Leirdjupet Trough occurred. In the interval c. 10 – 9 ka BP a rapidly increasing flux of benthic and planktic foraminifera, dominance of the benthic foraminiferal species *Cassidulina neoteretis*, and low of $\delta^{18}\text{O}$ values represent the Holocene temperature optimum at the study area and the strongest warm Atlantic water inflow for the Holocene. The mid-Holocene (8.3 – 4 ka BP) represents a transition period with relative stable environmental conditions. Increasing deposition of IRD indicates sea ice and icebergs arriving at the core site and is probably related to decrease in sea surface temperature. In the late Holocene climatic conditions became cooler. The dominant benthic species *Cassidulina reniforme* and *Islandiella norcrossi* indicate cooling of the bottom water. The dominance of *Neogloboquadrina pachyderma* sinistral (s) and *Turborotalia quinqueloba* with increasing trend of *N. pachyderma* sinistral (s) is related to the continuous decreasing of surface water temperature in the area. The decreasing trend in temperature continues during the late Holocene and the influence of Atlantic water in the area diminished further.

Acknowledgements

Great thanks to my supervisor Professor Tine Lander Rasmussen for excellent leading throughout this Master Thesis. I remember course GEO-3111 (Reconstructing Quaternary Environments) where I first met Professor Tine L. Rasmussen. After this course I decided to write a Master Thesis about the Paleoclimate reconstruction.

Special thanks to the laboratory staff. Trine Dahl and Ingvild Hald helped me with laboratory equipment. Lot of months we worked together in the laboratory.

My best wishes for the captain and crew of the research vessel R/V Helmer Hanssen.

I am thankful to my family. Special thanks to my wife Ilze for the patience and looking after my two kids Elizabete and Kristians throughout these years.

University in Tromsø is the great place to study geology. I met high grade teachers and kindhearted students. And I am very glad that studied geology here.

Boriss Kovalenko

December, 2015

Contents

1 Introduction	1
1.1 Objectives	1
1.2 The study area and core location	2
1.3 Oceanographic setting	4
1.4 Holocene climate	11
1.5 Last Glacial Maximum	14
1.6 Distribution of surface sediments and Foraminifera in the study area.....	17
1.6.1 Distribution of benthic foraminiferal species in the study area	20
2 Material and Methods	23
2.1 Coring and sampling	23
2.2 Lithology log.....	23
2.3 Magnetic susceptibility measurements and Color spectrophotometry	23
2.4 X-Radiography.....	25
2.5 Grain size and ice-rafted debris (IRD) analysis.....	25
2.5.1 Flux calculations.....	26
2.6 Foraminiferal analysis	27
2.7 Stable isotope analysis.....	27
2.8 Radiocarbon dating.....	28
3 Results.....	29
3.1 Age model and sedimentation rate	29
3.2 Core description and sediment properties	31
3.3 Lithological units.....	33
3.3.1 Lithological unit 1.....	39
3.3.2 Lithological unit 2.....	39
3.3.3 Lithological unit 3.....	39
3.3.4 Lithological unit 4.....	40
3.3.5 Lithological unit 5.....	40
3.4 Foraminiferal units.....	41
3.4.1 Foraminiferal unit 1	44
3.4.2 Foraminiferal unit 2	44
3.4.3 Foraminiferal unit 3	45
3.4.4 Foraminiferal unit 4	45
4 Interpretation	47

4.1 Time interval c. 11 – 10.7 ka BP (Holocene transition).....	47
4.2 Time interval 10.7 – 8.3 ka BP (early Holocene).....	49
4.3 Time interval 8.3 – 4.0 ka BP (mid-Holocene)	54
4.4 Time interval 4.0 ka BP – present (late Holocene)	56
5 Discussion and correlations	59
5.1 Paleoceanographic interpretation.....	59
5.1.1 Holocene transition (c. 11 – 10.7 ka BP).....	59
5.1.2 Early Holocene (10.7 – 8.3 ka BP)	60
5.1.3 Mid- Holocene (8.3 – 4.0 ka BP).....	63
5.1.4 Late Holocene (4.0 ka BP – present).....	64
5.2 Stable isotopes and ice rafted debris	67
5.3 Regional correlation of foraminiferal records	71
5.4 The Polar front observation.....	85
6 Summary and conclusions	89
7 References	91

1 Introduction

1.1 Objectives

The primary objective of this thesis is to reconstruct the paleoenvironment and paleoceanography in Leirdjupet, a small north-south stretching trough in the west-southwestern Barents Sea during the Holocene interglacial (Fig. 1.1). The study aims to detect changes in sedimentation and variations in the distribution patterns of marine microorganisms (Planktic and Benthic Foraminifera) and stable isotope values of their shells to reconstruct the variability of the inflow of Atlantic water to the study area. The results are compared to published paleodata records to investigate regional paleoceanographic processes in western Barents Sea and Svalbard region.

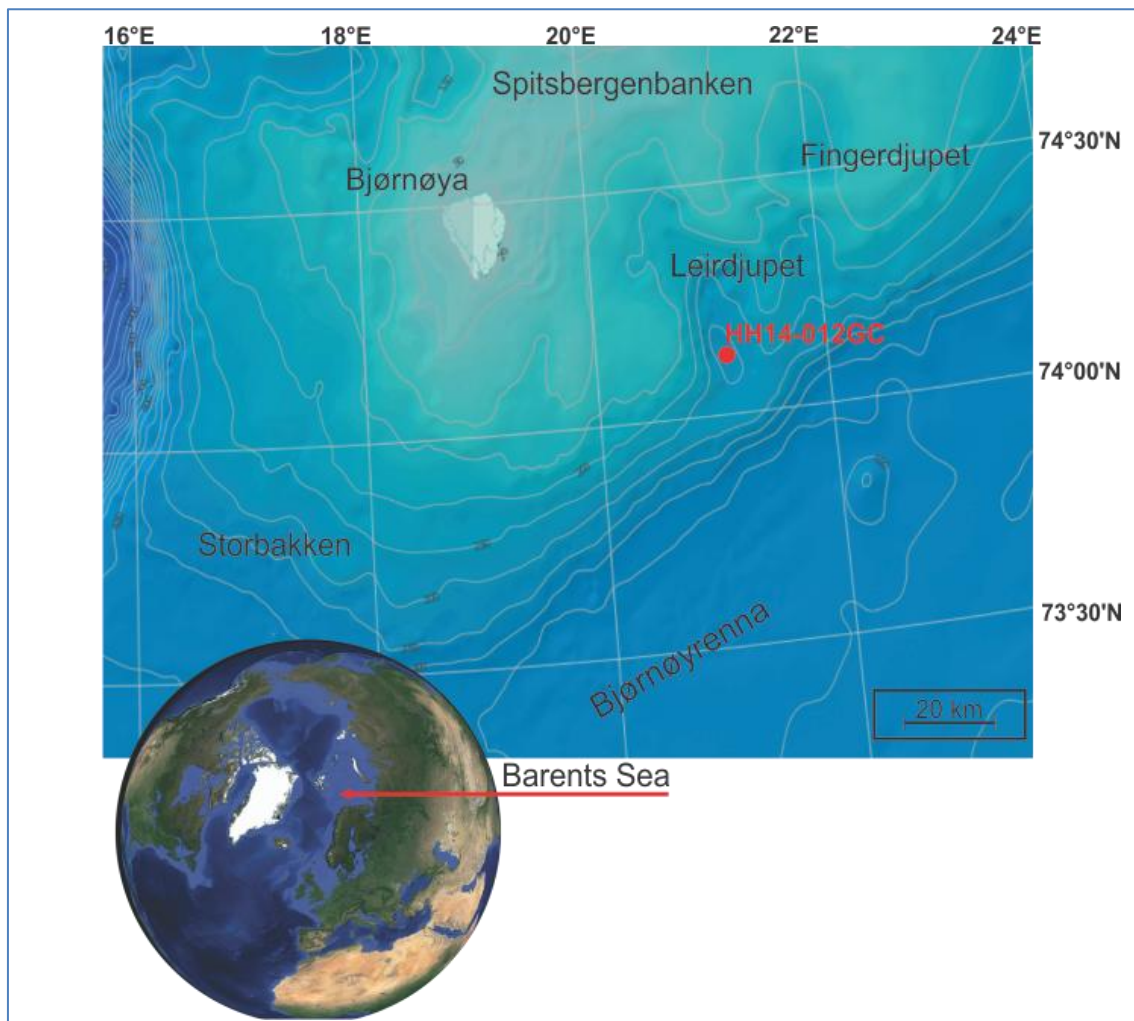


Figure 1.1. Bathymetric map showing the location of the sediment core HH14-012GC (Modified map from www.Mareano.no). Overview map of the North Atlantic and the Arctic Ocean is located in the lower left corners (Picture created by using Google Earth program).

1.2 The study area and core location

The study area is from the northern North Atlantic, the west-southwestern Barents Sea (Fig. 1.2). The Barents Sea is an epicontinental sea with an average depth of approximately 250 meters the deepest part reaches more than 500 meters. The Barents Sea has an area of approximately 1 424 000 km².

The Barents Sea is characterized by shallow banks and deep troughs (Fig. 1.2).

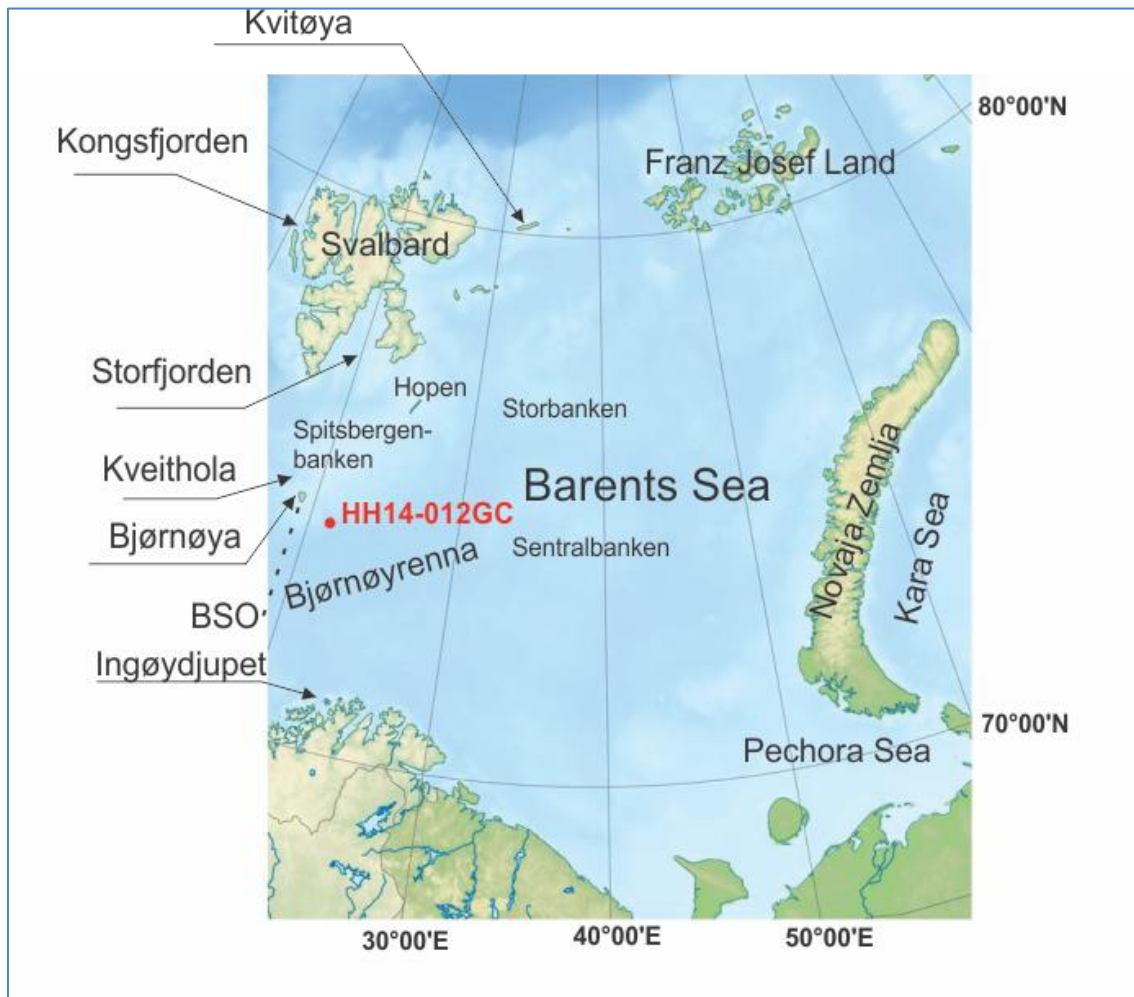


Figure 1.2. Overview map of the Barents Sea and core HH14-012GC location (Map modified from npolar.no).

The main features of the sea bed are related to the tectonics (Faleide et al., 1984). Local features such as shallow banks and moraine ridges are formed by glacial activity (Vorren et al. 2011) (Fig. 1.5). The geological history of the western Barents Sea occurred in three time intervals: Late Devonian-Carboniferous, Middle Jurassic-Early Cretaceous and Early Tertiary.

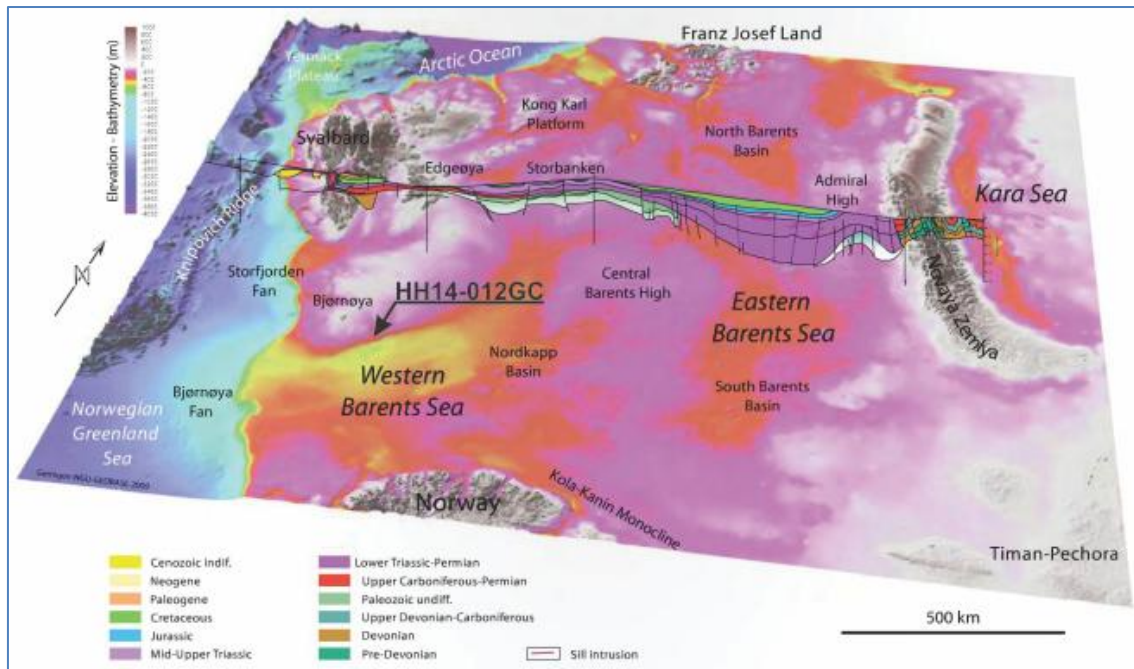


Figure 1.3. Three-dimensional bathymetry of the Barents Sea continental shelf and regional geological profile Modified from “Atlas. Geology history of the Barents Sea” (Smelror et al., 2009).

Core HH14-012GC (Latitude 21° 06' N; Longitude 74° 08'E) was taken in Leirdjupet at 343 m water depth in the central-western Barents Sea (Fig. 1.2).

Leirdjupet is a small trough located in the southern part of Spitsbergenbanken (Fig. 1.2). The trough is 40 km long and 16 km wide, stretching north-northwest to south-southeast. It opens into Bjørnøyrenna.

1.3 Oceanographic setting

The studies of the oceanographic environment and variability in inflow of Atlantic water into the Nordic Seas and Arctic Ocean have a long history. Scientific works by Helland-Hansen and Nansen (1909) “The Norwegian Sea” and by Knipovitsch (1905) “Hydrologische Untersuchungen im Europäischen Eismeer” laid the foundation for marine studies of this area.

The three main water masses flowing into the Barents Sea are: Coastal Water, (North) Atlantic Water and Arctic Water. Locally formed major water masses are Barents Sea Water and Bottom Water (Fig. 1.4.). The characteristics of the water masses are shown in Table 1.1. According to H. Loeng 1991, the inflowing of the warm Atlantic Water forms a major control of the climate in the Barents Sea area.

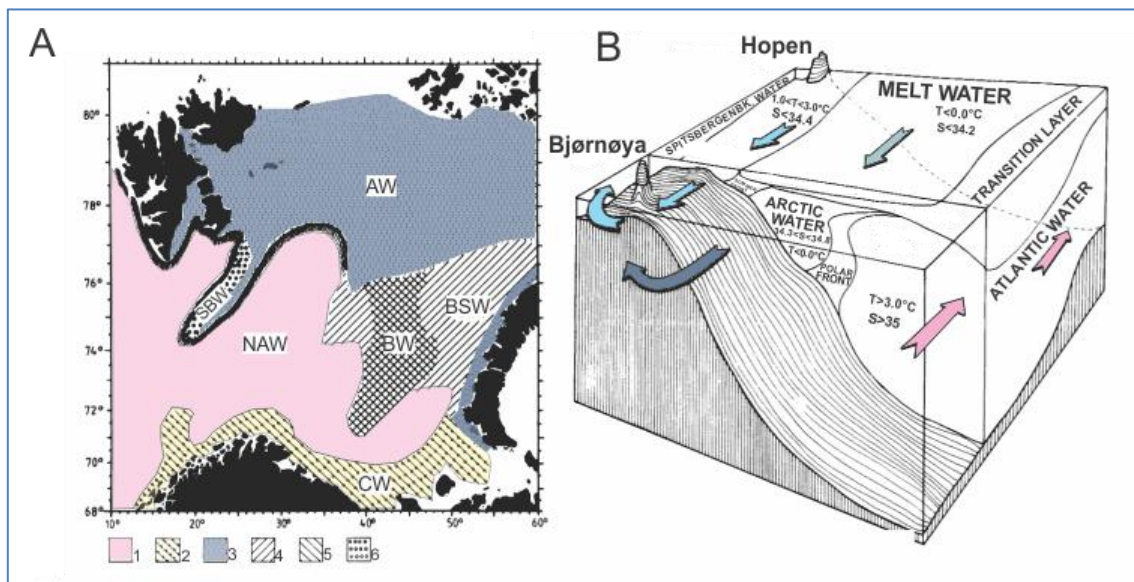


Figure 1.4. A) Main features of the water masses in the Barents Sea. 1 = (North) Atlantic Water (NAW); 2 = Coastal Water (CW); 3 = Arctic Water (AW); 4 = Barents Sea Water (BSW); 5 = Bottom Water (BW); 6 = Spitsbergenbanken Water (SBW). B) Water mass distribution at the eastern slope of Spitsbergenbanken during summer and autumn. The boundary between Arctic Water and Atlantic Water are referred to as the “Polar Front”. Pictures are modified from Loeng (1991).

Table 1.1. Characteristics of the water masses in the Barents Sea (Loeng, 1991).

Names of the water masses		Characteristics of the water masses	
		T, °C	S, psu
Coastal water	CW	>2.0	<34.7
(North) Atlantic Water	NAW	>3.0	>35.0
Arctic Water	AW	<0.0	34.3-34.8
Locally formed water masses:			
Melt Water	MW	<0.0	<34.2
Spitsbergenbanken	SBW	1.0-3.0	<34.4

Water			
Bottom Water	BW	<-1.5	>35.0
Barents Sea Water	BSW	-1.5-2.0	34.7-35.0
Polar Front Water	PW	-0.5-2.0	34.8-35.0

Table 1.1 continued.

The currents are highly dependent on the bottom topography and at the same time leads to a specific distribution of the water masses in the Barents Sea region. Variations in water mass properties (temperature and salinity) cause additional changes in water mass distribution (Loeng, 1991).

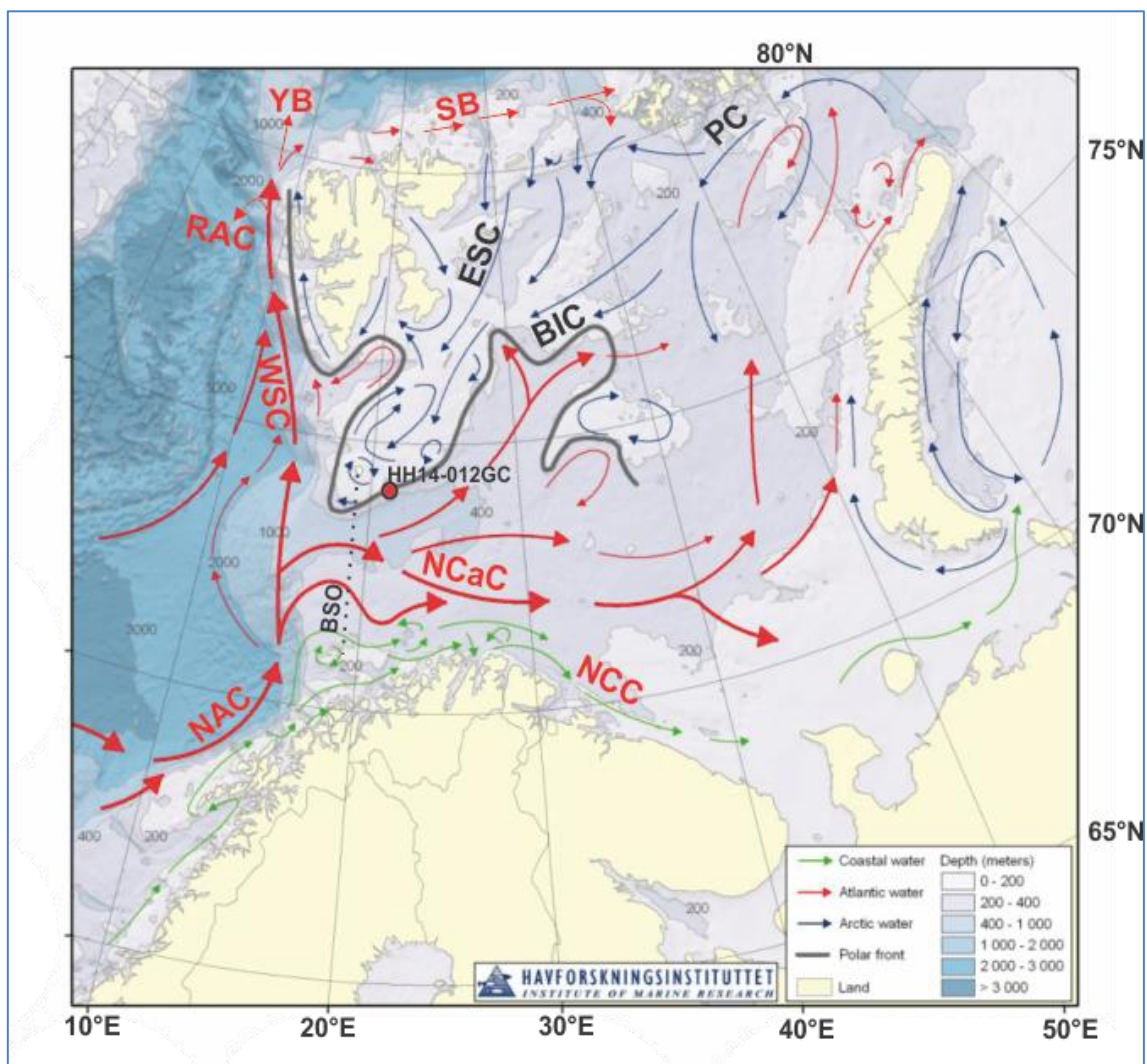


Figure 1.5. Major currents in the Barents Sea. NAC - Norwegian Atlantic Current; NCaC – North Cape Current; NCC – Norwegian Coastal Current; WSC – West Spitsbergen Current; RAC – Return Atlantic Current; YB – Yermak Branch; SB – Svalbard Branch; ESC – East Spitsbergen Current; BIC – Bear Island Current; PC – Persei Current. BSO – Barents Sea Opening. Map modified from www.imr.no (Institute of Marine Research).

The Norwegian Atlantic Current splits into two branches; the North Cape Current and West Spitsbergen Current, this process take place near the Barents Sea Opening (71 – 74 ° N) (Figs. 1.5 and 1.6). Warm Atlantic water masses flow into the Barents Sea through its topographic deepest part –

the Bear Island Trough (Bjørnøyrenna). Following changes in topography the North Cape Current also splits into two branches. One branch continues flowing to the east, the second branch takes a northern direction (Hopen Trench). Between Hopen and Storbanken and between Storbanken and Sentralbanken - the North Cape Current continue flowing as an intermediate current, below the lighter and colder Arctic Water. The Atlantic Water's temperature and salinity decrease towards the north and east. While the Norwegian Atlantic Current consists of an inner barotropic and an outer baroclinic branch, the North Cape Current is mostly abarotropic (Ingvaldsen, 2005).

The current flowing close to mainland Norway is called the Norway Coastal Current. This current differs from the North Cape Current by its slightly lower salinity due to influence by low-salinity runoff from land (salinity <34.7 ‰ and >35 ‰, respectively).

At approximately 79.5° N, the West Spitsbergen Current split into three branches: the Yermak Branch, the Svalbard Branch and the Return Atlantic Current. The Yermak Branch continues to flow as an intermediate layer into the Arctic Ocean (Manley, 1995). The Svalbard Branch supply Atlantic Water along the northern edge of the Barents Sea below a layer of Polar Water. The warm core of the Atlantic Water is located between 100 – 200 m and 600 – 800 m depth. The core temperature is 3 – 4.5 °C at 100 – 400 m water depth (Pfirman et al., 1994). The Arctic Water is formed by mixing of the warm Atlantic Water with the Polar Water. The East Spitsbergen Current brings the Arctic Water into the Barents Sea. This water mass seasonally covered by sea-ice. The boundary between the Polar Water and Arctic Water is called the Polar Front, in the western Barents Sea the boundary between Arctic Water and Atlantic Water is termed the Arctic Front (Hopkins, 1991).

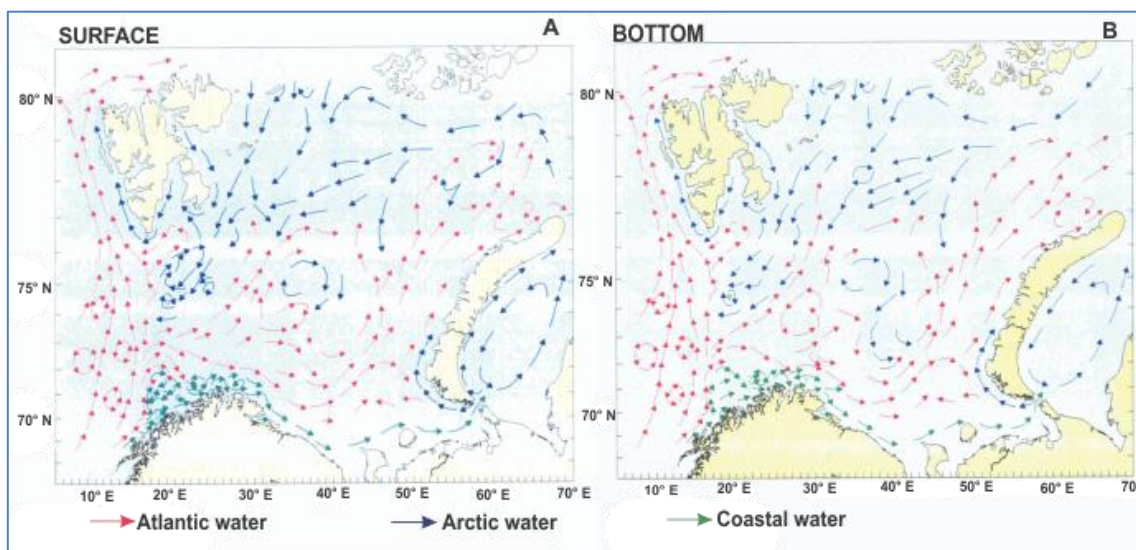


Figure 1.6. A) Surface currents in the Barents Sea. Because of the barotropic conditions, it is representative for the upper 100 m. B) Currents close to the bottom in the Barents Sea. Data modified from Loeng and Sætre, (2001).

The inflow of Arctic Water to the Barents Sea occurs between Spitsbergen and Frans Jozef Land, and between Franz Josef Land and Novaja Zemlja (Dickson et al., 1965). The Arctic Water has low salinity and temperature $<0^{\circ}\text{C}$ (its core has $T < -1.5^{\circ}\text{C}$ and $S > 34.4$ and < 34.7). In the winter period it occupies the upper 150 m of the water column and during summer melt-water with a thickness 5 – 20 m covers the Arctic Water. The East Spitsbergen Current flows along east Spitsbergen. South of Frans Josef Land it is called the Persei Current, it splits north of Sentralbanken (Fig. 1.5). Part of this current goes along the eastern slope of the Spitsbergenbanken and is here called as Bear Island Current. This Bear Island Current (Bjørnøya Current) has a great influence on the present study of Leirdjupet (Loeng, 1991).

The Bottom Water in the Barents Sea originates from the shallow shelf of Novaja Zemlja and at Sentralbanken. In winter, when the water temperatures decrease and meltwater supply diminishes, the density of the surface water increases. Also, when ice formation takes place, the salinity increases, due to brine rejection, this process further increases the water density (Midttun, 1985).

Also, along the boundary between the North Atlantic Water and the Arctic Water at the southeastern slope of Spitsbergenbanken Bottom Water formation can take place (Sarynina, 1969).

In the eastern part of the Barents Sea mixing between Atlantic Water with Arctic Water together with brine rejection forms Barents Sea Water.

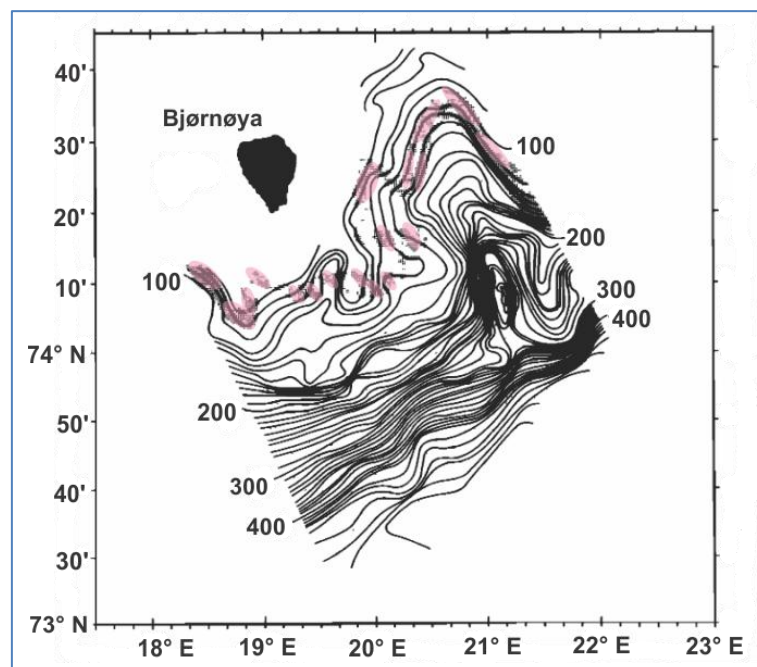


Figure 1.7. Correlation between the bathymetry and the position of the Polar front. The front is indicated by the shaded band (additionally colored in pink), which is the zone of the largest horizontal temperature gradient. Picture modified from Johannessen and Foster, (1978).

Figure 1.7 was created by combining the bathymetry and with the areas of strong temperature gradients at the surface (colored in pink). Johannessen and Foster (1978) established that “the position of the Oceanic Polar Front in the Barents Sea is locked to the outer part of the shelf and in general follows the 100-m isobath”¹. In other words, the geographical position of the boundary between the Arctic water and Atlantic water at the sea surface shows a good correlation with the 100 m isobaths. In a later study, Ingvaldsen (2005) found that “the location of the Polar Front south of Bear Island is not as stationary as earlier believed. The location of the front varies in phase with the climate of the Barents Sea. In warm periods with strong winds, the front is located further upslope than in cold periods”².

Harris et al., (1998), investigated the water mass distribution of the southern Spitsbergen Bank and found: existence of Modified Atlantic Water ($T < 1.0$ °C and $34.95 < S < 35.10$ psu) on the southeast slope of the Spitsbergen Bank, mostly between the 100 m isobaths and the deepest part of the Bjørnøyrenna and on the shallow Sentralbanken to the east. Modified Atlantic water is formed at the Polar front, when meltwater overlay Atlantic water (Harris et al. 1998). Modified Atlantic water is produced via convection. The Barents Sea polar front water masses are locally produced, through isopycnal mixing of Arctic and Atlantic waters (Parsons et al., 1996).

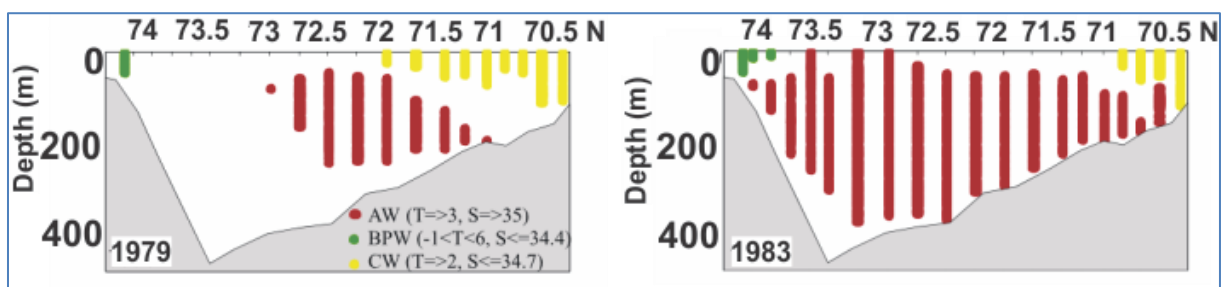


Figure 1.8. Distribution of water masses in August for the cold year 1979 and for the warm year 1983. Arctic Water (red color), Barents Polar Water (green color) and Coastal Water (yellow color). Modified from Ingvaldsen, (2005).

The North Cape Current comprises a two-core current system during warm periods and only one wider core in cold periods (Ingvaldsen, 2005). A positive North Atlantic Oscillation (atmospheric pressure at sea level between the Icelandic low and the Azores high) index provides stronger south westerlies in the south, at this time the North Cape Current is close to the Norwegian coast. Positive NAO also often generates stronger north easterlies in the north, moving the Arctic water and the front to the north, creating preconditions for increase in temperature and width of the North Cape Current (Ingvaldsen, 2005).

¹ Johannessen, O. M. & Foster, L. A. A note on the topographically controlled oceanic polar front in the Barents Sea. *J. Geophys. Res. Ocean.* **83**, 4567–4571 (1978) p. 1.

² Ingvaldsen, R. B. Width of the North Cape Current and location of the Polar Front in the western Barents Sea. *Geophys. Res. Lett.* **32**, 1–4 (2005) p. 4.

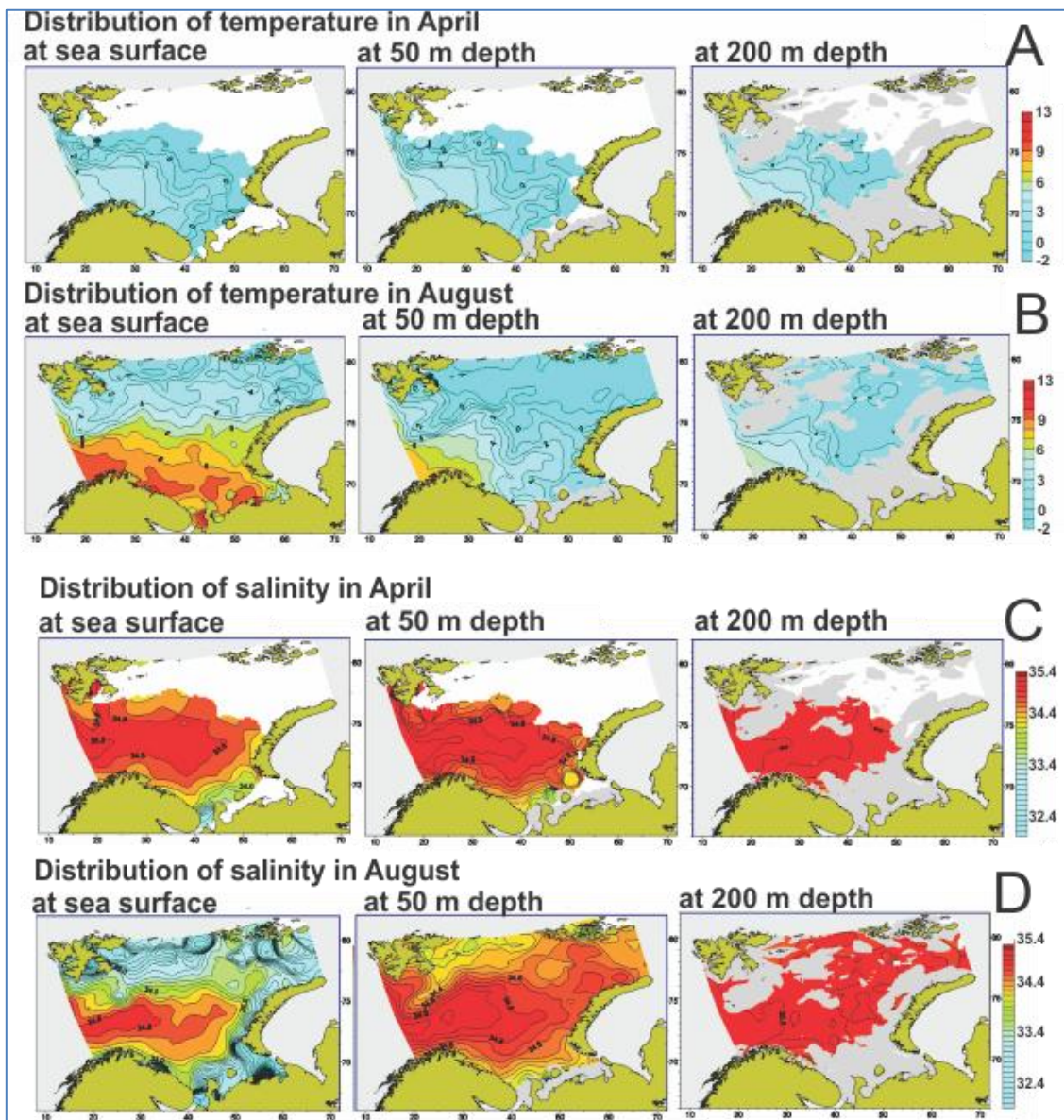


Figure 1.9. Monthly mean temperature ($^{\circ}\text{C}$) and salinity (psu) distribution in the Barents Sea. Data obtained from National Centers for Environmental Information (www.noa.gov).

Figure 1.9. shows the monthly mean temperature and salinity distribution in the Barents Sea. Panel A represent the temperature in the study area in April, after a long cold winter period. Close to the core site the temperature at the sea surface is about $-1 - 0^{\circ}\text{C}$, at 50 m water depth it is around 2°C , at 200 m $1 - 2^{\circ}\text{C}$. The temperature in August (Fig. 1.9, panel B) is higher. At the sea surface the temperature reaches $3 - 4^{\circ}\text{C}$, at 50 m water depth it is 3°C , and at 200 m water depth it is $2 - 3^{\circ}\text{C}$. Isotherm at the southeastern slope of Spitsbergenbanken are placed close one to each other. The study area (Leirdjupet) is close to the boundary of the Atlantic and Arctic Waters; Bottom Water formation take place at this area by cascading from Spitsbergenbanken during winter (Invalgsen, 2005). The study area also is close to the winter sea ice margin. Panel C and D (Fig. 1.9) show distribution of salinity (psu).

In August, at the sea surface, the area with high salinity value (red color) is smaller than in April. Sea ice melting and runoff from the mainland decrease salinity during the summer months.

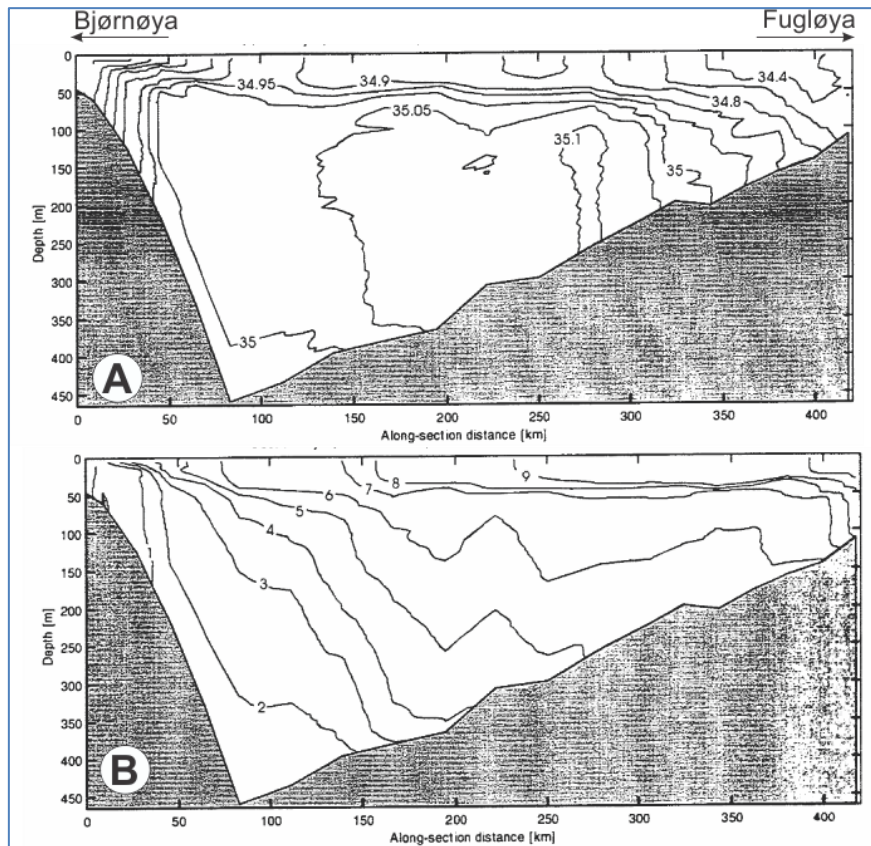


Figure 1.10. Vertical sections of salinity (psu, panel A) and temperature ($^{\circ}\text{C}$ lower panel B) at the Bear Island – Fugløya section as observed in the period August 21-22 1997. Modified from Asplin et al. (1998). BSO location is shown in Fig. 5.

Salinity and temperature distribution through Barents Sea opening are shown in Figure 1.10. Spitsbergenbanken is to the left and mainland Norway to the right. The Coastal Water ($T > 2^{\circ}\text{C}$ and $S < 34.7$ psu) is positioned directly at the Norwegian coast. The Atlantic Water masses ($T > 3^{\circ}\text{C}$ and $S > 35.0$ psu) is found in the central part. Mixing between Arctic Water and Atlantic Water produce the Barents Sea Water (temperature -1.5 - 2.0°C and salinity 34.7 - 35.0 psu) (Loeng, 1991).

The Modified Atlantic Water is produced by convection ($T < 1.0^{\circ}\text{C}$ and $34.95 < S < 35.10$ psu) (Harris et al. 1998). Results from Finger Canyon (Fingerdjupet located close to the study area, Fig. 1.1.) investigated by Parsons et al., (1996) show that in summer the Barents Polar Water ($-1 < T < 6^{\circ}\text{C}$ and $S < 34.4$ psu) occurs in the upper c. 50 m of the water column, the interval 50 - 100 – 120 m is the interval of isopycnal mixing, at 100 – 120 c. 210 m depth the interval of diapycnal mixing, the deeper part represents the North Atlantic Water (Parsons et al., 1996).

1.4 Holocene climate

The climate of the Holocene (c. 11,500 cal yr BP to Present) relates to a warm interval (interglacial) period (Lowe and Walker, 1984).

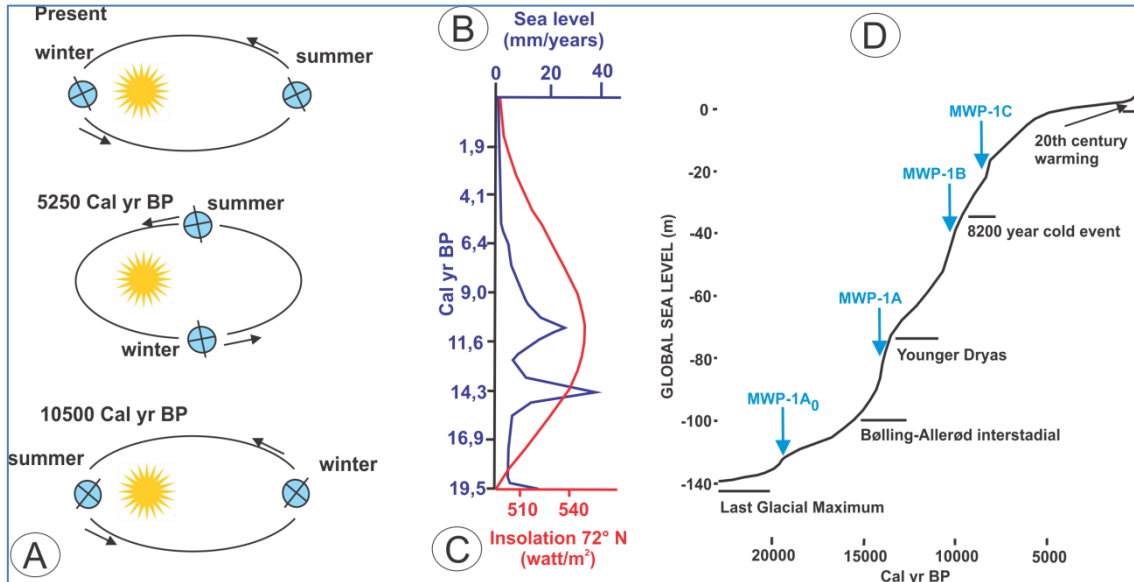


Figure 1.11. A) Precession of the equinox, redrawing from (Lowe and Walker, 1984). B) Global meltwater flow rate is drawn from Fairbanks (1989). C) June insolation 72° N (Berger and Loutre, 1991). D) Generalized sea level rise since the last ice age, redrawn from Gornitz (2013).

At present, the Northern Hemisphere winter is close to the sun (perihelion), while the summer occurs at the furthest point of the orbit (aphelion) (Lowe and Walker, 1984). Decreased obliquity diminishes the amplitude of seasonal differences at high latitudes (Lowe and Walker, 1984).

Panel D on Figure 1.11. shows the Global sea level rise, blue arrow indicate meltwater pulses: MWP-1A₀ (19,600 - 18,800 cal yr BP), MWP-1A (14,600 – 13.800 cal yr BP), MWP-1B (11,000 - 8800 cal yr BP) and MWP-1C (8200 ÷ 7600 cal yr BP) (Gornitz, 2013). The Holocene is commonly divided into the early-, mid- and late Holocene. Based on climatic fluctuations, five chronozones have been defined. The Early Holocene includes the Preboreal (10 - 9 ¹⁴C ka) and Boreal (9 - 8 ¹⁴C ka). The Mid-Holocene includes the Atlantic (8 - 5 ¹⁴C ka) and Subboreal (5 – 2.5 ¹⁴C ka). The Late Holocene includes the Subatlantic (2.5 ¹⁴C ka to present) (Mangerud et al., 1974).

In the early Holocene continued inflow of the Atlantic water into the western Barents Sea was recorded (e.g., Duplessy et al., 2005; Ślubowska-Woldengen et al., 2007; Chistyakova et al., 2010; Skirbekk et al., 2010; Rasmussen et al., 2012; Klitgaard-Kristensen et al., 2013; Groot et al., 2015). The Middle Holocene was characterized by stable, but colder environmental conditions. The Late Holocene can be described as a period with unstable conditions at the surface and bottom.

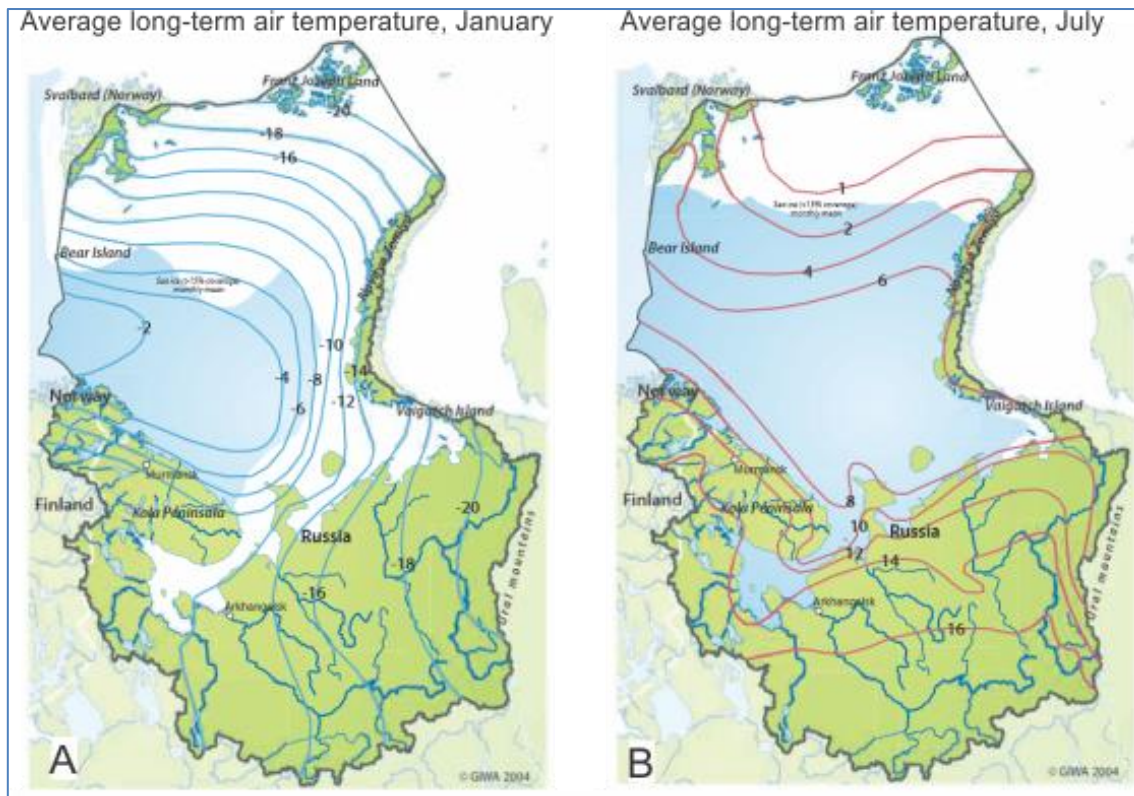


Figure 1.12. Average long-term air temperature: panel A – in January and panel B – in July. Areas colored by white show sea ice distribution (>15 % coverage, monthly mean). Modified from Matishov et al., (2004).

The area located in the transition zone between sea ice and the open sea is called the marginal ice zone (Fig. 1.12.). The marginal ice zone is affected by sea ice and variably weather conditions, and thus is very dynamic. In this area a relatively short, but intense production of phytoplankton occurs (Carstens et al., 1997). A large part of the biological production sinks to the bottom, and provides food for the benthic organisms.

Carstens et al., (1997) investigated the distribution patterns of the planktic foraminiferal faunas in the three distinct oceanographic regions in the Fram strait (78° to 80° N, and between 10° W to 10° E). Results show that during summer in the ice-free zone, the absolute abundances is between 100 and 500 ind/m³; in the ice margin absolute abundances are up to 1250 ind/m³ and in the ice-covered area absolute abundances are below 50 ind/m³. The mesh size for research of planktic foraminifera at high northern latitudes is important, especially for the study of times of colder climate in the Holocene (Carstens et al., 1997). Mesh sizes of >150 μm or >200 μm caught only 30% to 10% of the population recoverable with a 63 μm mesh size; in addition the species composition also changed significantly. The percentage changes of species abundances: 60% *Neogloboquadrina pachyderma* and 38% *Turborotalita quinqueloba* (fraction >63 μm); >80% *N. pachyderma* (fraction >150 μm) and >90 % *N. pachyderma* (fraction >200 μm) (Carstens et al., 1997).

Investigations of lake sediments of Bjørnøya (c. 178 km² area) present reconstruction of the palaeoenvironmental development of the climate in the area of Spitsbergenbanken during the Holocene (Wohlfarth et al., 1995). Until 9800 ¹⁴C BP (11.2 cal ka BP) Bjørnøya was covered by local glaciers. After a large-scale deglaciation glacial sediments were deposited in the lake basin. Between 9800 ¹⁴C BP (11.2 cal ka BP) and 9500 ¹⁴C BP (10.7 cal ka BP) organic production began and temperature increased gradually. Between 9500 ¹⁴C BP (10.7 cal ka BP) and 8300 ¹⁴C BP (9.3 cal ka BP) the climatic conditions were more continental with strong seasonal contrasts of cold winters and warm summers. Mean July temperatures were c. 9° C (4-5° C higher than present), and mean January temperatures around -12° C (5-6 °C lower than present). At 9500 ¹⁴C BP (10.7 cal ka BP) a rapid increase in the organic production was observed. At 8500 ¹⁴C BP (9.5 cal ka BP) increased freeze/thaw processes and increase erosion took place. The influx of minerogenic and organic material from the catchment area increased. At 8000 ¹⁴C BP (8.9 cal ka BP) conditions were relative calm; but a gradual decrease in temperature began at that time.

1.5 Last Glacial Maximum

During the last glacial maximum (LGM) the Barents Sea was covered by a c. 2000 m thick ice sheet (Landvik et al., 1998). Thick glacial sediments were deposited on the continental shelf and shelf break areas (Vorren et al., 1986). The Bjørnøyrenna Ice stream is the largest in the Barents Sea, and reaches a length of more than 600 km and a width of 165 km (Vorren and Laberg, 1997). The Bjørnøya Trough Mouth Fan occupies 215,000 km² and is the largest fans in the Nordic seas (Andreassen and Winsborrow, 2009).

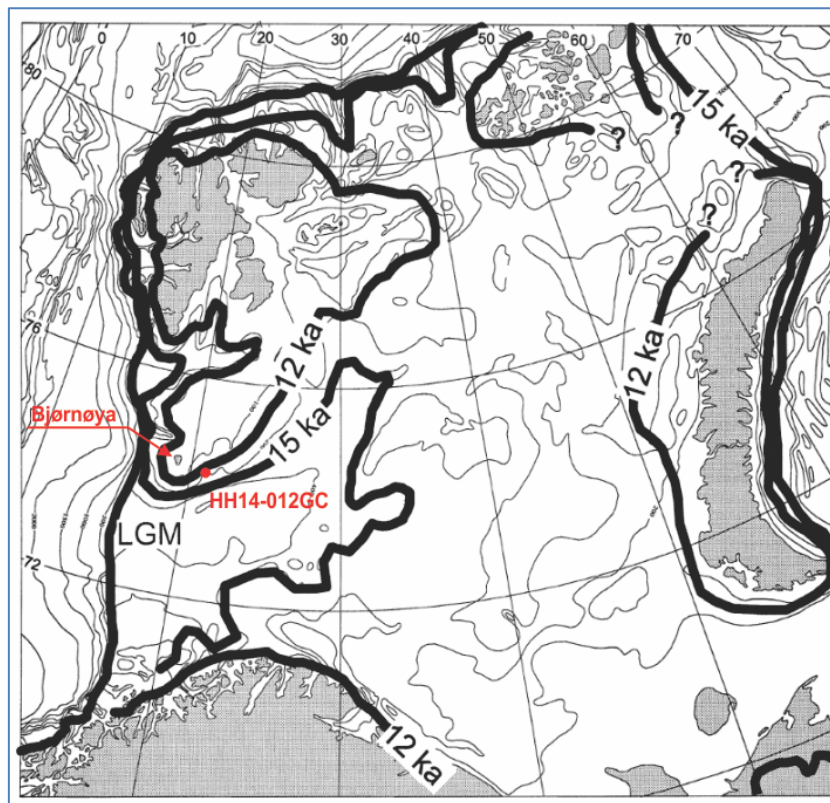


Figure 1.13. Reconstructed ice extent for the Last Glacial Maximum and the deglaciation. Map modified from Landvik et al., (1998).

The period of the peak glaciations of the LGM was relatively short, and deep Bjørnøya Trough shelf was glaciated for only a few thousand years (Landvik et al., 1998). The deglaciation began at c. 19 and continues to 11.7 cal ka BP (Fig. 1.13).

A 5-stage deglaciations model was proposed (Winsborrow et al., 2010).

During stage 1 (until 19 ka BP) the entire Barents Sea shelf was covered with ice (Fig. 1.14). Stage 2 (19-17 ka BP) includes a significant retreat of the ice margin in Storfjordrenna and Bjørnøjrenna. During stage 3 (17-16 ka BP) Nordkappbanken and Djuprenna Ice Streams readvanced. Bjørnøjrenna Ice Stream was still active. Stage 4 (15-12 ka BP) was characterized by a complete

deglaciation of the southern Barents Sea. The ice margin had retreated to the outer-fjord areas of northern Norway. In stage 5 ice retreat began on the Kola Peninsula, while in northern Norway the ice retreated continuously inland (Winsborrow et al., 2010).

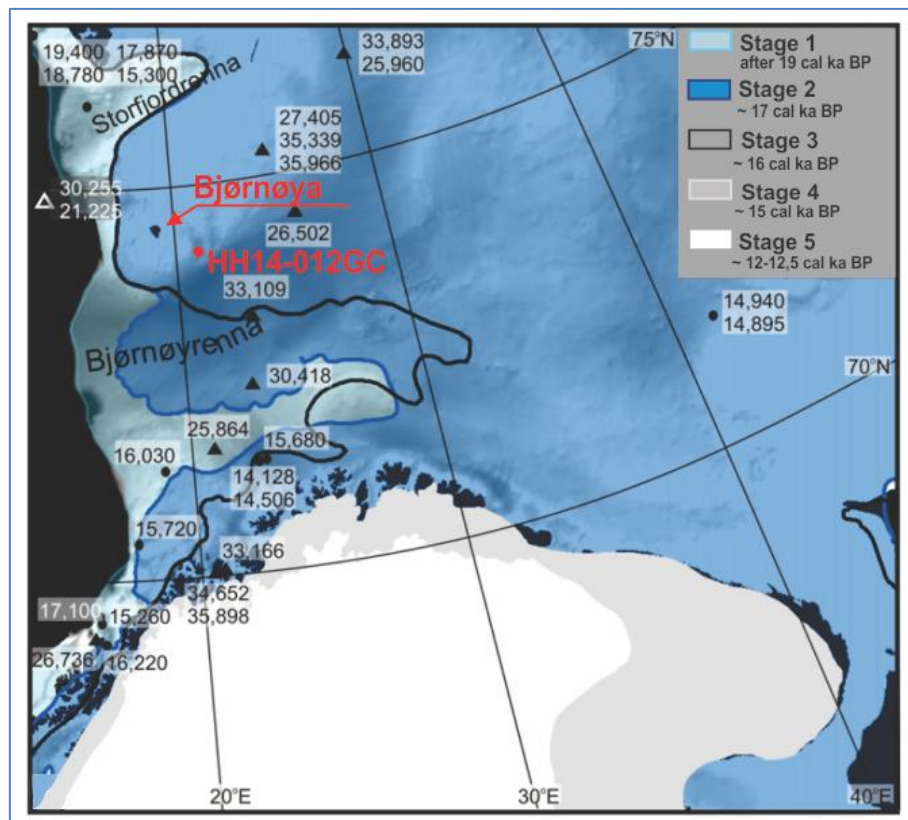


Figure 1.14. Ice marginal positions during the Late Weichselian deglaciation in the southern Barents Sea. Black triangles show dates from till units giving maximum estimates for the onset of glaciation and black dots show dates from glaciomarine sediments giving minimum estimates for the onset of deglaciation. Modified from Winsborrow et al., (2010).

Paleorecords from the Storfjorden Trough shows that the ice sheet was retreated from the shelf edge before 16,310 ¹⁴C years BP (Rasmussen et al., 2007). Results from Ingøydjupet show a date of circa 18,600 cal years BP, when the ice retreated (Aagaard-Sørensen et al., 2010). A core with coordinates 70° 30' N and 21° 30' E, indicated ice free conditions at 18,700 cal years BP. Further south at 71° 09' N and 23° 00' E the ice retreated c. 15,000 cal years BP, and a core site closer to mainland Norway, deglaciated at c. 15,000 – 14,000 cal years BP (Junttila et al., 2010). Inflow of Atlantic water can be related to a high content of smectite in the sediments, while glacial erosion from the Fennoscandian Ice Sheet and the Bjørnøyrenna Ice Stream was characterized by high content of illite and kaolinite in the sediments (Junttila et al., 2010). The Kveithola Trough west of Spitsbergenbanken and c. 100 km from core HH14-012GC in Leirdjupet was fully deglaciated before c. 14,2 cal ka (Bjarnadóttir et al., 2013) (see Fig. 1.15 for location of core site).

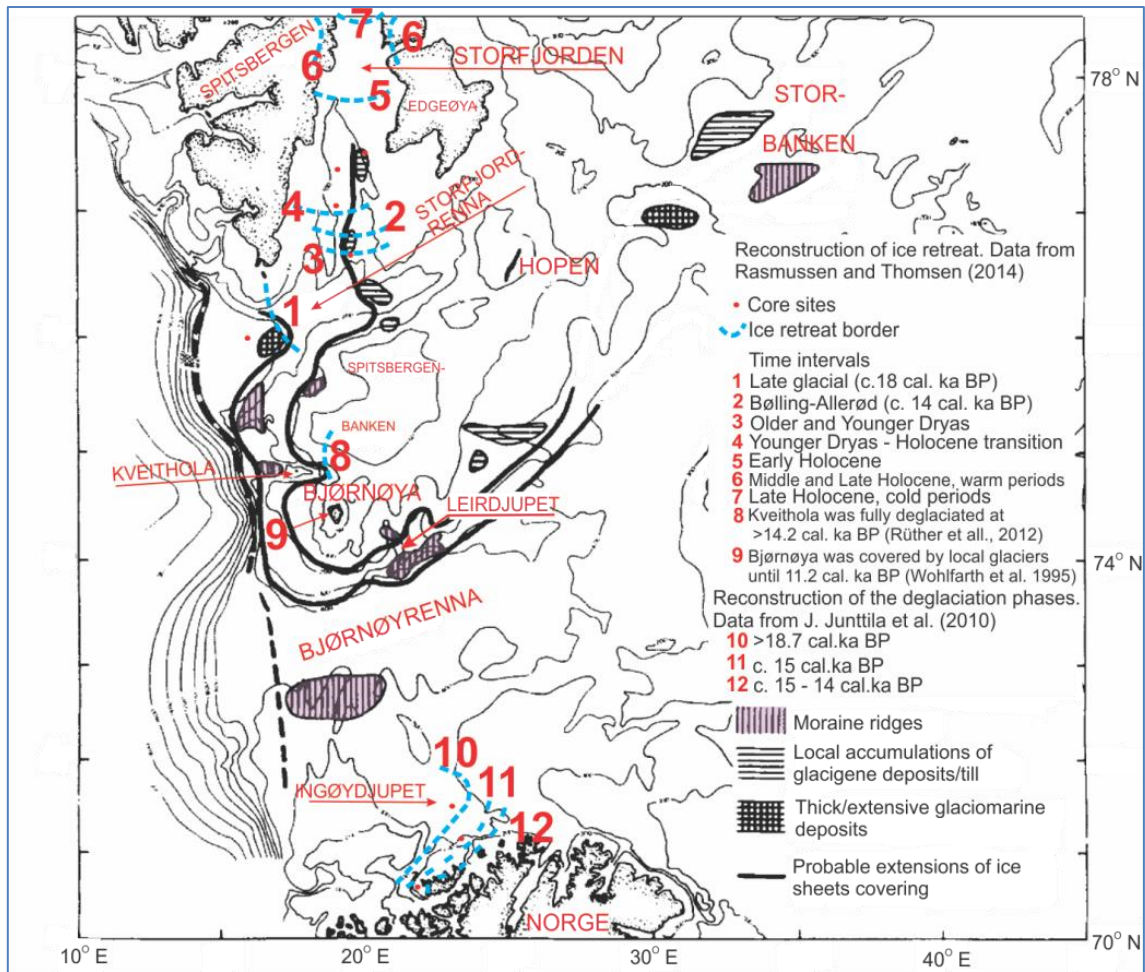


Figure 1.15. Bathymetric map showing features related to former ice margins in the western Barents Sea. Modified from Elverhøi and Solheim (1983).

A sill interpreted as a moraine ridge is located at the outer part of Leirdjupet (Fig. 1.15). The height of the ridge is c. 100 m and the width is c. 10 km. This feature appears to be deposited by a glacier flowing in Leirdjupet (Elverhøi and Solheim, 1983). Vorren and Elvsborg (1979) suggest that the moraine is part of a moraine complex rather than a single end moraine. The shelf moraines were deposited by ice (Rekoengen and Bugge, 1979).

1.6 Distribution of surface sediments and Foraminifera in the study area

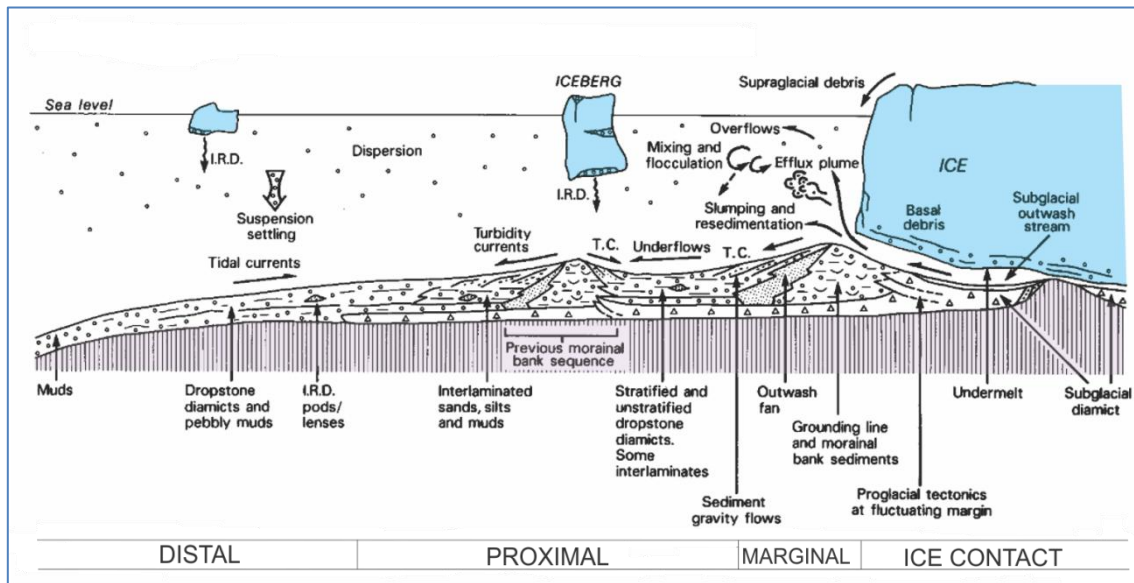


Figure 1.16. Warm based glaciomarine tidewater fjord/bay environment. Modified from Hart and Roberts (1994).

The major agents of ice-rafting are icebergs and sea ice (Gilbert, 1990). The ice-rafted sediments provide information about the extent of glacial processes and the characteristics of the glaciated seas. The approximate range in grain size of ice-rafted sediments from icebergs include all grain-size fractions from boulders to clay. Sea-ice transport mostly rounded cobbles, rounded grains in the sand-size fraction, along with some silt particles. Most clay and silt sediments are deposited during suspension settling (Fig. 1.16). In the glacier-proximal zone high concentrations of suspended particulate material is observed. At shallow-water depth iceberg plough marks can be found. The modern day icebergs are delivered mostly from glaciers on Franz Josef Land and Svalbard (Zubov, 1943). The predominant trajectory is southwesterly, which follows the main surface water flow (Vinje, 1985). During the melting season the sea-ice edge rapidly retreats from approximately 76°N to 82°N (Vinje, 1985; Rey et al., 1987).

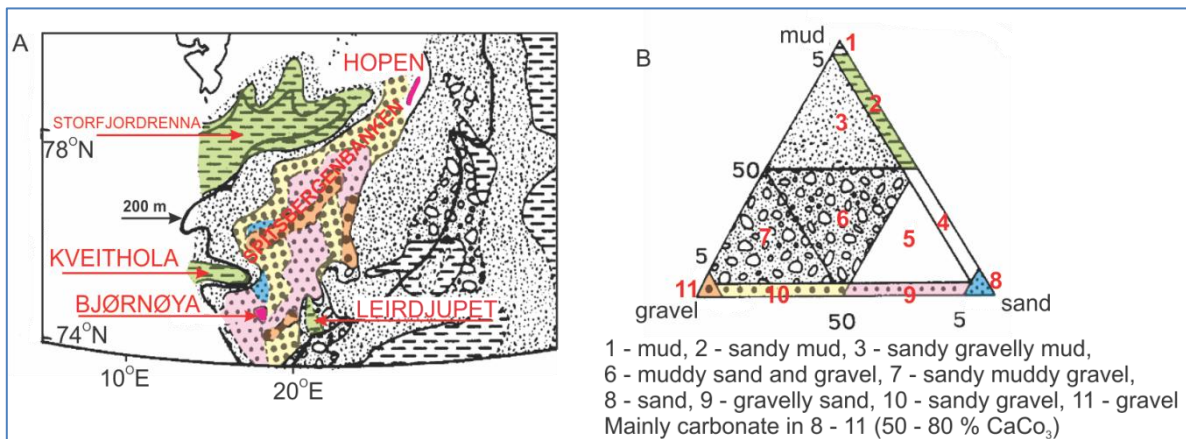


Figure 1.17. Surface-sediment distribution (A) and composition (B) in the study area. Modified from Elverhøi and Solheim (1989).

Around Spitsbergenbanken an important sedimentary boundary is found with diamict sediments dominating above 200 m water depth and mud below the 200 m contour (Fig. 1.17 A). On the southern slope of Spitsbergenbanken some diamicton and sand- and gravel-rich sediments are also found down to a water depth of 300 m (Elverhøi and Solheim, 1983). On Spitsbergenbanken current-related sediment structures (ripple marks) in carbonate sand are found. Sediment erosion occurs down to 60 – 80 m water depth by high current velocities and probably also by storm surges (Bjørlykke et al., 1978).

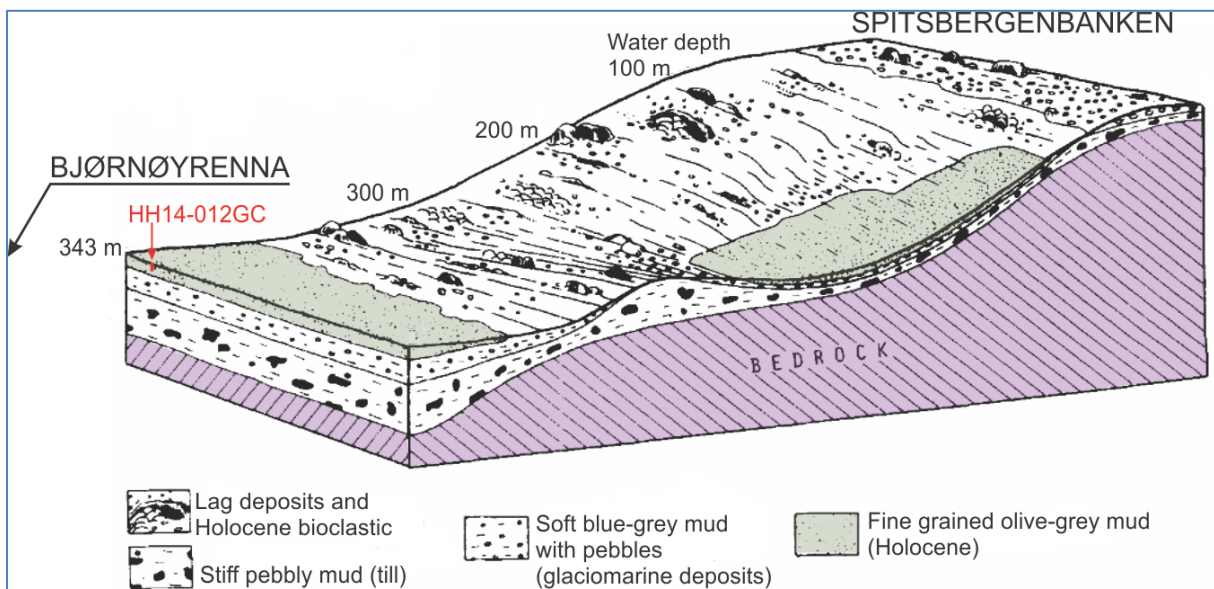


Figure 1.18. Generalized block diagram illustrating the sediment distribution on the slope south of Spitsbergenbanken and northern part of Bjørnøyrenna. Modified after Elverhøi and Solheim (1983).

An overview of the sediment types, distribution and composition of the southern slope of Spitsbergenbanken is shown in Figure 1.18. The stiff pebbly mud (Late Weichselian) is covered by soft, blue-grey muds with pebbles (“proximal” glaciomarine sediments). The thickness of the glaciomarine sediments in regions >300 m water depth are 15 – 20 m. The glaciomarine sediments are overlain by fine-grained, olive grey Holocene mud (“distal” glaciomarine) (Elverhøi et al., 1989). The Holocene mud is rich in foraminifera. The distribution of moraine ridges provides information about the extension of an ice sheet (Elverhøi and Solheim, 1983).

During the summer of 1971 detailing sampling of bottom surface sediments in the western part of the Barents Sea was arranged (Fig. 1.19). The highest benthic foraminiferal content of the sediment on Spitsbergenbanken are in range from 1300 to 8400 shells per gram of sediment (Østby and Nagy, 1982). In Bjørnøyrenna and Storfjordrenna the benthic foraminiferal content of the sediment is 11 to 410 shells per gram.

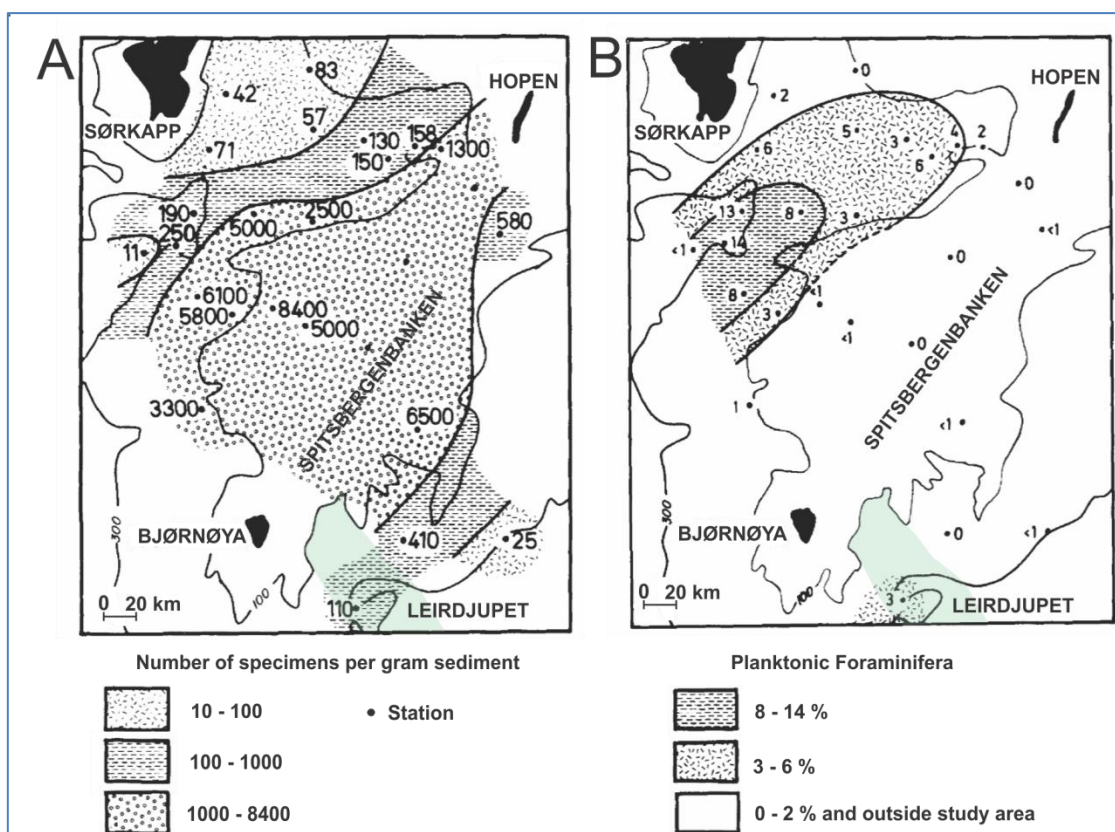


Figure 1.19. Distribution of foraminiferal shells (A), and planktonic foraminifera (B) in the surface sediments. Modified after Østby and Nagy (1982).

The maximum values of foraminiferal shells per unit surface sediment is reached on Spitsbergenbanken, where the strong abrasion, breakage and transport of shells out of the bank area

are observed (Østby and Nagy, 1982). The relatively low concentrations in Bjørnøyrenna and Storfjordrenna must be explained by increased sedimentation rates, mainly of clay and silt.

The amount of planktic foraminifera on the Spitsbergenbanken is 0 or less than 1 % (Fig. 1.19 B). In Storfjordrenna the distribution of the planktonic foraminifera generally increases with increasing depth and is related to the inflowing current of Atlantic water. On the northern flank of Storfjordrenna the amount of planktonic foraminifera is smaller than at similar depth on the southern flank. This difference caused by the cold East Spitsbergen Current, flowing in this area (Østby and Nagy, 1982). The amount of planktonic foraminiferal shells in the southern part of Bjørnøyrenna reaches 49 % (Jarke, 1960), while on its northern flank it is 0 – 3%. The small amounts of planktonic foraminifera on the northern flank of Bjørnøyrenna can be related to the Bjørnøya Current transporting Arctic water towards the southwest.

1.6.1 Distribution of benthic foraminiferal species in the study area

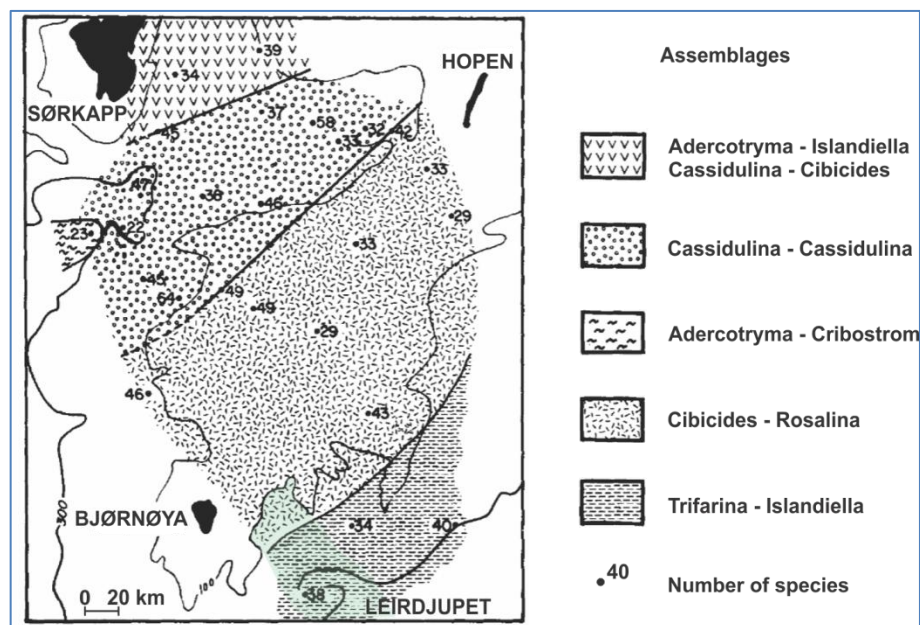


Figure 1.20. Surface distribution of benthic foraminiferal assemblages and number of species in surface samples. Modified after Østby and Nagy (1982).

The high energy environment of Spitsbergenbanken is dominated by the Cibicides – Rosalina assemblage. This assemblage includes *Cibicides lobatulus* (40–68 %), *Cassidulina reniforme* (6–25 %), *Astrononion gallowayi* (3–20 %), and *Elphidium excavatum* (1–9 %). *Rosalina spp.* may account for 15 % of the assemblage (table 1.2 and Fig. 1.20).

On the northern side of Bjørnøyrenna the Trifarina – Islandiella assemblage are predominant. It is dominated by *Trifarina fluens* (15–20 %), *Islandiella norcrossi* (10–16 %), *Cibicides lobatulus* (10–14

%), and at a depth of 300 m by *Melonis barleeanus* (13-14 %). This cold-water fauna appears connected to the Bjørnøya Current.

The Cassidulina – Cassidulina assemblage are located in the central and southern parts of Storfjordrenna. The dominant species are *Cassidulina laevigata*, *C. reniforme* (as *C. crassa*) and *Elphidium excavatum*.

The Cassidulina – Cibicides assemblage is present on the northwestern side of Storfjordrenna. The assemblage is dominated by *Cibicides lobatulus* and *C. reniforme*. Important species are *Elphidium excavatum*, *M. barleeanus* and *Islandiella norcrossi*. Generally the assemblage is related to cold conditions, but the occurrence of *C. laevigata* (up to 8 %) reflects temperatures around 0° C (Burmistrova, 1967).

The Adercotryma – Islandiella assemblage are located in the northeastern part of Storfjordrenna. The dominant species is *Adercotryma glomeratum* (7-24 %), *Islandiella norcrossi* (11-21 %), *Elphidium excavatum* (5-25 %), *Nonionellina labradorica* (3-15 %), and *Cassidulina reniforme* (7-11 %).

Both the Cassidulina – Cibicides and Adercotryma – Islandiella assemblages are limited to the area affected by the East Spitsbergen Current.

In the deepest part of Storfjordrenna the Adercotryma – Cribrostomoides assemblage is found. The dominant species are *Adercotryma glomeratum* and *Cribrostomoides crassimargo*; common species are *Ammotium sp.* and *Recurvoides turbinatus*. The bottom water temperature in this area is < -1° C.

Table 1.2. Foraminiferal assemblages, their environments and supposed ages. Reprinted from Østby and Nagy (1982).

Assemblage	Environment	Supposed age
<i>Cibicides lobatulus</i> – <i>Rosalina</i> spp.	Open shelf bank	Holocene
<i>Trifarina fluens</i> – <i>Islandiella norcrossi</i>	Open shelf trench	
<i>Adercotryma glomeratum</i> – <i>Cribost. crassimargo</i>		
<i>Cassidulina crassa</i> – <i>Cibicides lobatulus</i>	Semiglacial shelf	Late Weichselian – Early Holocene in south
<i>Adercotryma glomeratum</i> – <i>Islandiella norcrossi</i>		
<i>Nonion labradoricum</i> – <i>Cassidulina crassa</i>		Late Weichselian – Recent in north
<i>Elphidium excavatum</i> – <i>Cassidulina crassa</i>	Glacial shelf	Weichselian

2 Material and Methods

2.1 Coring and sampling

Marine gravity core HH14-012GC was received during a cruise with RV Helmer Hanssen in 2014. The core was retrieved from Leirdjupet at 350 m water depth in July. On board, the inner plastic liner (length 441 cm and 9.8 cm inner diameter) was cut into 5 sections and stored in a cooling room at 4 °C. After the cruise cores were placed in cooling storage in Tromsø

Work began with the opening of the core in February 2015 using a Marinetechnik Kawohol sediment liner saw. The core was split into two parts using an osmotic knife cutting from the bottom to the top of the core. Thereafter, the core surface was cleaned carefully. One part was immediately wrapped in plastic foil and stored as the “archive” half. The other half marked “work” was sampled continuously in 1 cm-thick slices. They were packed in plastic bags and immediately weighted. All samples were dried using a freeze-dryer. Each 5 cm slices were prepared for grain size and foraminiferal analysis. The “archive” part of the core was used for lithological description, X-Radiography, magnetic susceptibility measurement and color spectrophotometry.

2.2 Lithology log

After the opening of the core color was described using a Munsell’s soil chart (Munsell 1994). Notes were made about sediments characteristics.

2.3 Magnetic susceptibility measurements and Color spectrophotometry

For these measurements the GEOTEK Multi Sensor Core Logger was used.

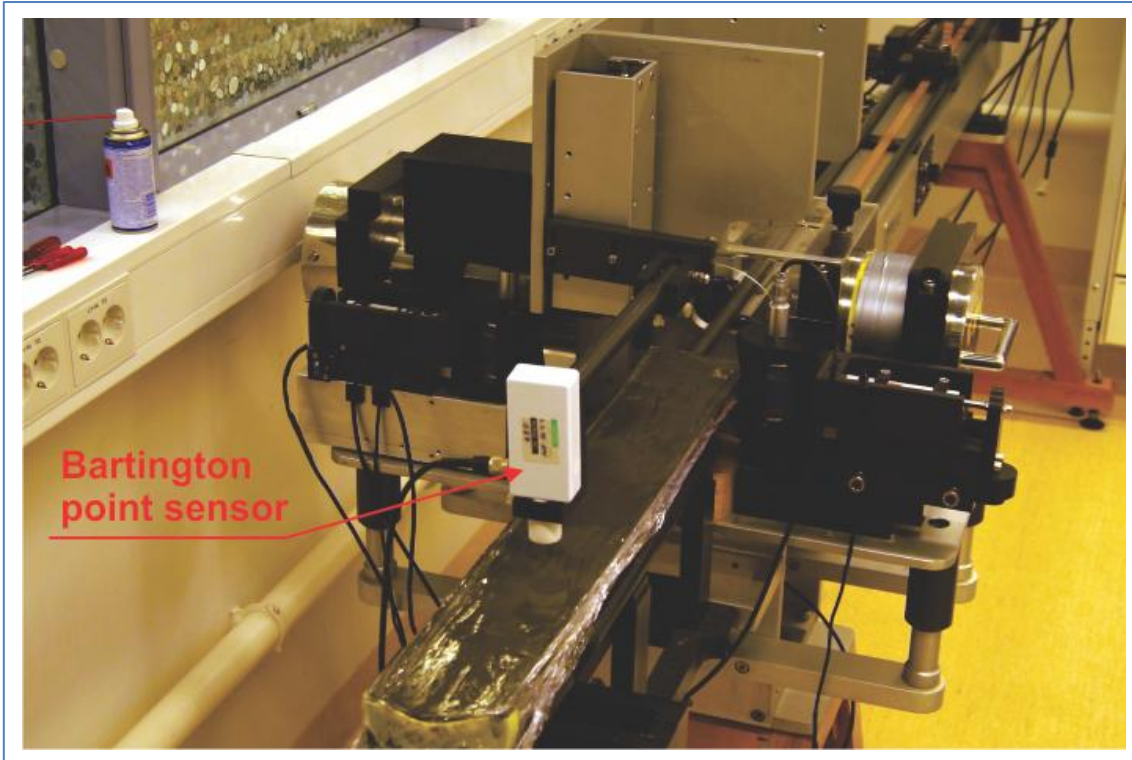


Figure 2.1. Magnetic susceptibility measurements with point sensor mounted on the GEOTEK logger.

Before carrying out measurements, the core halves were taken from the cooling room into the laboratory and staying 24 hours to obtain room temperature. Magnetic susceptibility was measured using a point sensor (Bartington MS2E) (Fig. 2.1). The measurement took 10 seconds at 1 cm intervals. Color Spectrophotometry measurements were performed in August 2015, seventh months after the opening of the core with a Konica Minolta CM-700d spectrophotometer (Fig. 2.2).

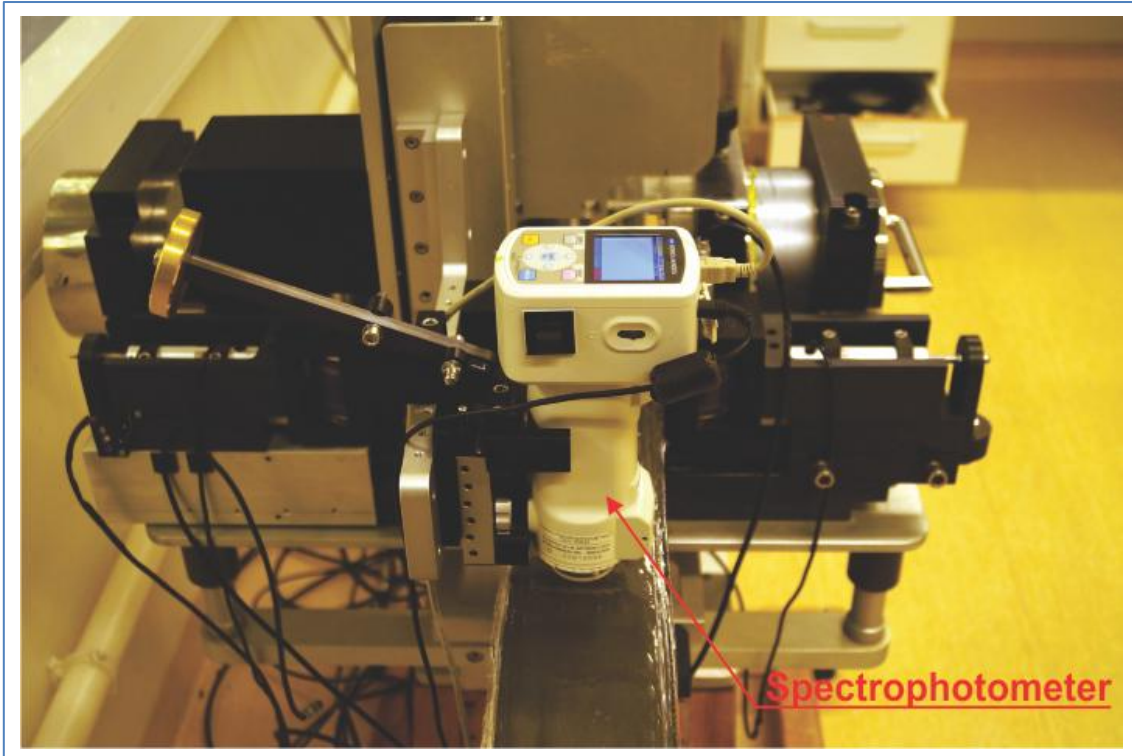


Figure 2.2. Spectrophotometer Konica Minolta CM-700d.

2.4 X-Radiography

In February 2015 the core was x-rayed using a Geotek MSCL-XCT x-ray imaging machine (Fig. 2.3). The images present the highest-density material by white color. Shells and shell's fragments were located based on the X-Ray images and sampled for radiocarbon datings. The composition and structures reflected on the images were also used in generating lithological log of the core.

2.5 Grain size and ice-rafted debris (IRD) analysis

All samples were weighed (measured wet weight), freeze-dried, and reweighed (measured dry weight). A total of 87 samples at 5 cm intervals were selected for wet-sieving over mesh sizes of 63 μm , 100 μm and 1 mm. The residues were dried and weighed. Thereafter, the residues 0.1-1 mm was dry sieved over mesh sizes 150 μm , 250 μm and 500 μm . All size fractions were weighed. The percentages of the individual size fractions were calculated relative to the total dry weight sediment. In the fractions >1 mm, 500 and 250 μm all minerogenic grains was counted, while in the size-fraction 150-250 μm at least 200 grains was counted. The number of IRD grains per gram dry weight sediment was calculated (concentration). For all four IRD fractions also the fluxes as number/cm²*kyr were calculated. These calculations were based on data of dry bulk density (g/cm³), number IRD grains per dry sediment and sedimentation rate (see below). Sedimentation rates were calculated assuming linear sedimentation rates between dating points (see below).



Figure 2.3. Geotek MSCL-XCT x-ray imaging machine.

2.5.1 Flux calculations

Dry and wet bulk density (g/cm^3), water percentage (%), and porosity (g/cm^3) were calculated using the formula given by Ehrmann and Thiede (1986). The volume of 1 cm-thick slice was calculated as 37.72 cm^3 .

Weight of water in gram (g) per sample was calculated as wet weight (g) subtracted by the dry weight (g) of the sediment.

The water percentage (%) per sample was calculated using the formula: water weight (g) / sediment wet weight (g) * 100 (%).

The sediment porosity (g/cm^3) was calculated using the formula: (sediment wet weight (g) – sediment dry weight (g)) / 37.22 cm^3 , where 37.22 cm^3 is the volume of the 1-cm thick sample.

Total wet density (g/cm^3) was calculated as sediment wet weight (g) / 37.22 cm^3 , where 37.22 cm^3 is the volume of 1-cm thick sample.

Dry bulk density (g/cm^3) was calculated as the sediment wet density (g/cm^3) – (1.025 * porosity (g/cm^3)).

Linear sedimentation rates (cm/kyr): (depth of the second calibrated radiocarbon date – depth of the first calibrated radiocarbon date) / (second calibrated radiocarbon date – first calibrated

radiocarbon date) * 1000. Example of the calculations: $(118.5 \text{ cm} - 39.5 \text{ cm}) / (5389 \text{ years} - 2525 \text{ years}) * 1000 = 27.58 \text{ cm/kyr}$.

To calculate the linear sedimentation rates for the interval between the first radiocarbon date (interval 39 – 40 cm) and top of the core (interval 0 – 1 cm), was calculated with the assumption that top of the core represent the present.

The linear sedimentation rates between the last (fifth) radiocarbon date and the fourth date is 80 cm/kyr. This value was extrapolated for the interval between the core bottom and the fifth radiocarbon date (393 – 394 cm) and the age of the bottom of the core (429 – 430 cm) was calculated.

Sediment mass accumulation rates ($\text{g/cm}^2\text{kyr}$) were calculated by multiplying the dry bulk density (g/cm^3) and the linear sedimentation rate (cm/kyr).

The benthic foraminifera accumulation rates (BFAR) were based on of the following calculations: $\text{BFAR} = \text{number of benthic foraminifera (No.)} / \text{sediment dry weight (g)} * \text{sediment mass accumulation rates (g/cm}^2\text{kyr)}$. Similar calculations have been done for flux of ice rafted debris in the various size-fractions, and planktic foraminifera accumulation rates (PFAR).

2.6 Foraminiferal analysis

From size fraction 100 μm to 1 mm all planktic foraminiferal specimens, and at least 350 calcareous benthic foraminiferal specimens were picked from a picking tray under a binocular microscope. All planktic and benthic foraminifera were identified to species level. Benthic agglutinated species were also picked from the exact same squares on the picking tray as the calcareous specimens and the percent of agglutinated specimens calculated relative to the total benthic foraminifera. The foraminiferal analysis was based on the methods in Feyling-Hanssen (1958) and Meldgaard and Knudsen (1979). The percentages of individual species were calculated relative to the total fauna separately for planktic and for calcareous and agglutinated species. The concentration of foraminifera was calculated as number per gram dry weight sediment. The flux (accumulation rate) of planktic and benthic foraminifera was calculated as $\text{number/cm}^2\text{kyr}$ using the dry bulk sediment density, accumulation rate and number of specimens per gram dry sediment (see above).

2.7 Stable isotope analysis

The planktic species *Neogloboquadrina pachyderma* sinistral (s) (specimens with 4 chambers in the last coil and similar size c. 200 μm , >30 tests per sample) and two benthic species *Cibicides*

lobatulus and *Melonis barleeanus* (>10 and >15 tests per sample, respectively) were picked for oxygen and carbon isotope analysis. Stable isotopes measurements were performed at the Geological Mass Spectrometer (GMS) laboratory at the University of Bergen using a Finnigan 253 mass spectrometer and the standard Vienna Pee Dee Belemnite (V-PDB). Values were corrected for ice-volume effect using the Fairbanks (1989) curve. In addition, oxygen isotope data was corrected for isotopic disequilibrium (vital effect correction) of +0.64 ‰ for *Cibicides lobatulus* (Shackleton, 1974) and +0.40 ‰ for *Melonis barleeanus* (Duplessy et al., 1980).

2.8 Radiocarbon dating

Five accelerator mass spectrometer (AMS) ^{14}C dates were measured at the Chrono Centre, Queen's University, Belfast, UK. Four dates were obtained from various bivalve shells and one from mixed benthic foraminiferal assemblages and bivalve shell fragments (Table 3.1). The radiocarbon ages were calibrated to calendar years Before Present (cal years BP) using the Calib 7.0.4 program (Stuiver et al., 2005) and the Marine13 curve (Reimer et al., 2013). A regional reservoir age of 400 years and regional ΔR value of 67 ± 37 years was used (Mangerud and Gulliksen, 1975). For comparison with published records an age model based on ^{14}C years was also made. For this model a reservoir effect correction of -440 years was applied (Mangerud and Gulliksen, 1975). Linear interpolation was used to obtain values between given sample points under the assumption of constant sedimentation rates between dating points. No abrupt changes in lithology, or erosional features that would indicate large changes in sedimentation rates were observed.

3 Results

3.1 Age model and sedimentation rate

Five accelerator mass spectrometry (AMS) radiocarbon dates have been obtained from core HH14-012GC during this study. Mainly marine mollusks were dated. The most suitable specimens of marine fauna used for radiocarbon dating are shown in Figure 3.1.

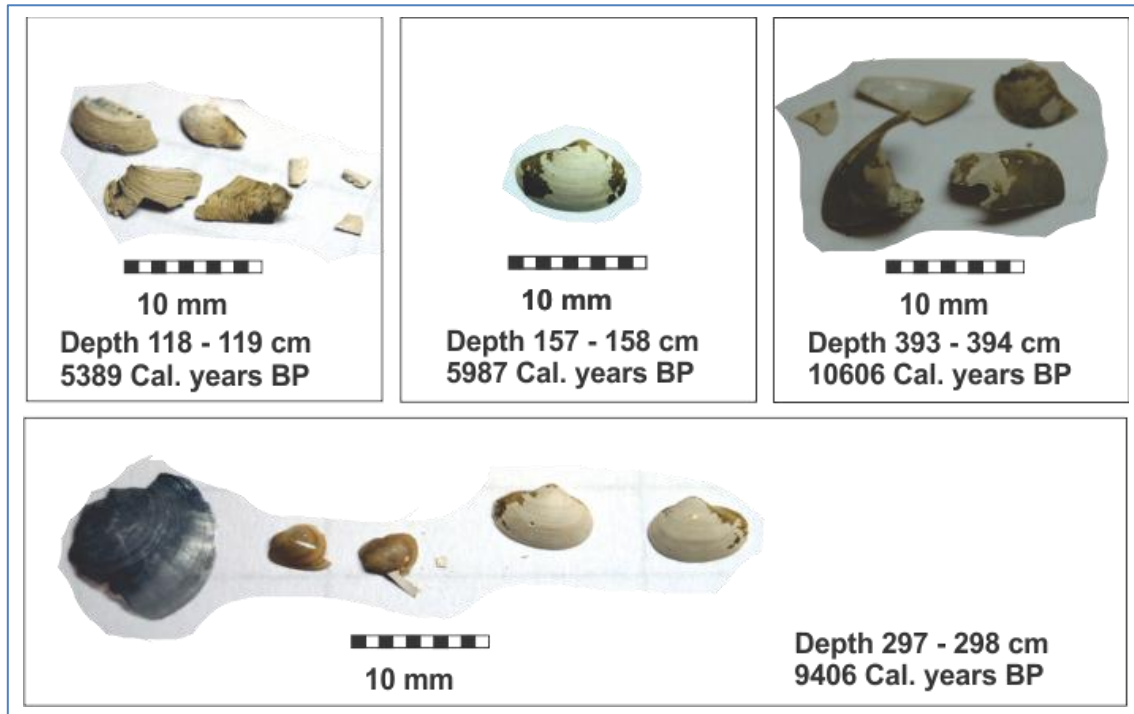


Figure 3.1 Shells and parts of shells, which have been selected for radiocarbon datings. The youngest sample for radiocarbon dating (depth 39 – 40 cm) consisted benthic foraminifera and a few very small bivalve shell fragments.

The conventional AMS ^{14}C dates were calibrated to calendar years Before Present (Table 3.1). The ages are in chronological order (Fig. 3.2 right panel). This may indicate that there were no significant disturbances. The dates indicate that the sediments are all of Holocene age. Age data can be improved by using additional samples of radiocarbon data as well as using correlation with already published records.

Table 3.1 AMS ¹⁴C dates and calibrated dates for core HH14-012GC.

Lab reference UBA No.	Depth (cm)	Dated material	AMS ¹⁴ C	Calibrated age years BP (16 mean and ± 16 range)
29300	39-40	Benthic foraminifera mixture with few small shell parts	2847 ± 22	2525 ± 88
28814	118-119	Bivalves	5119 ± 39	5389 ± 68
28815	157-158	Bivalves	5669 ± 31	5987 ± 69
28816	297-298	Bivalves	8795 ± 40	9406 ± 60
28817	393-394	Bivalves	9774 ± 52	10,606 ± 78

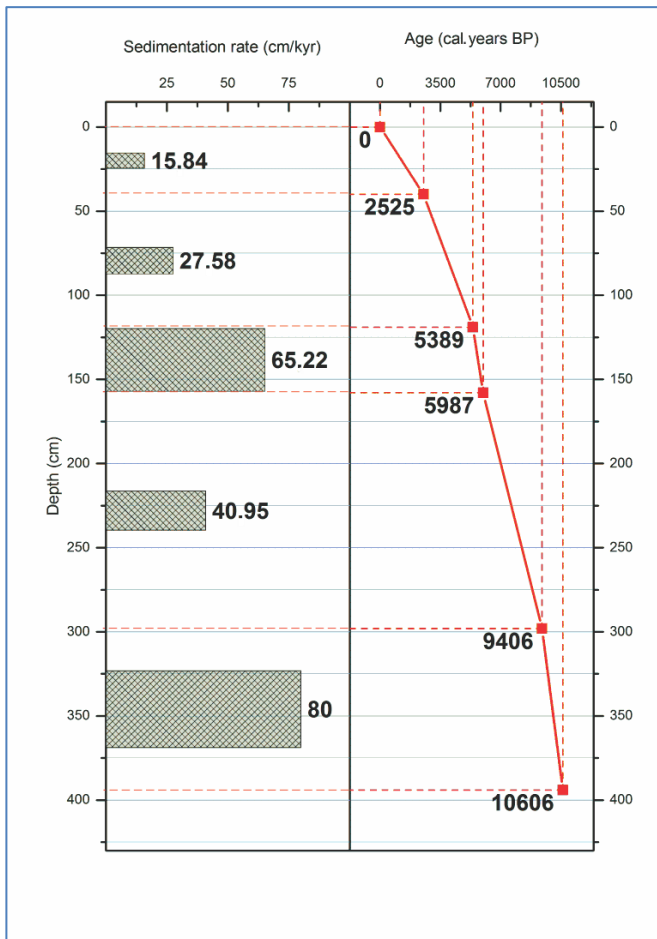


Figure 3.2 Age model and sedimentation rate of HH14-012GC. Linear interpolation was used between calibrated ages.

Sedimentation rates were calculated and are presented in Figure 3.2 (left panel). Largest value of sedimentation rate is 80 cm/kyr or respectively 0.8 mm per year. This value is found in the early Holocene in the time interval 10,606 to 9406 cal years BP, (394 – 297 cm depth).

Between 9406 and 5987 cal years BP (depth interval 298 – 157 cm) sedimentation rate decrease c. 41 cm/kyr. In the time range 5987 – 5389 cal years BP (depth interval 158 – 39 cm) sedimentation rate increase and reaches c. 65 cm/kyr. After 5389 cal years BP, sedimentation rates gradually decrease to 27.6 cm/kyr and 15.8 cm/kyr, respectively.

Large variations in sedimentation rates are observed in the Holocene. The largest value of 80 cm/kyr occurs at start of the Holocene and the rate drops to 15.84 cm/kyr in the late Holocene, which is 5 times lower. The main trend is a decrease towards the present.

3.2 Core description and sediment properties

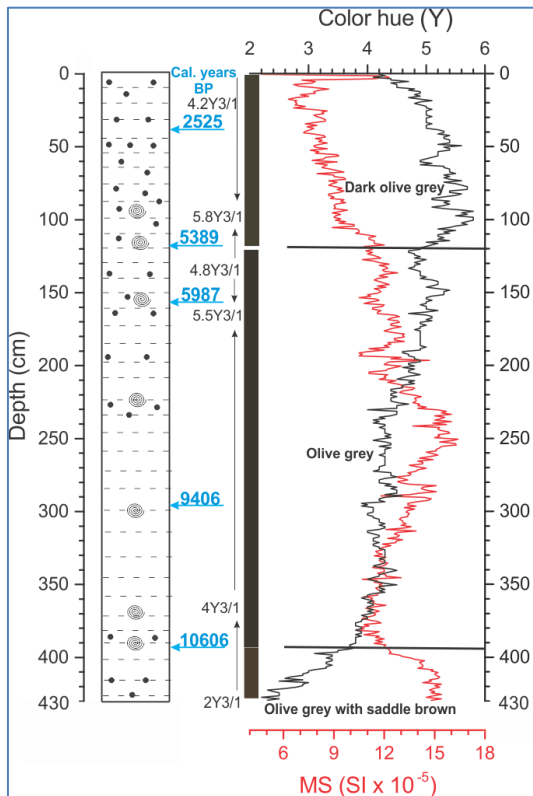


Figure 3.3 Sedimentological log plotted along magnetic susceptibility (MS) and color hue. Black dots represent ice rafted debris and spirals are shells. Horizontal dashed lines are hemipelagic sediments.

The sedimentological log is illustrated in Figure 3.3. The core consists mainly of hemipelagic clay sediments of homogeneous structure. It was not possible to visually determine the presence of ice rafted debris (IRD). Ice rafted debris and shell abundance based on the results after wet sieving. Only seven IRD grains >1 mm (diameter c. 2 - 4 mm) were found. The inspection of the X-ray images also did not reveal any larger dropstones. Color change of the sediment can be distinguished, which has been visually determined using the three color zones of the Munsell Soil Colour Charts. From the core bottom to a depth of circa 390 cm sediment the color changes from olive grey with saddle brown to olive grey (2Y3/1 - 4Y3/1). From a depth of c. 120 cm and to the core top the sediment color becomes dark olive grey.

For more accurate color determination a Konica Minolta CM-700d spectrophotometer was used (Fig. 3.4). The results can be presented in different formats; the Munsell chart color system, CIE Color L a b, CIE XYZ, and RGB (red green blue). In geology the common Munsell color system, is based on Hue, Value and Chroma. Hue distinguishes five principal hues (Red, Yellow, Green, Blue and Purple) and five intermediate (Yellow-Red, Green-Yellow, Blue-Green, Purple-Blue and Red-Purple). Value or lightness ranges from black (value 0) to white (value 10). Chroma varies in range from 0 to 12. Value 0 represents less pure (more diluted with white, as in pastels) and value 12 represents more intense, saturated color.

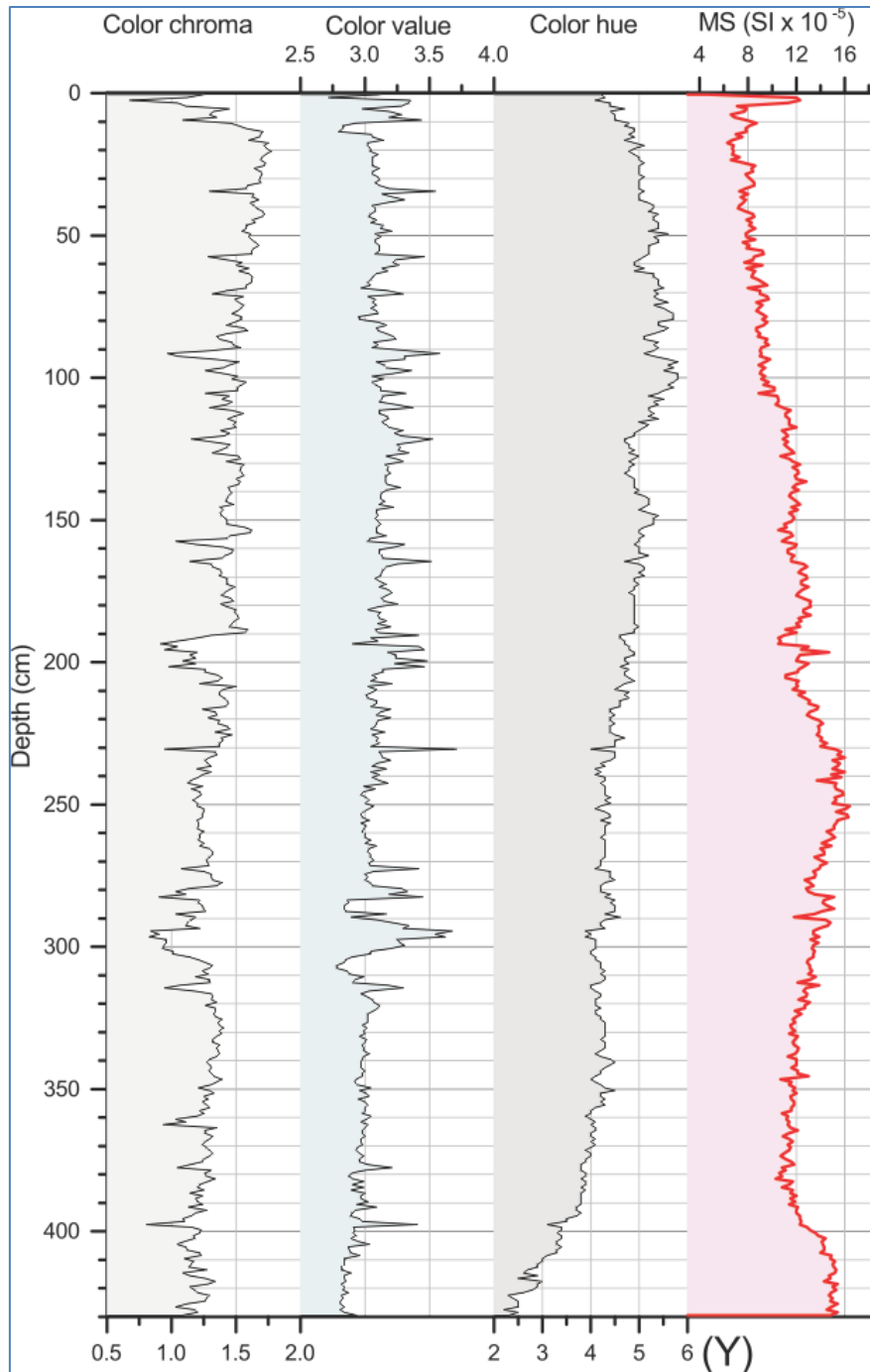


Figure 3.4 Magnetic susceptibility (MS) with color characteristics (Hue, Value and Chroma).

The point sensor (Bartington MS2E) was used to measure magnetic susceptibility (Fig. 3.4). Point sensor data are more detailed than loop sensor data, because it measures over an interval of 1 cm, while the loop measures over c. 10 cm. Magnetic susceptibility (MS) was measured each centimeter. Results are shown in Figure 3.3 (red line). The MS values decrease from bottom of the core to a depth of c. 380 cm (14.8×10^{-5} to 10.8×10^{-5} SI). Further, there is a gradual increase in MS values from 380 cm to 250 cm to a maximum of 16.4×10^{-5} SI. From 250 cm to the top of the core the

MS values decrease. Close to the core top the MS are at minimum (4.8×10^{-5} SI) followed by an increase in MS at the top of the core.

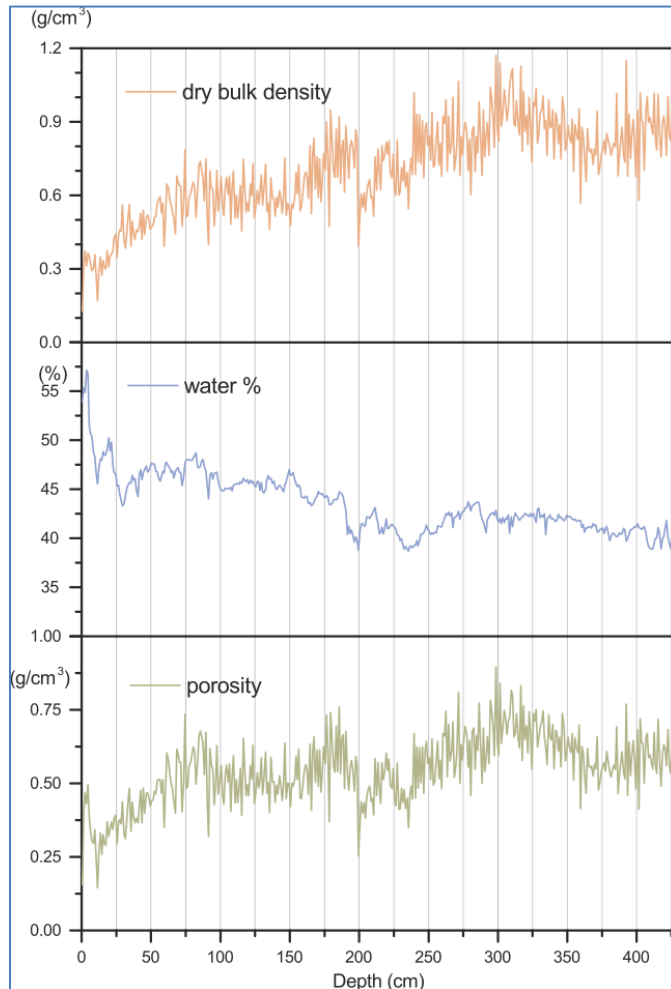


Figure 3.5 Sediment properties plotted against depth.

3.3 Lithological units

Core visual inspection, X-ray images, magnetic susceptibility, grain size analysis, the weight percent of the various size fractions and count of minerals per gram dry weight sediment were used to identify specific lithological units in the core. The Udden-Wentworth Grain size classification for clastic sediments is represented in Table 3.2. Results show an absence pebbles (dropstones), and very rare granules and very coarse sand. Most grains occur in the fine sand fraction, here 0.25 – 0.15 mm with some in the medium sand fraction 0.5 – 0.25 mm.

The dry bulk density (DBD) is the ratio of the mass of the sediment to the total volume. The results show that DBD values generally increases with depth (Fig. 3.5 upper panel). Grain size analysis show that the size fraction <0.063 mm constitutes 97 % of the total through the whole core. This indicates that DBD changes occur under the influence of sediment compaction.

The percentage of water decreases with depth. At the top of the core the water content reaches 56.7 % and close to the bottom c. 40 %.

Specific sediment porosity (g/cm^3) generally follows the distribution of the DBD (Fig. 3.5 lower panel).

Table 3.2. The Udden-Wentworth grain-size scale for clastic sediments (partially represented).

The Udden-Wentworth grain-size scale for clastic sediments		
mm	µm	Name
4 - 2	4000 - 2000	Granules
2 - 1	2000 - 1000	Very coarse sand
1 - 0.5	1000 - 500	Coarse sand
0.5 - 0.25	500 - 250	Medium sand
0.25 - 0.125	250 - 125	Fine sand
0.125 - 0.063	125 - 63	Very fine sand
0.063 - 0.0039	63 - 3.9	Silt (include 4 subdivisions)
<0.0039	<3.9	Clay

Grain size data in the very fine sand fraction may provide useful information about the current strength of the inflowing Atlantic Water to the Barents Sea. Fine particles can be moved by stronger bottom currents and very small particles can be transported in suspension (Nichols, 2009). Generally, variation in the content of fine particles can also reflect changes, which occur with transport agents (sea ice, icebergs, wind, and water flow. Most mineral grains larger than 150 µm is considered as ice rafted by either sea ice or icebergs (Gilbert, 1990).

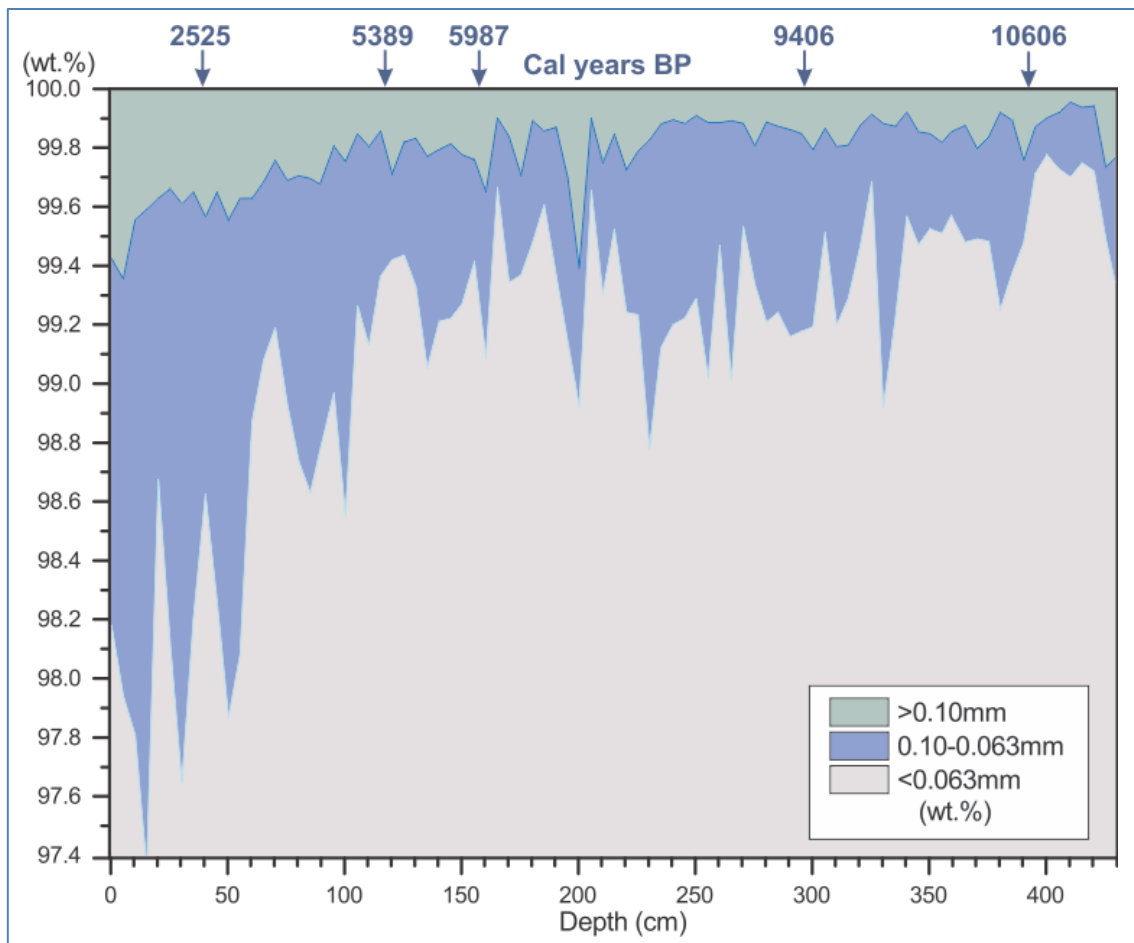


Figure 3.6 Cumulative grain sizes as weight percentages.

The results of the grain-size analysis demonstrate that the silt and clay grain-size fractions are dominant (Fig. 3.6). This fraction is present in all samples and reaches a maximum value 99.78 weight percentage and minimum value of 97.35 weight percentage. The Hjulstrom diagram shows the relationship between the velocity of a water flow and the transport of loose grains. From this diagram for grain sizes >0.1 mm deposition start at a flow velocity of less than 7 cm/sec. For grain sizes >0.063 mm deposition start at flow velocity less than c. 3.5 cm/sec.

All other size-factions together constitute 0.12 – 2.24 weight percentage. The second most common fraction is very fine sand (0.10 – 0.063 mm), also represented in all samples.

Five lithological units are shown in Figures 3.7, 3.8 and 3.9. Numbering starts at the bottom of the core.

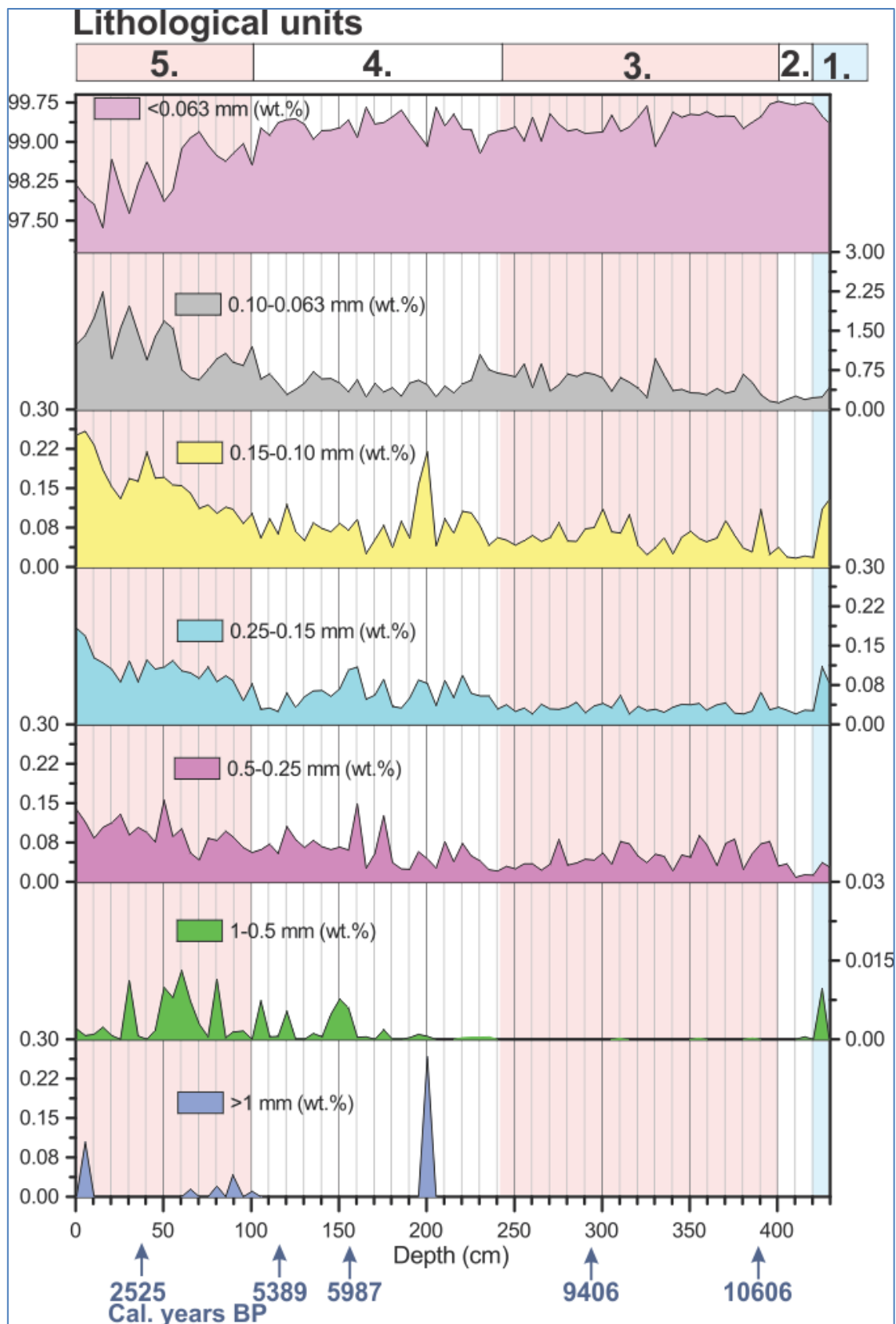


Figure 3.7 Lithological units. Percentage of the various grain size fractions plotted versus depth.

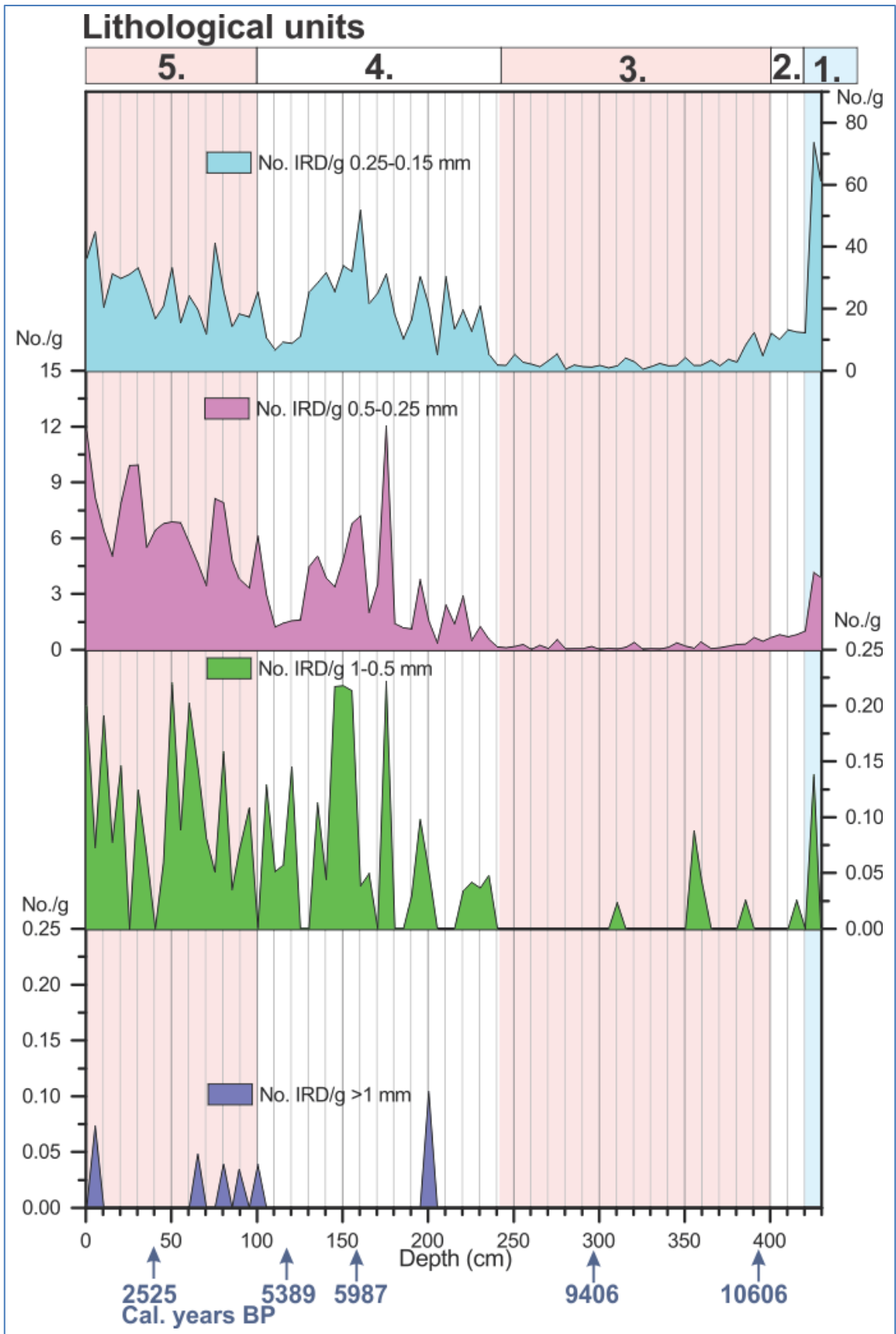


Figure 3.8. Concentration of IRD as number of mineral grains per gram dry weight sediment.

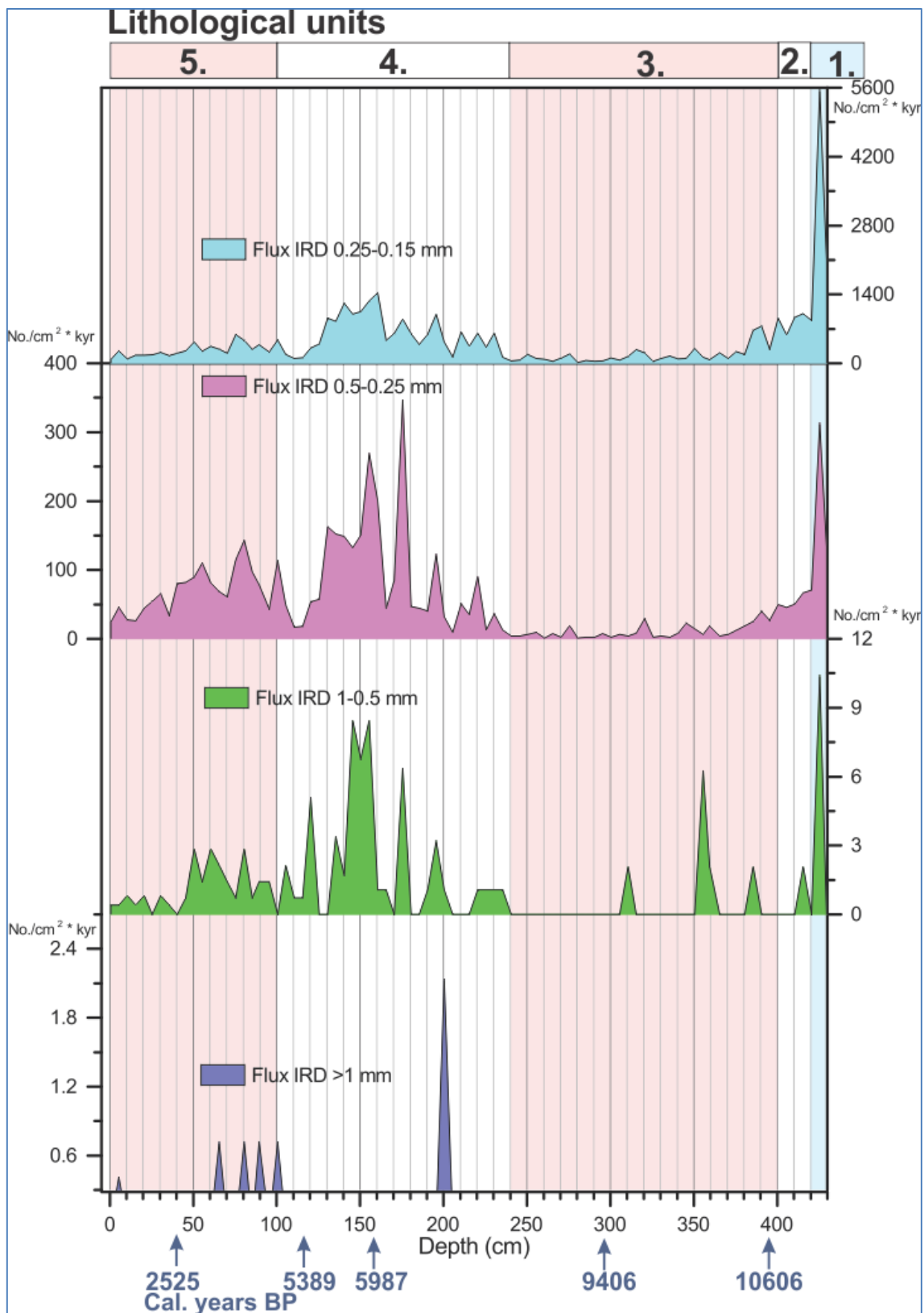


Figure 3.9. The flux of IRD grains in the various grain size fractions plotted versus depth.

3.3.1 Lithological unit 1

Lithological unit 1 (LU 1; depth interval 430 – 420 cm; c. 11.0 – 10.9 ka BP) is defined based on the high sedimentation rates (80 cm/kyr), and high magnetic susceptibility (MS) values (Fig. 3.2). The sediment is fine-grained and consists of homogenous clay and silt. The flux of grains in three size fractions 0.15-0.25, 0.25-0.5 and 0.5-1 mm is high (Fig. 3.9). The color is olive grey with saddle brown. The lower limit of LU 1 is not recorded.

3.3.2 Lithological unit 2

The second lithological unit (LU 2; depth interval 420 – 400 cm; 10.9 – 10.6 ka BP) is defined by high sedimentation rates 80 cm/kyr, and high magnetic susceptibility values. At 414 and 404 cm, small fragments of shells probably from the same shell (c. 8 mm long) are found. As in LU 1, the sediment consists of homogenous clay and silt and with the same color (Fig. 3.3).

The flux of grains in the various size fractions are low compared to LU 1 with a moderate flux of grains 0.5 – 0.25 mm and 0.25 – 0.15 mm, but larger than average for the whole of the core (Fig. 3.9).

3.3.3 Lithological unit 3

Lithological unit 3 (LU 3; depth interval 400 – 240 cm; 10.6 – 8.0 ka BP) is characterized by high sedimentation rate in the interval 400 – 297 cm (80 cm/kyr). At 297 cm sedimentation rate rapidly drop to 40.95 cm/kyr (Fig. 3.2). The sediment consists of homogenous clay and silt of olive grey color (Fig. 3.3). The magnetic susceptibility increases gradually to a maximum value of $16.4 \cdot 10^{-5}$ SI at the top of the LU 3 (Fig. 3.4).

LU 3 is richer in remains of marine macrofaunas than the previous units. At a depth of 375 cm a fish tooth (approximately 18 mm long and 1 – 3 mm in diameter) is found. Here, paired bivalve shells (c. 3.5 mm long) also occur. At 288 cm part of a crab leg (c. 9 mm long) was found. A large paired bivalve shell is found at a depth of 275 cm (c. 23 mm long). Shells also are found at a depth of 370, 323, 305, 303, 289 and 288 cm.

Number of IRD grains per dry weight sediment and the flux of the size fractions 0.25 – 0.15 and 0.5 – 0.25 mm are minimal throughout this unit. Some small increases in the size fraction 1 – 0.5 mm are observed (Figs. 3.8 and 3.9).

3.3.4 Lithological unit 4

Lithological Unit 4 (LU 4; depth interval 240 - 110 cm; 8.0 – 5.0 ka BP) also consists of homogenous clay and silt (Fig. 3.3). The unit shows a change of color from olive grey to dark olive grey at a depth of c. 120 cm. The magnetic susceptibility decrease close to the top of LU 4 (Fig. 3.4).

At 96 cm a fish tooth (c. 8 mm long, 1 – 2.5 mm in diameter) is found. Some paired bivalves shells are identified at a depth of 232, 136, 103, 95, 94 and 76 cm. There is also an increase in the abundance of broken shells.

The sediment is fine grained, but the concentration of coarser grains in all size fractions increase towards the top of the unit (Fig. 3.7).

The flux of IRD grains in all size fractions show high values (Fig. 3.9). In comparison with the other lithological units, the flux of fractions >1 mm and 0.5 – 0.25 mm is at maximum maximal, while in fractions 1 – 0.5 mm and 0.25 – 0.15 mm the second largest flux is observed.

3.3.5 Lithological unit 5

Lithological unit 5 (LU 5; depth interval 110 – 0 cm; c. 5.0 ka BP – present) consists of homogenous, dark olive grey clay and silt (Fig. 3.3). The magnetic susceptibility (MS) values range 12.1 – 4.7 *10⁻⁵ SI. Near the core top at 2 – 3 cm depth, MS reaches 12.3 *10⁻⁵ SI (Fig. 3.4).

Macrofossils are rare in this unit. Some small shells parts were found at 34 and 37 cm.

The weight percentage of the fraction 1 – 0.5 mm has a maximum compared with other LU, and show peak values in the interval 30 – 80 cm. Grains larger than 1 mm is found at 5 and 60 – 100 cm (Fig. 3.7). Most size fractions >0.063 mm show an increasing trend in weight percentages as does the number of IRD grains per dry weight sediment (Fig. 3.8). The flux of IRD is low (Fig. 3.9).

3.4 Foraminiferal units

Four foraminiferal units (FU) are defined based on the percentage distribution of the benthic foraminiferal species, the concentration of planktic and benthic foraminifera and the flux data. The values of FU thickness varies in intervals of 10 – 20 cm to 100 – 150 cm (Figs. 3.10, 3.11 and 3.12).

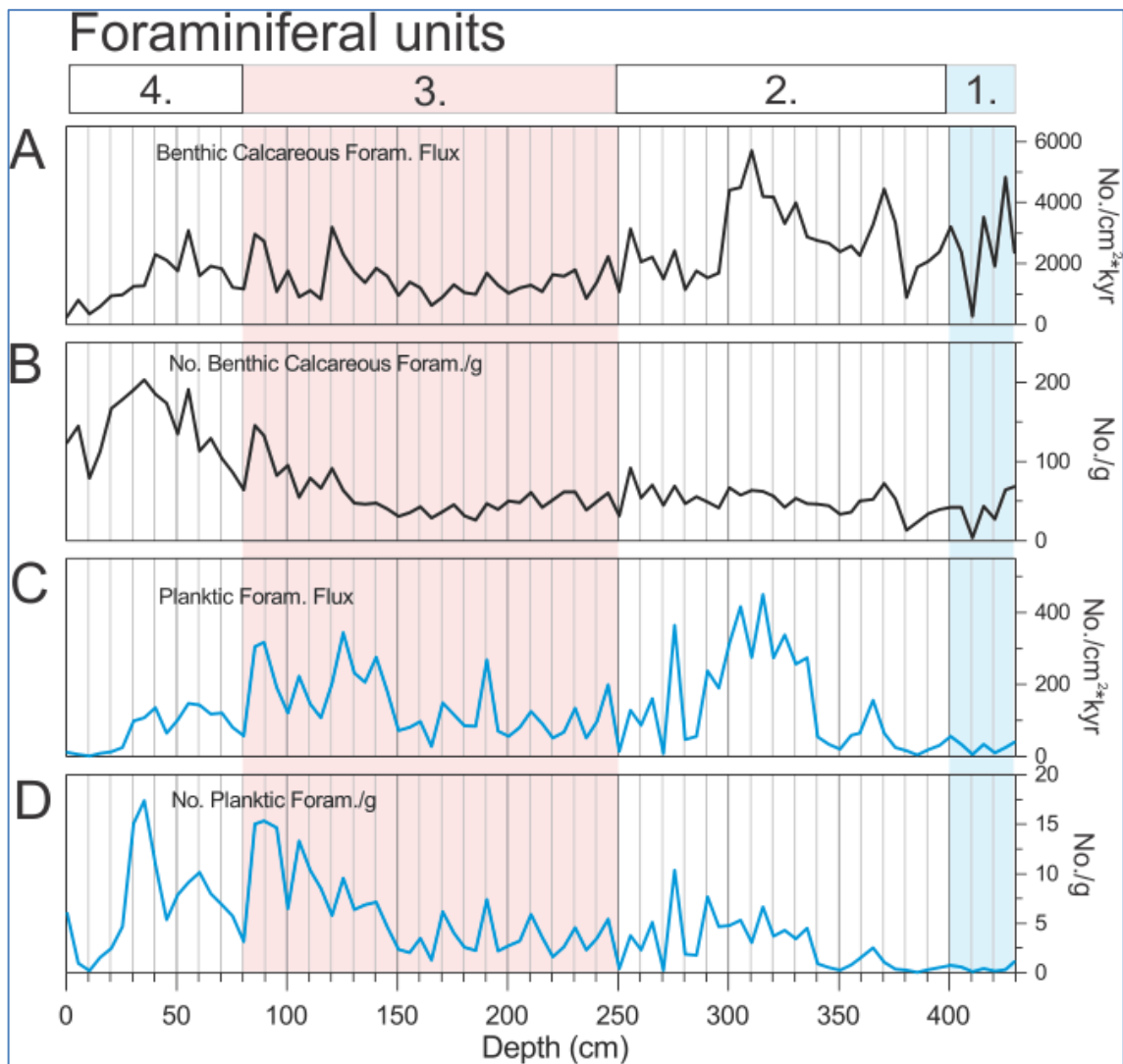


Figure 3.10. Benthic calcareous foraminifera A) concentration (No./g) and B) flux (No./cm²*kyr); planktic foraminifera C) concentration (No./g) and D) flux (No./cm²*kyr) plotted versus depth.

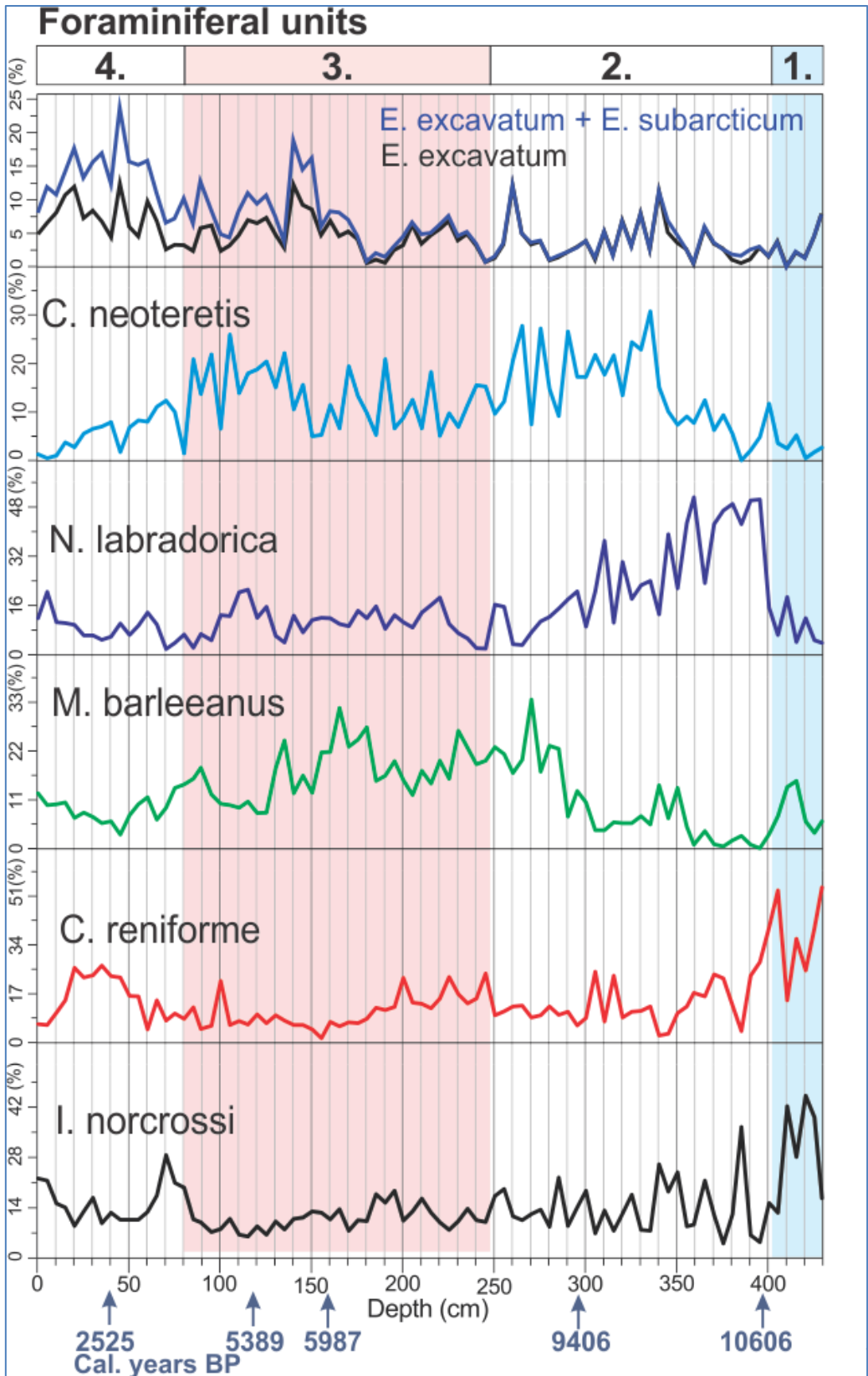


Figure 3.11. Percent distribution of dominant benthic foraminiferal species versus depth in core HH14-012GC.

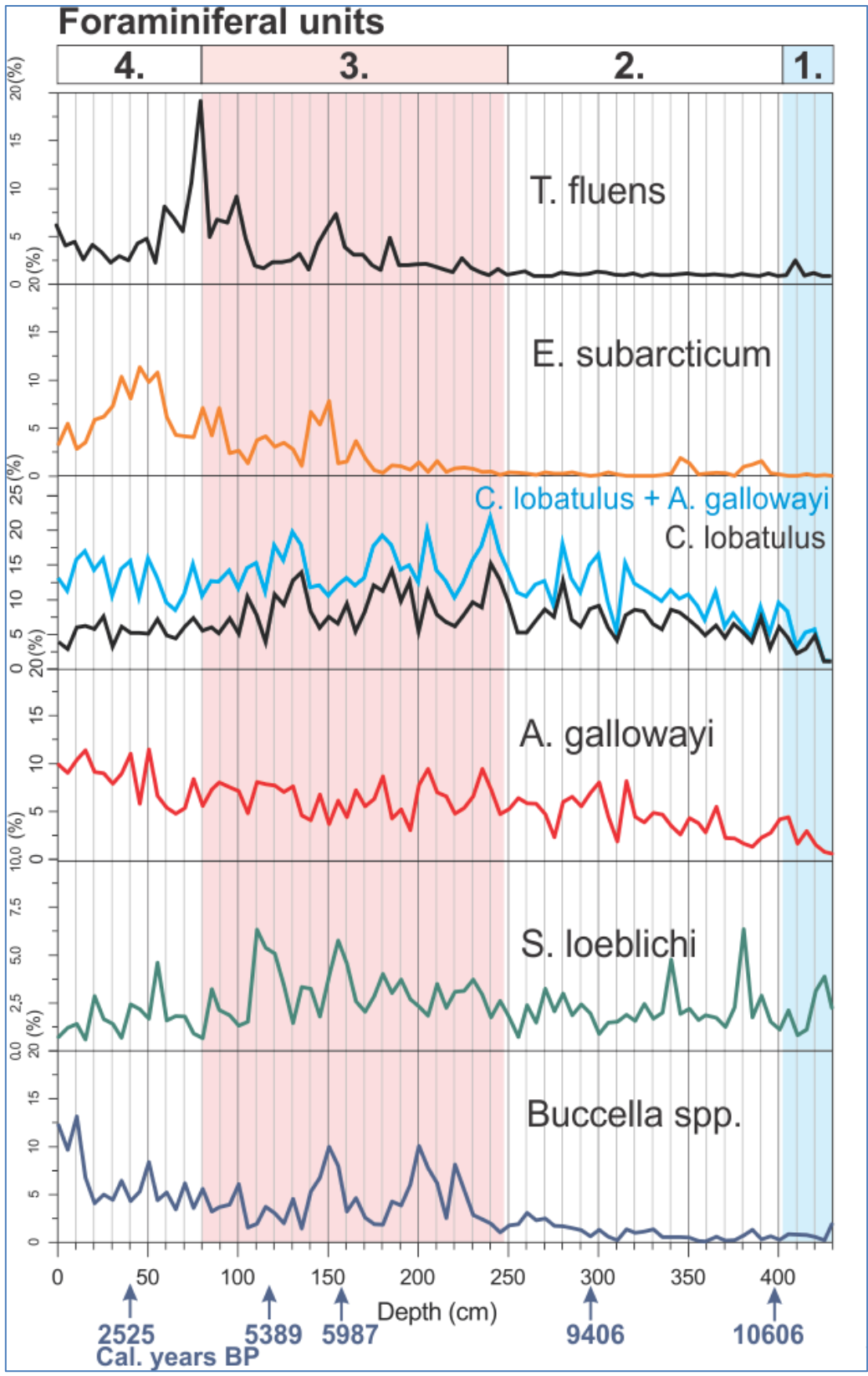


Figure 3.12. Percent distribution of dominant benthic foraminiferal species versus depth in core HH14-012GC.

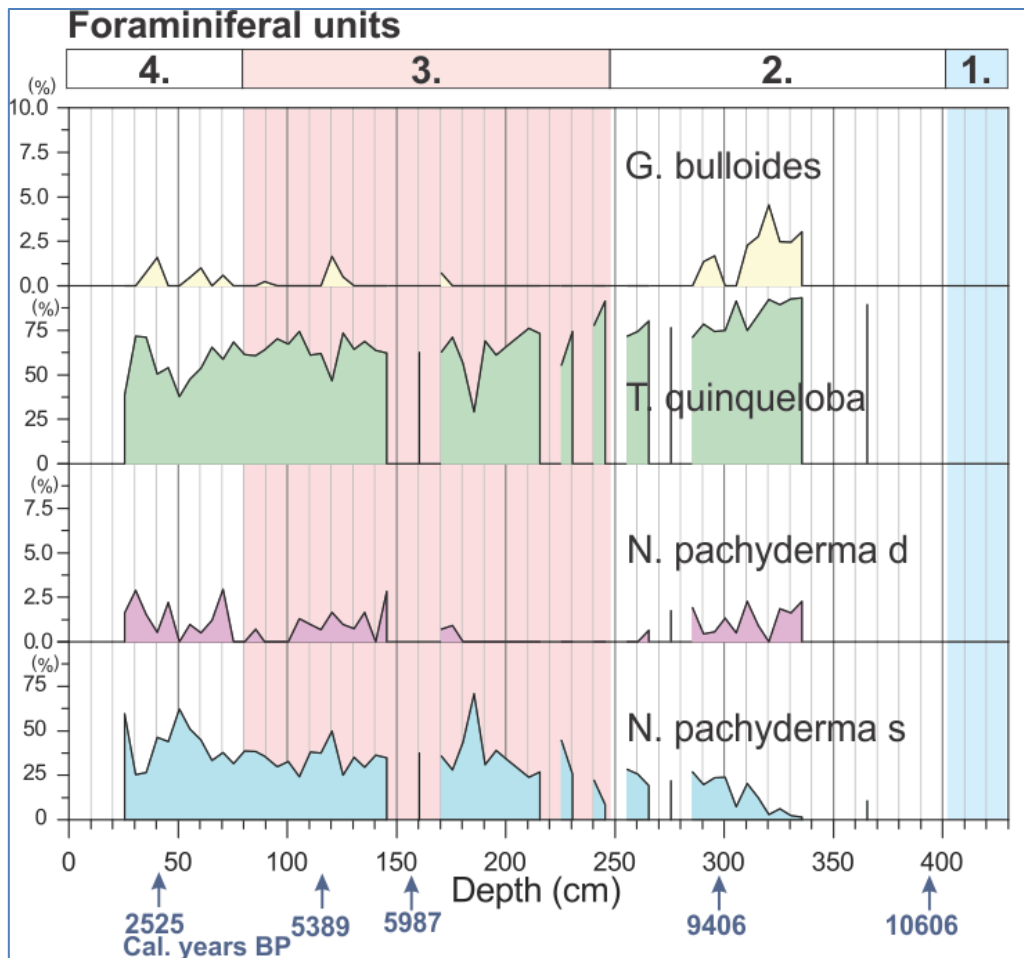


Figure 3.13 Percent distribution of planktic foraminiferal species versus depth in core HH14-012GC. Only samples more than 50 specimens per one sample are shown. The benthic foraminiferal units are indicated.

3.4.1 Foraminiferal unit 1

Foraminiferal unit 1 (FU 1; depth interval 430 – 400 cm; c. 11.0 – 10.7 ka BP) is defined based on the high benthic foraminiferal flux and moderate benthic foraminiferal concentrations (Fig. 3.10). The flux and concentration of planktic foraminifera are minimal. FU 1 is dominated by *Cassidulina reniforme* (c. 37 %) and *Islandiella norcrossi* (c. 31 %) (Fig. 3.11). The subdominant species are *Nonionellina labradorica* and *Melonis barleeanus* each constituting c. 8 % (Figs. 3.10 and 3.11). At the bottom of the core the abundance of *Elphidium excavatum* reaches c. 7.8 %.

3.4.2 Foraminiferal unit 2

Foraminiferal unit 2 (FU 2; depth interval 400 – 250 cm; 10.7 – 8.3 ka BP) is characterized by moderate benthic foraminifera concentration and high flux (Figs. 3.10 and 3.13). The planktic foraminiferal concentration and flux in the depth interval 400 – 360 cm are low, in the depth interval 360 – 250 cm they are moderate and high, respectively. The dominant benthic foraminiferal species

are *N. labradorica* (c. 25 %), *Cassidulina neoteretis* (c. 14 %), *C. reniforme* with *I. norcrossi* (c. 13 % each), and *Melonis barleeanus* (c. 9.7 %). The subdominant species are *Cibicides lobatulus*, *Astrononion gallowayi* and *E. excavatum* (c. 6.2 %, 4.4 % and 3.5 %, respectively) (Figs. 3.11 and 3.12).

At the start of FU 2 *N. labradorica* shows a sharp and rapid increase in percentage. *C. neoteretis* shows increase at c. 340 cm depth. The percentages of *M. barleeanus* increase at c. 290 cm depth. FU 2 is characterized by a decrease in percentages of *C. reniforme* and *I. norcrossi* (Fig. 3.11).

3.4.3 Foraminiferal unit 3

Foraminiferal unit 3 (FU 3; depth interval 250 – 80 cm; 8.3 – 4.0 ka BP) is defined by moderate concentration and flux of benthic foraminifera (Fig. 3.10). The concentration of benthic foraminifera shows a weak increase at c. 120 cm. The planktic foraminiferal concentration and flux are moderate, and show an increase at c. 140 cm. The unit is dominated by *M. barleeanus* (c. 17 %), *C. neoteretis* (c. 12.7 %), *I. norcrossi* (c. 11 %), *C. reniforme* (c. 10.7 %), and *N. labradorica* (c. 10.5 %) (Figs. 3.11 and 3.12).

3.4.4 Foraminiferal unit 4

Foraminiferal unit 4 (FU 4; depth interval 80 - 0 cm; 4.0 ka BP - present) is characterized by a maximum concentration of benthic foraminifera and relatively moderate flux (Fig. 3.10). The planktic foraminifera concentration and flux are high and moderate, respectively, and decrease after c. 30 cm.

The dominant benthic species are *C. reniforme* (c. 15.7 %) and *I. norcrossi* (c. 15 %). The subdominant species are *N. labradorica* (c. 8.9 %), *M. barleeanus* (c. 8.7 %), *A. gallowayi* (c. 8.4 %), *E. excavatum* (c. 7 %), *Elphidium subarcticum* and *Buccella spp.* (each c. 6.4 %) (Figs. 3.11 and 3.10).

The general trend of FU 4 is an increase of *C. reniforme*, *I. norcrossi*, *E. excavatum*, *E. subarcticum*, *A. gallowayi* and *Buccella spp.* In FU 4 a decrease in % of *C. neoteretis* is observed.

4 Interpretation

Core HH14-012GC were divided into four time intervals based on the radiocarbon data, the benthic and planktic foraminiferal concentration and flux, the dominant and subdominant benthic foraminiferal distribution patterns, the oxygen isotope data of benthic and planktic foraminifera, the percentage of the various grain size fractions, the concentration and flux of ice rafted debris, and the magnetic susceptibility:

Time interval c. 11 – 10.7 ka BP (Holocene transition);

Time interval 10.7 – 8.3 ka BP (early Holocene);

Time interval 8.3 – 4.0 ka BP (mid-Holocene);

Time interval 4.0 ka BP – present (late Holocene).

4.1 Time interval c. 11 – 10.7 ka BP (Holocene transition)

In the Holocene transition period a high content of the fine fraction (<0.063 mm) of the sediment is observed, which may be indicative of a moderate bottom water flow (Fig. 4.1). At the bottom of the core high concentration and flux of ice rafted debris are found (Fig. 4.2). Both transport agents of sea ice and icebergs can deliver IRD (Gilbert, 1990). High sedimentation rate in conjunction with moderate bottom water flow indicates sediment supply mainly by sea-ice and icebergs. This is characteristic of distal glaciomarine environments (Gilbert, 1990; Bischof, 1994). During this period the magnetic susceptibility values are relatively high and stable; this can indicate sediment supply with similar and high magnetic properties, which may have the same place of origin.

At the earliest part of the Holocene transition (until c. 10.9 ka BP) the dominant benthic foraminiferal species are *C. reniforme* (c. 57 %), *I. norcrossi* (c. 16.7 %), *E. excavatum* (c. 7.8 %) and *M. barleanus* (c. 6.2 %). *C. reniforme* and *E. excavatum* indicates cold, unstable conditions and glaciomarine environments (and most likely reflects predominantly polar conditions) (Jennings et al., 2004). Probably at longer sea-ice season and extensive sea-ice cover existed at that time over the core site, with sporadic break-ups allowing for ice rafting. The occurrence of *I. norcrossi* and *M. barleanus* can be associated with inflow of Atlantic water, and increase in productivity (Figs. 4.4 and 4.5). The high flux and moderate benthic foraminifera concentration also could indicate higher productivity, which is associated with inflow of Atlantic water (Fig. 4.3). Low concentration and flux of planktic foraminifera indicate low subsurface water's temperature and probably extended sea ice cover (Carstens et al., 1997; Ślubowska et al., 2005).

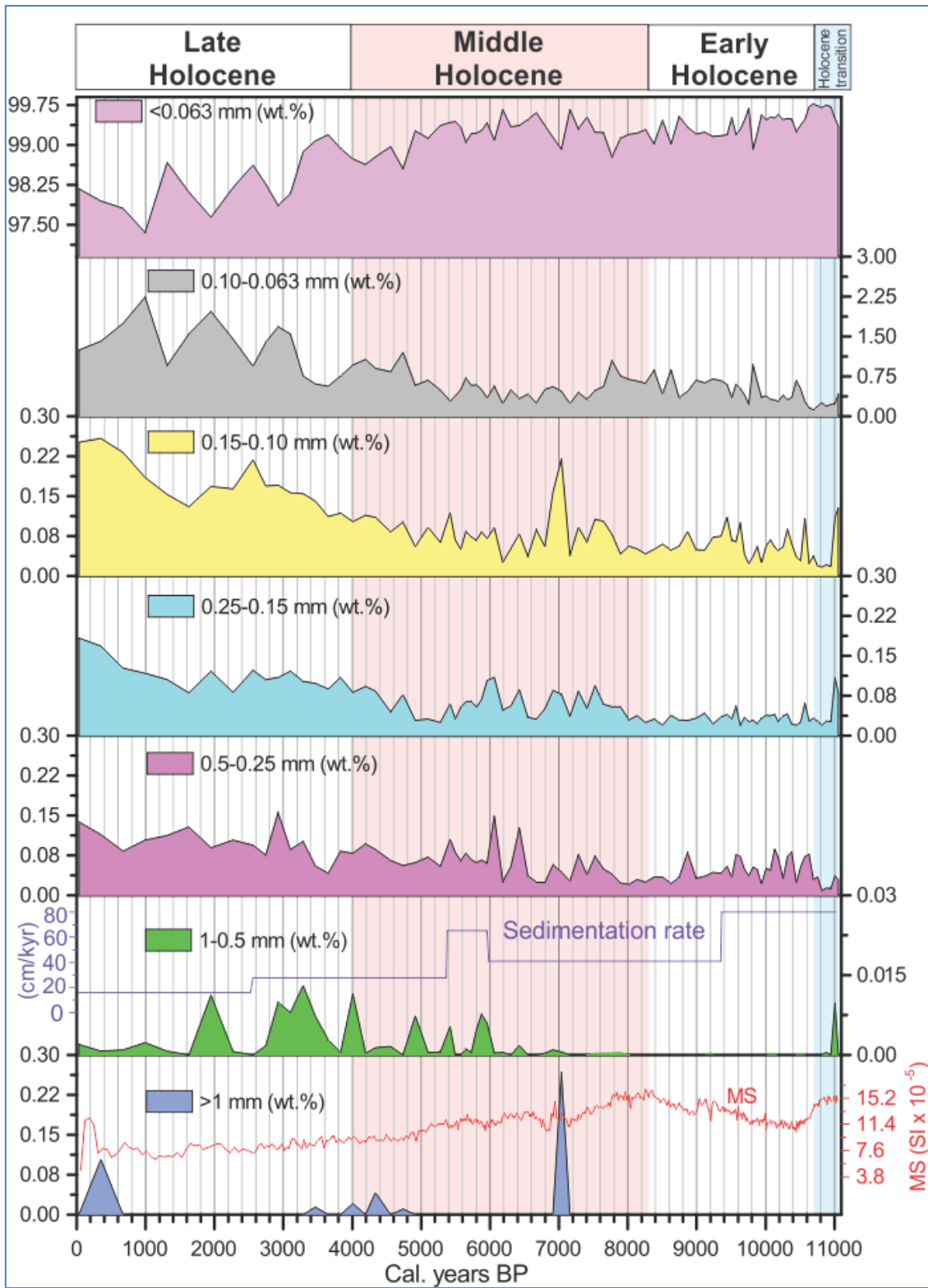


Figure 4.1. Percentage of the various grain size fractions plotted versus age. Red line represents magnetic susceptibility (MS). Purple line represents sedimentation rate.

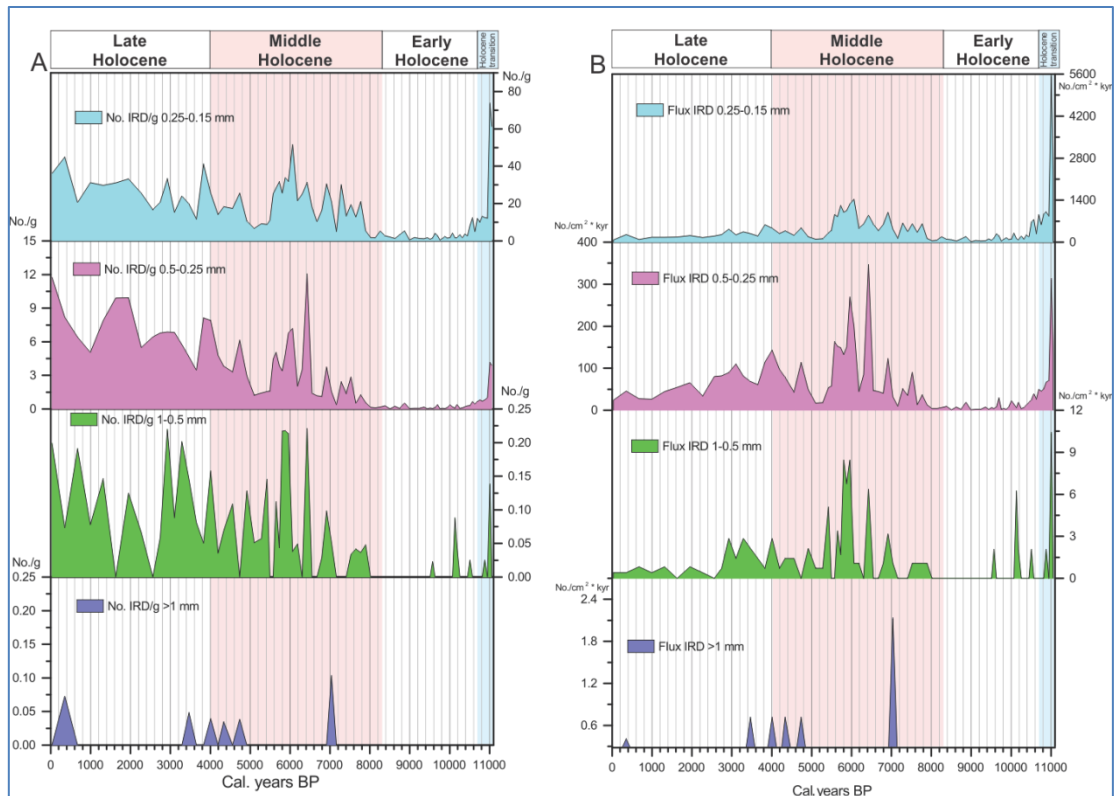


Figure 4.2. A) Concentration of IRD as number of mineral grains per gram dry weight sediment and B) the flux of IRD grains in the various grain size fractions plotted versus age.

In time interval c. 10.9 – 10.8 ka BP the relative abundance of *I. norcrossi* (45%), *M. barleeanus* (15%), *N. labradorica* (18.7%), and *C. neoteretis* (5%) increase. The percentage of *C. reniforme* (14 – 25%) and *E. excavatum* (0 – 1.3%) decreases (Fig. 4.4). The species assemblage indicates increased inflow of Atlantic water. The environment is characterized by higher productivity and longer ice-free seasons. The bottom water temperature is low.

At c. 10.8 ka BP a rapid decline in the concentration of foraminifera occur, which could indicate a deterioration of environmental condition (Fig. 4.3). After this cold event the relative abundance of *C. reniforme* increases from 14.6 to 53% indicative of an environment period with prolonged seasons of sea-ice cover.

4.2 Time interval 10.7 – 8.3 ka BP (early Holocene)

During the early Holocene large changes occurred in the benthic foraminiferal faunas (Fig. 4.3). A significant increase of *N. labradorica* (from 4 to 50%) indicates an increased inflow of Atlantic water (Hald and Korsun, 1997). Probably the margin of the Polar front moved closer to the core site. The bottom water was still cold, but probably slightly more saline than during the transition period. At c. 10 ka BP the conditions may have deteriorated as the concentration and flux of planktic and benthic foraminifera decreases (Fig. 4.3). After c. 10 ka BP the concentration and flux of planktic

foraminifera significantly increase. Probably the conditions in the subsurface water column became more favorable. Also, the relative abundance of *C. neoteretis* increase, indicating seasonal ice-free conditions and high seasonal productivity (Fig. 4.4). The increase of the subpolar species *C. neoteretis* are associated with chilled Atlantic water in the Arctic region (Mackensen and Hald, 1988).

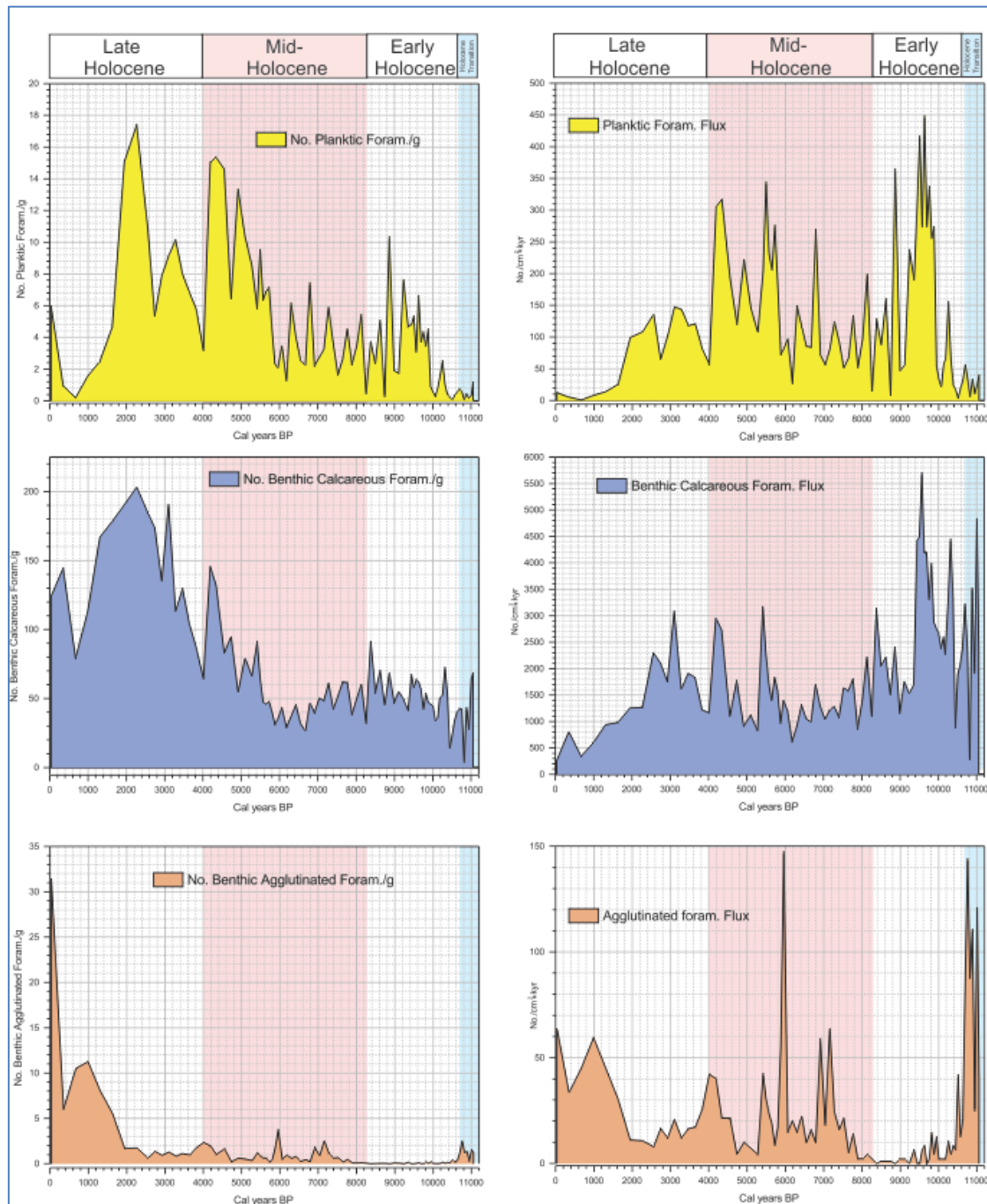


Figure 4.3. Upper panel (yellow color) planktonic foraminifera, middle panel (blue color) benthic calcareous foraminifera, and lower panel benthic agglutinated foraminifera concentration (No./g) and flux (No./cm² *kyr) plotted versus age.

At c. 9.1 ka BP the percentages of *M. barleeanus* increase (Fig. 4.4). This species is an arctic-boreal species that prefers higher salinities (Hald and Steinsund, 1992), and which indicates high and stable supply of organic matter, deep-water formation and cascading. High concentration of *M. barleeanus* can be a result of a change from supply of fresh organic matter to more degraded (Korsun and Polyak, 1989).

In the interval c. 10 - 9 ka BP the relative abundance of *Turborotalita quinqueloba*, *Globigerina bulloides* and *Neogloboquadrina pachyderma* dextral (d) increase (Fig. 4.6). *G. bulloides* and *N. pachyderma* dextral (d) are warm water indicators (Hald et al., 2007). The dominance of *T. quinqueloba* can be related to the presence of the Arctic Oceanic Front (AOF), separating Arctic and Atlantic water masses (Hald et al., 2007).

The foraminiferal oxygen isotope data show minimum values, which can be associated with stronger Atlantic water inflow (Fig. 4.7 B) indicating warming in accordance with the increase in subpolar planktic foraminiferal species.

The content of sediment of the fine fraction (<0.063 mm) decreases at the end of the period, possibly because the bottom currents became stronger (Fig. 4.1). Absence of IRD >1mm, and low amounts of IRD in the 1-0.5 mm size fraction are observed (Fig. 4.2). The percentage of fractions 0.10-0.063 mm and 0.15-0.10 mm, and the magnetic susceptibility values increase at the end of the period, which indicate supply of material with higher magnetic susceptibility. Magnetic susceptibility values increase until c. 8.3 ka BP. Perhaps this is due to the stronger currents bringing sediments with higher magnetic susceptibility to the core site.

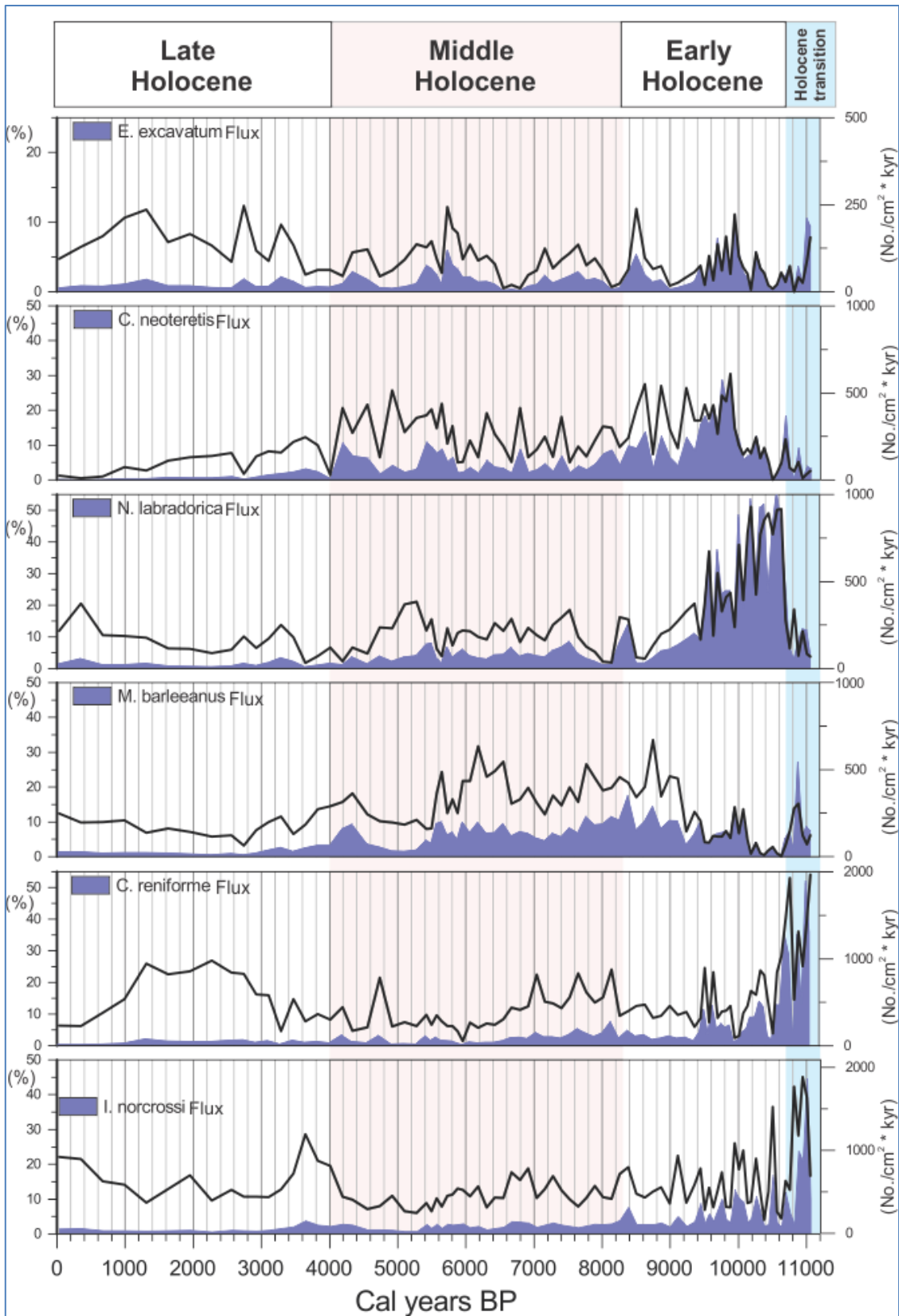


Figure 4.4 Percent distribution (bold black line and left scale) and flux (purple area and left scale) of dominant benthic foraminiferal species versus age in core HH 14-012GC.

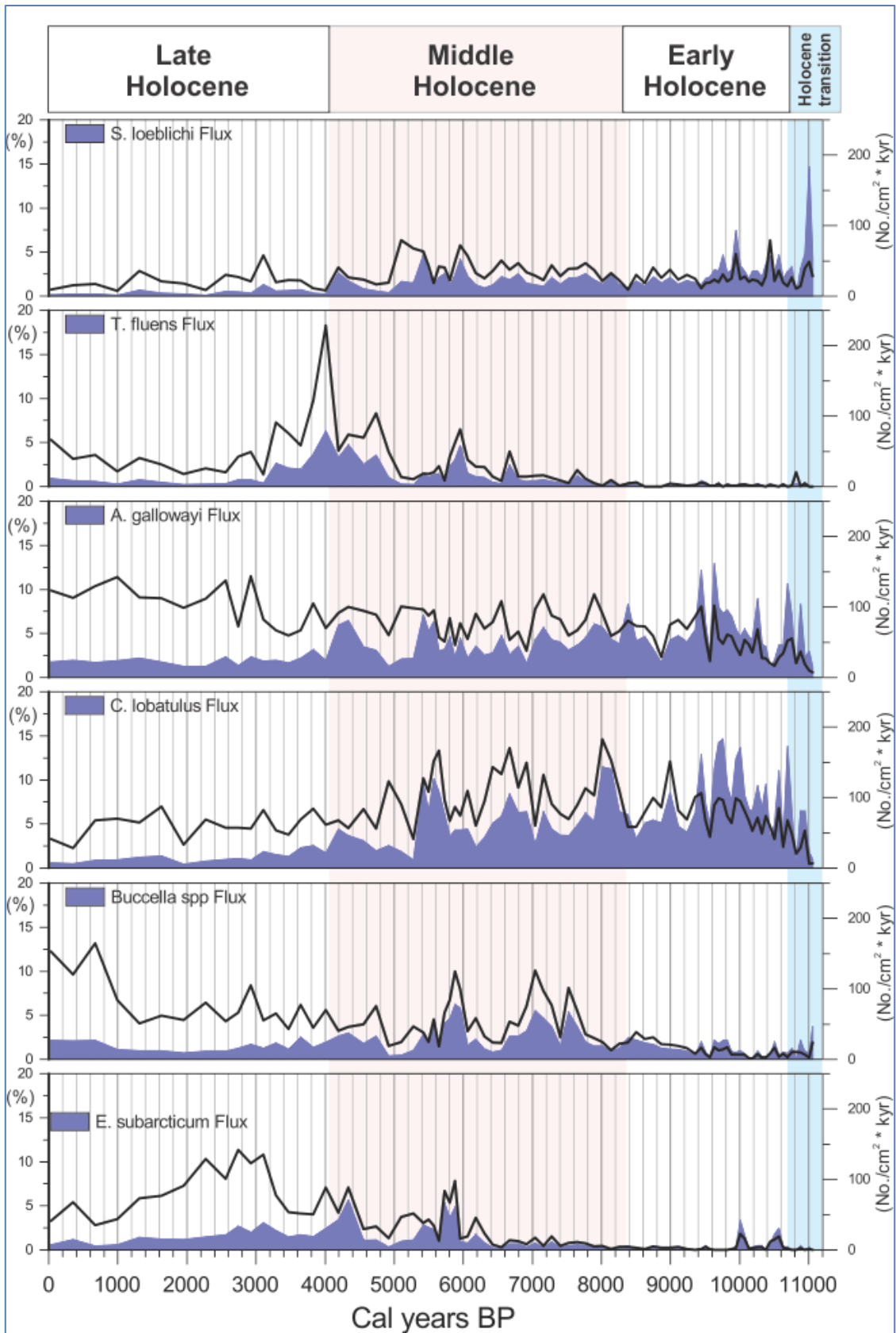


Figure 4.5. Percent distribution (bold black line and left scale) and flux (purple area and left scale) of dominant benthic foraminiferal species versus age in core HH 14-012GC.

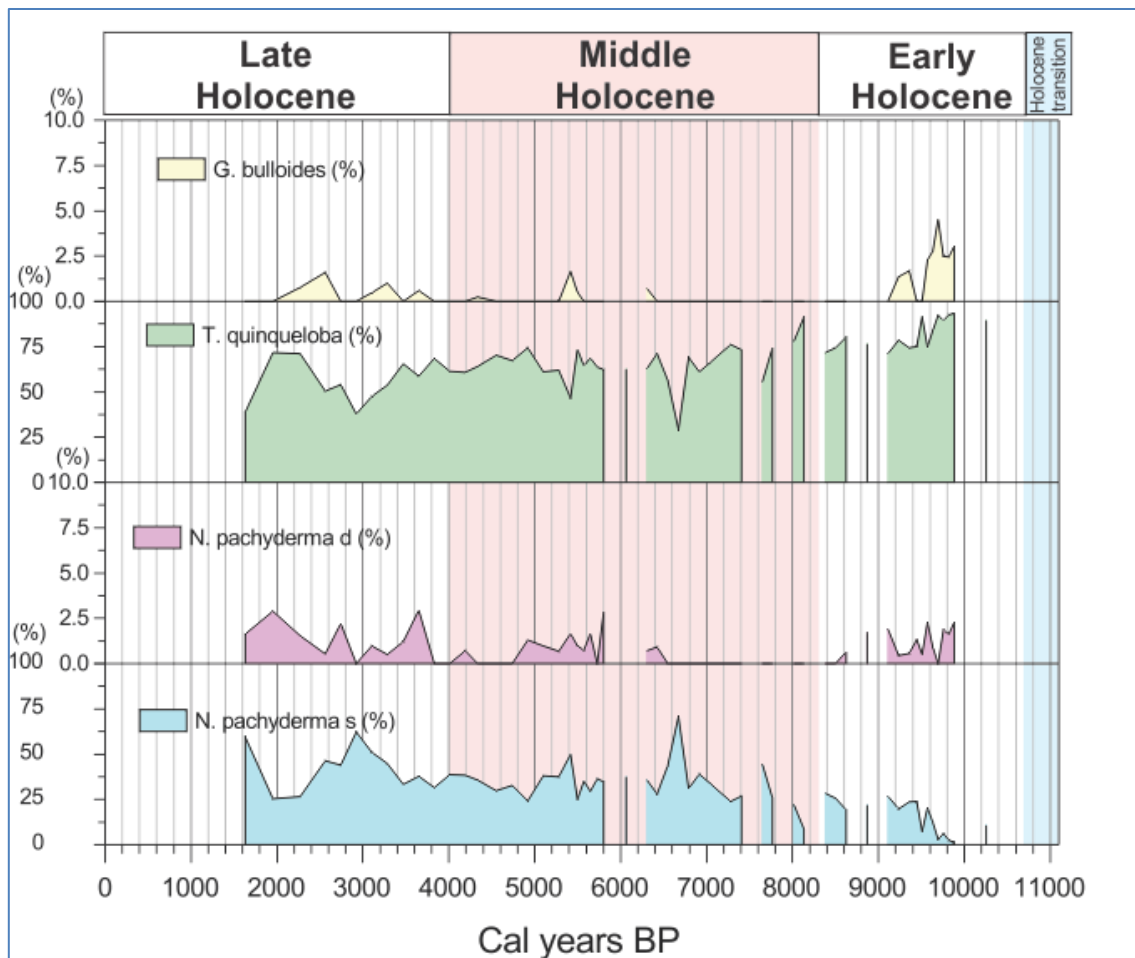
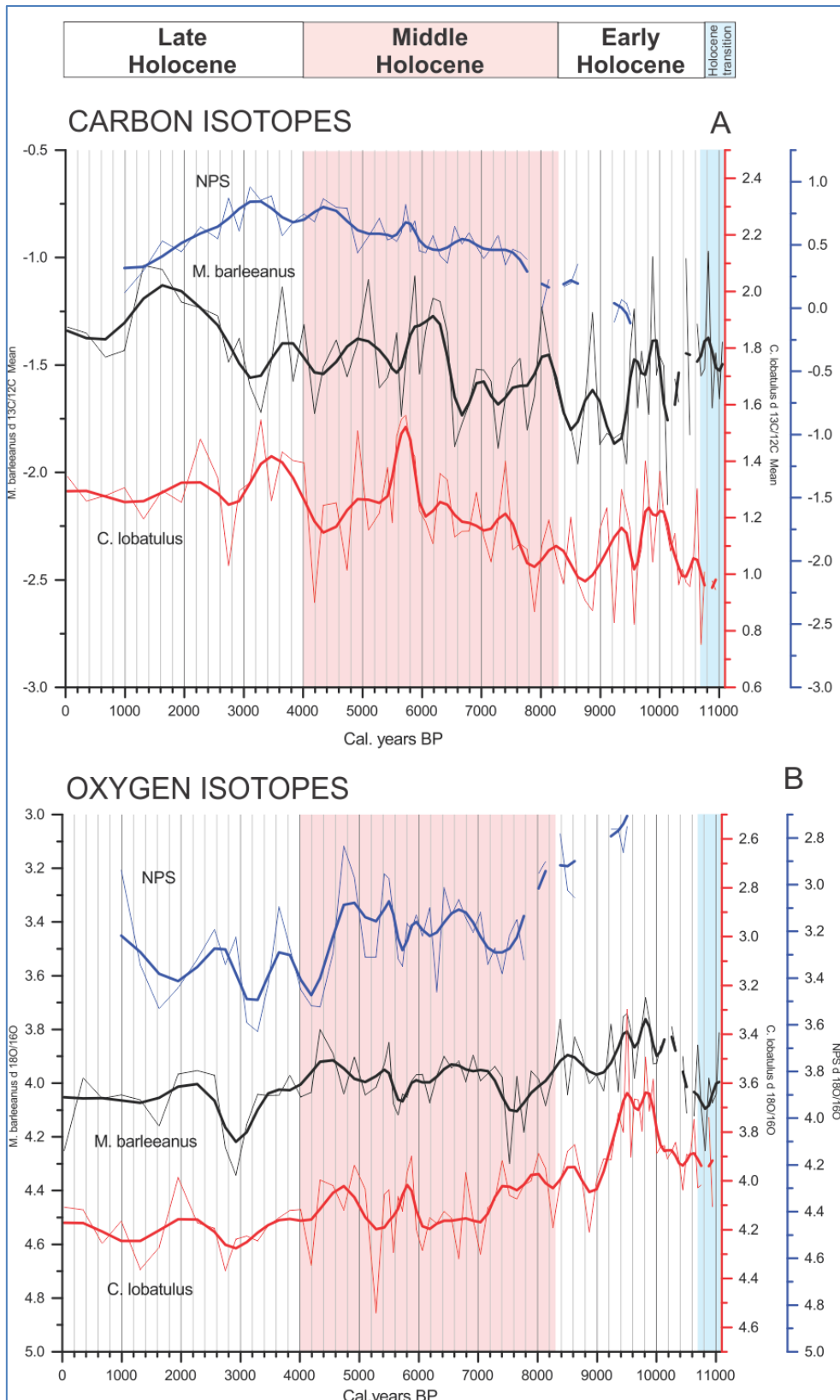


Figure 4.6. Percent distribution of planktonic foraminiferal species versus age in core HH14-012GC. Only samples with more than 50 specimens per one sample are shown.

4.3 Time interval 8.3 – 4.0 ka BP (mid-Holocene)

During the time interval 8.3 – 4.0 ka BP the dominant sediment fraction is the fine fraction <0.063 mm, which indicate a moderate bottom water flow (Fig. 4.1). Compared with the early Holocene, the IRD content in the middle Holocene increases (Fig. 4.2), indicating that more icebergs spread over the core site. The magnetic susceptibility decreases. The sedimentation rate has a decreasing trend, with a small increase at c. 6 – 5.4 ka BP. Generally during the middle Holocene the sedimentation rate decreases. After c. 6 ka BP IRD in the size fraction 1 – 0.5 mm and 0.5 – 0.25 mm rises (Fig. 4.2), indicating that more sea-ice and/or icebergs propagate to the core site.



Until c. 6.2 ka BP the concentration and flux of planktic foraminifera is moderate, while the concentration and flux of benthic calcareous foraminifera decrease (Fig. 4.3). It is possible that in this time period the environmental conditions deteriorated. At c. 6.2 ka BP the concentration and flux of both benthic and planktic foraminifera are low, showing a worsening of environmental conditions. After c. 6.2 ka BP the absolute abundance and flux of foraminifera increase, which indicate that the environment became more fertile.

In the interval 8.3 – 6 ka BP the dominant species are *M. barleeanus* (c. 20.2 %) which can be associated with chilled Atlantic water; *C. reniforme* (c. 13.4 %) indicate colder bottom water; *I. norcrossi* (12.2 %), *C. neoteretis* (11.2 %) and *N. labradorica* (10.5 %) are associated with cold Atlantic water (Hald and Korsun, 1997). The presence of *I. norcrossi* are associated with seasonal sea-ice cover (Hald and Steinsund, 1996). Compared to the early Holocene *C. lobatulus* (9.1 %) and *A. gallowayi* (6.3 %) increase, this event may be associated with higher current speed (see chapter 4.2). Probably the location of the core was close to the summer sea-ice margin, which affected the food supply for *M. barleeanus*, *N. labradorica* and *Buccella* spp (Figs. 4.4 and 4.5).

After c. 6 ka BP *C. neoteretis* (14.6 %) increases slightly, probably indicating influence of modified, cold Atlantic water (Mackensen and Hald, 1988; Steinsund, 1994; Seidenkrantz, 1995). *C. reniforme* and *I. norcrossi* decrease slightly also indicating cold bottom water temperature.

The dominant planktic species is *T. quinqueloba*, which shows a falling trend, while the percentage of the polar species *N. pachyderma* sinistral (s) increases. This can be related to the general cooling of the subsurface water (Hald et al., 2007).

4.4 Time interval 4.0 ka BP – present (late Holocene)

The noticeable reduction of sediment in the fraction <0.063 mm together with the low sedimentation rate indicates a reduction of sediment supply. The proportions of grains in the size fractions from 0.5 to 0.063 mm show increasing trends (Fig. 4.1). Perhaps lower sedimentation rate and increased bottom current affected the sedimentation. The magnetic susceptibility continues the decreasing trend. Low values of IRD >1 mm and higher values of IRD 1 – 0.5 mm probably indicate an increased role of sea ice in in the area (Fig. 4.2).

The high concentration of benthic foraminifera probably indicates a more stable environment with steady food supply (Fig. 4.3). The flux of benthic foraminifera increases until c. 3 ka BP and decreases to the present. The concentration and the flux of planktic foraminifera decrease after c. 2 ka BP, indicating the deterioration of the subsurface conditions. *C. reniforme* and *I. norcrossi* together

dominate in this time, pointing to a cold environment. The percentage of *C. neoteretis* is greatly reduced (from 10.6 to 1.6 %). Probably the period of sea-ice cover became longer.

After c. 2 ka BP relative abundance of agglutinated species increase, probably indicating the existence of cold saline, dense bottom water. This is known to cause increase in the concentration of CO₂ at the sediment-water interface (Steinsund and Hald, 1994). As a consequence calcareous foraminiferal tests may be dissolved. The low sedimentation rate negatively affects the preservation of calcareous foraminifera (see references in Rasmussen and Thomsen, 2014).

The percentage of the planktic species *T. quinqueloba* (c. 56 %) dominates slightly over *N. pachyderma* sinistral (s) (c. 42 %) in the time interval 4 – 1.6 ka BP. The relatively similar proportions of these two species can be identified as a result of interplay of Atlantic and Arctic waters at the core site. Probably the peaks in relative abundance of *N. pachyderma* sinistral (s) at c. 2.9 and 1.6 ka BP represent colder events in the subsurface water column (Fig. 4.6).

5 Discussion and correlations

5.1 Paleoceanographic interpretation

The sedimentological and foraminiferal proxy data collected from core HH14-012GC represents the Holocene time interval. The record was divided into five lithological units (LU) and four foraminiferal units (FU):

The Holocene transition period includes the FU 1, and LU 1 and partially LU 2;

The early Holocene period includes the FU 2, LU 3 and partially LU 2:

The mid-Holocene period includes the FU 3, LU 4 and some parts of LU 3 and LU 5;

The late Holocene period includes the FU 4 and LU5.

The results show significant changes in the benthic and planktic foraminiferal faunas and sedimentological data. During the Holocene transition the benthic fauna indicate higher inflow of Atlantic water which caused an increased flux of foraminifera. The flux of ice rafting debris (IRD) and increase in percentages of *C. reniforme* and *I. norcrossi* at this time indicate cold temperatures at the bottom. Absence of planktic foraminifera and presence of IRD indicate cold subsurface water temperatures. In the early Holocene an intensification of inflow of Atlantic water occurred. The environmental conditions became more fertile, as indicated by a high flux of planktic and benthic foraminifera. In the mid-Holocene the temperatures began to decrease gradually. The late Holocene was characterized by a continued trend in decreasing temperatures.

5.1.1 Holocene transition (c. 11 – 10.7 ka BP)

In the Holocene transition period several peaks in relative abundance of the glaciomarine indicator-species *C. reniforme* (at c. 11, 10.9 and 10.75 ka BP) are observed (Fig. 4.4). At c. 11 ka BP the % of *E. excavatum* increases, which reflects an environment with more extensive sea ice cover and high turbidity (Hald and Korsun, 1997). This suggests spreading of conditions of cold, unstable and low salinity waters at the bottom. At the surface periods with longer sea ice seasons are indicated. The high flux of ice rafted debris suggests sea ice and icebergs over the core site and cold subsurface water (Fig. 4.2 B). This is supported by the low value of planktic foraminifera. Interpretation of isotope data also points to a cold environment at the bottom (Fig. 4.7 B). *M. barleeanus* oxygen isotope (OI) data vary highly, but the mean value is slightly lower than the late Holocene mean value. *C. lobatulus* OI data shows that the mean values are significantly different from the mean value of the late Holocene (c. 3.9 and c. 4.18 ‰, respectively) (Fig. 4.7 B).

Between the two peaks of *C. reniforme* (at c. 11 and c. 10.75 ka BP) an increase in percentage of *I. norcrossi* and a small increase of *N. labradorica* occur (Fig. 4.4). The presence of *I. norcrossi* is associated with seasonal sea ice cover/proximity of the sea ice margin (Korsun and Hald, 1998). It can be concluded that the dominance of *I. norcrossi* indicates a change in the ice-edge zone. The peaks in relative abundance of *S. loeblichii* at c. 10.9 ka BP are also connected to sea ice cover (Steinsund, 1994) (Fig. 4.5). The increased inflow of Atlantic water in the period of dominance of *I. norcrossi* suggest the presence of cold bottom water with stable and higher salinity.

The environment deteriorates at c. 10.8 ka BP, which can be seen in reduced concentration of planktic and benthic foraminifera (Fig. 4.3). The % *I. norcrossi*, *C. reniforme* and *M. barleeanus* decline rapidly, but at the same time *N. labradorica* increases (from 4 to 18.7 %) accompanied by a small increase in % *E. excavatum* (from 0 to 3.68 %) (Fig. 4.4). More severe environmental conditions prevailed at this time with cold water temperatures, probably near-permanent sea ice cover and associated decrease in food supply.

The low concentration of planktic foraminifera suggests polar conditions at the surface in the late Holocene in the northern Svalbard (Ślubowska et al., 2005), perhaps the low concentration of planktic foraminifera similarly can indicate polar conditions in Leirdjupet Trough during the Holocene transition.

Rapid increase in concentration of benthic foraminifera and harsh conditions at the surface indicate inflow Atlantic water below a cold Polar Water layer at the surface.

5.1.2 Early Holocene (10.7 – 8.3 ka BP)

In the early Holocene a high flux of planktic foraminifera and a moderate flux of benthic foraminifera, along with a low concentration of IRD are observed (Figs. 4.2 (B) and 4.3). The environmental conditions were considerably improved and the icebergs declined.

The early Holocene period can be subdivided into three events: 1) rapid increase in percent of *N. labradorica* (from 6.4 to 50.4 %) at c. 10.6 ka BP; 2) increase of *C. neoteretis* (from 3.5 to 30.4 %) at c. 9.88 ka BP, and 3) increase of *M. barleeanus* to 33.5 % at c. 9.2 – 8.75 ka BP (Fig. 4.4).

The increase in relative abundance of *N. labradorica* can be related to improvement of the environmental conditions at c. 10.7 – 10.0 ka BP, which was probably caused by inflow of Atlantic water. This inflow of Atlantic water meeting polar nutrient richer water creates mixing and high seasonal productivity associated with the presence of an oceanic front, conditions which are highly favored by *N. labradorica* (Hald and Korsun, 1997; Jennings et al., 2004). The Atlantic water inflow

probably caused a northward shift of the oceanic front from the core site. The subdominant species are *I. norcrossi* and *C. reniforme* which points to a seasonal sea ice cover and proximity to the ice edge (Hald and Steinsund, 1996).

The foraminiferal oxygen isotope data (corrected for ice volume change) show lower values than at present and probably reflect a higher influx of the Atlantic water with higher temperatures (Fig. 4.7 B).

The subpolar species *Turborotalia quinqueloba* is dominant during this period. This species is associated with the oceanic fronts (Johannessen et al., 1994) (Fig. 5.17). *T. quinqueloba* also are sensitive to changes in productivity (Reynolds and Thunell, 1985) (Fig. 4.6).

The increase in percentage of *C. neoteretis* (at c. 9.88 ka BP) also accompanied with a small increase of *E. excavatum* (until c. 10 %), while the relative abundance of *N. labradorica* is still high (c. 24 %). The subpolar species *C. neoteretis* is associated with chilled Atlantic water in the Arctic region (Mackensen and Hald, 1988). Fluctuations in % of *E. excavatum* indicate high water turbidity (Hald et al., 1994) (Fig. 4.4). The rise in percent of *C. lobatulus* and *A. gallowayi* indicate enhanced current activity of the bottom waters (Murray, 1991) (Fig. 4.5). The fine sediment fraction (<0.063 mm) slightly decreases, probably due to the higher bottom current activity. Stronger bottom currents might be related to the sea level rise in the Early Holocene (e. g. Forman et al., 2004; Taldenkova et al., 2012) (Fig. 4.1). The increase of *C. neoteretis* coincides with lower oxygen isotope values and is probably related to the strongest inflow of Atlantic water at the Holocene optimum temperatures (Fig. 4.7 B).

The largest flux of benthic and planktic foraminifera indicates a large improvement of the environmental conditions compared to the Holocene transition. The dominant planktic species is *T. quinqueloba*. The maximum occurrence of planktic foraminifera in the Barents Sea is found together with high relative abundance of the benthic foraminiferal species *C. neoteretis* (Mackensen and Hald, 1988; Hald and Steinsund, 1996). The recent distribution of planktic foraminifera and *C. neoteretis* on the Eurasian Arctic shelf coincides with areas influenced by Atlantic-derived water, generally flowing as a subsurface current (Khusid and Polyak, 1989; Jennings and Helgadóttir, 1994; Lubinski et al., 2001). In the early Holocene, the peaks of *C. neoteretis* well correlated with peaks of planktic foraminifera at c. 10.7, 10.3, 9.8-9.2, c. 8.9 and 8.6 ka BP. During c. 10 – 9ka BP Atlantic water spread close to the surface, improving the subsurface environment.

The oxygen isotope data show lower values (mean $\delta^{18}\text{O}$ *C. lobatulus* – 3.65 ‰ and *M. barleeanus* – 3.8 ‰ for this period) and are related to the probably maximum of inflow of Atlantic

water to the core site. According to Shackleton (1974), if salinity stays constant and the modern mean $\delta^{18}\text{O}$ values is around 4.2 ‰ for *C. lobatulus* and 4.05 ‰ for *M. barleeanus* the increase in water temperature may be as high as 2.4 °C (*C. lobatulus*) and 1.2 °C (*M. barleeanus*) (both corrected for species-specific vital effects important for the interpretation of stable oxygen records (Zająckowski et al., 2010)) (Fig. 4.7 B). *C. lobatulus* prefers to live in coarse sediment, with strong bottom water currents (Sejrup et al., 1981; Mackensen et al., 1985; Hald and Korsun 1997), whereas *M. barleeanus* is an intermediate infaunal species that lives in a muddy substrate (Caralp, 1989). It is highly adaptable to environmental changes, and can change habitat from infaunal to epifaunal (Linke and Lutze, 1993).

The early Holocene temperature optimum correlates with the time of higher-than-present summer insolation in the Northern Hemisphere (Berger and Loutre, 1991) (Fig. 1.11 C) and a strong inflow of Atlantic water and heat advection northward (Hald et al., 2007). The occurrence of the thermophilous mollusk *Mytilus edulis* at the western Svalbard coastal areas (Salvigsen et al., 1992) and increasing foraminiferal biodiversity in Leirdjupet at c. 10 – 9 ka BP suggest that the inflow of Atlantic water impacted both areas.

After of the peaks in relative abundance of *N. labradorica* and *C. neoteretis* *M. barleeanus* increases at c. 9.2 – 8.75 ka BP (Fig. 4.4). The modern distribution of *M. barleeanus* is linked to presence of fine-grained sediments enriched with organic detritus, which are usually redeposited from shallow areas (Korsun and Polyak, 1989). The continuing inflow of Atlantic water to the western Barents Sea occurs with a rise in concentration of *M. barleeanus* and a slight rise in benthic foraminifera concentration. The drop in concentration of IRD is associated with the furthest retreat of glaciers onshore during the early and mid- Holocene (Svendsen and Mangerud, 1992) (Fig. 4.2 A). The icebergs were located in the inner fjords and mostly melted in or close to fjord heads (Dowdeswell, 1989).

In Hald and Korsun (2008) the correlation between the initial freshwater drainage of the proglacial Lake Agassiz (North America) (8.2 ka BP) and the proxy record of Van Mijenfjorden (western Svalbard) is discussed. A high-resolution record from Van Mijenfjorden show significant changes at that time. The $\delta^{18}\text{O}$ values measured in the benthic foraminiferal species *C. reniforme* decreased (may imply a decline in salinity) together with an increase in percentage of the cold/freshwater foraminiferal species *E. excavatum* and *C. reniforme*. This important cooling event also correlates with a cold anomaly in GISP and NGRIP (the ice core drilling station in Greenland) and indicates this event also affected areas of the European Arctic. The freshwater discharge from the proglacial Lake Agassiz led to cooling at c. 8.2 ka BP by forcing a shutdown or slow-down of the meridional overturning circulation (MOC) in the North Atlantic Ocean (Barber et al., 1999; Clarke et

al., 2004). The decrease in MOC may have changed the inflow of Atlantic Water in Van Mijenfjorden and increased dominance of fresher Arctic Water (Hald and Korsun, 2008).

In the studied core HH14-012GC, between c. 8.5 – 8.1 ka BP, observed: 1) decrease in percent of *C. neoteretis* and increase in *E. excavatum* (diminished Atlantic water inflow, increased turbidity at the bottom and more extensive sea-ice cover) (Fig. 4.4); 2) increase in percent of *N. labradorica* and *I. norcrossi* (first species indicates change in the location of the Polar front (Hald and Korsun, 1997), the second indicates cold bottom conditions, seasonal sea ice cover and/or close proximity to the sea ice margin (Hald and Steinsund, 1996) and 3) increase in percent of *C. reniforme* which an indicator of glaciomarine conditions (Polyak et al., 2002). To explain the reduction in deposition of IRD, the presence of more perennial sea ice, probably hampered the movement of icebergs.

In connection with the 8.2 ka BP cooling event (time interval around c. 8.5 – 8.1 ka BP), the studied core shows a fairly clear decrease in concentration and flux of planktic foraminifera (Fig. 4.3), increase in relative abundance of the polar planktic species *N. pachyderma* (s) (Fig. 4.6) and some decrease in concentration and flux of benthic foraminifera with increase in percent of *C. reniforme*. The benthic foraminiferal oxygen isotope data show a significant fluctuation at this time ($\delta^{18}\text{O}$ values *C. lobatulus* 3.9 – 4.2 ‰ and *M. barleeanus* 3.85 – 4.05 ‰) (Fig. 4.7 B).

5.1.3 Mid- Holocene (8.3 – 4.0 ka BP)

The concentration and flux of planktic and benthic foraminifera gradually decrease until c. 6 ka BP (Fig. 4.3). The dominant species is *M. barleeanus*, pointing to high food availability (Polyak et al., 2002), *C. reniforme* indicate a colder environment and longer sea ice seasons (Hald and Korsun, 1997), and periodically increase in percent of *I. norcrossi*, which prefers the high productivity zone near ice fronts (Polyak et al., 2002) (Fig. 4.4), increased % of *C. lobatulus* and *A. gallowayi* reflect higher bottom water currents (Sejrup et al., 1981; Mackensen et al., 1985) (Fig. 4.5). In the interval 8.3 – 7 ka BP the second dominant species is *C. reniforme*, but at 6 – 4 ka BP *C. neoteretis* becomes more abundant; this correspond to decreasing $\delta^{18}\text{O}$ values.

The significant increase in concentration of IRD indicates increase in the presence of icebergs (Fig. 4.2 A). The largest flux of IRD is observed at c. 6.5 – 5.5 ka BP (Fig. 4.2 B). The sedimentation rate in the interval c. 6.0 – 5.4 ka BP shows an increasing trend (Fig. 3.2). During the mid- Holocene a decreasing trend in proportion of the fine grain-size fraction (<0.063 mm) is observed (Fig. 4.1). Until c. 6 ka BP this trend is only small, but after 6 ka BP become more pronounced.

According to modeling experiments by Ådlansdvik and Loeng (1991), high ocean temperatures occur during periods of relatively low air pressure, cyclonic circulation, low sea-ice cover and

increased influx of warm Atlantic Water. Hald and AsPELLI (1997) discuss a cooling period at c. 6.5 ka BP in core T-88-2/NP90-57 (southern part of the continental slope off the western Barents Sea) and relate this to high atmospheric pressure, which on turn would lead to warm summers on land. Probably the cold event at c. 6 ka BP in the Leirdjupet belongs to changes in atmospheric circulation at this time.

After c. 6 ka BP the dominant benthic foraminiferal species is again *C. neoteretis*, which is connected to presence of chilled Atlantic Water. At c. 5.2 ka BP the % of *N. labradorica* increases and at same time the flux of planktic and benthic foraminifera decreases, indicating more severe environmental conditions in the study area. Presence of IRD indicates iceberg activity (Fig. 4.2 A). Oxygen isotope data shows highly fluctuating values and the values are higher than in the early Holocene (Fig. 4.7 B). This complex of proxies indicate a cold environment.

5.1.4 Late Holocene (4.0 ka BP – present)

The late Holocene is characterized by decreasing sedimentation rates (Fig. 3.2). The flux of IRD becomes lower and indicates decrease of sediment delivery by sea ice/icebergs (Fig. 4.2 B). On land glaciers are growing (Svendsen and Mangerud, 1997; Hald et al., 2004), and slightly enhanced iceberg calving or ice rafting occur near the core site. The high oxygen isotope values indicate a cooling of 2.4 °C according to Shackleton (1974) (assuming stable salinity), compared with the Holocene temperature optimum. The mean $\delta^{18}\text{O}$ value measured in *C. lobatulus* during the late Holocene is c. 4.2 ‰ and during the Holocene climatic optimum 10 – 9ka BP the average value was 3.6 ‰ (Fig. 4.7 B). *C. reniforme* and *I. norcrossi* are the dominant species and reflects a cold environment (Steinsund, 1994). Increase in % of *E. excavatum* indicates more severe environmental conditions and enhanced glacial influence (Jennings et al., 2004) (Fig. 4.4). The high abundance of foraminifera indicates a slightly improved environment relating to the food supply. In Leirdjuprt (c. 2.5 – 2 ka BP) an increase in benthic and planktic foraminiferal abundances indicate ameliorated conditions which may correlate with the Roman Warm Period (Holzhauser et al., 2005), which represent warm climatic phases in Europe, begins in Leirdjupet by increase in planktic foraminiferal abundances (Fig. 4.3). At c. 2.2 ka BP a rapid decline of foraminiferal abundance is observed. This may correlate in time the Dark Ages Cold Period (1.5 – 1.1 ka BP) (Grauel et al., 2013). At 1 ka BP agglutinated species increase in abundance (from 2 to 12 No./g), this period may also correlate with the Dark Ages Cold Period. The most persistent agglutinated species is *Reophax scorpiurus*. From the study of Rasmussen and Thomsen (2015) the agglutinated species attaining maxima during the colder phases of the late Holocene, the Dark Ages Cold Period and the Little Ice Age c. 600-100 a BP in the Storfjorden during the last 4 ka BP.

Figure 5.1 shows the correlation in time between the foraminiferal (core HH14-012GC) and proxy data from land studies (northern and southern Norway). The high flux of foraminifera (c. 10 – 9 ka BP) correlates with cold climate in land records (Lake Ifjord, Jostedalsglacier). Looking more closely it appears that, peaks in the foraminiferal flux correlate with temperature increase in Lake Ifjord at c. 9.6 ka BP. Warm climate of the Holocene Optimum on land apparently correlates with a reduction of temperature in the study area (Leirdjupet). The 8.2 ka BP cold event, which affected the foraminiferal abundance in Leirdjupet, show decreased temperature in Lake Ifjord and increase in Jostedalsglacier activity. The low value of foraminifera at c. 6.2 ka BP is preceded by glacier activity of Jostedalsglacier at c. 6 ka BP. Rapid decline in foraminiferal abundance at c. 4 ka BP correlate well with increasing activity of the Lyngedals glacier. The large-scale oceanic and atmospheric circulation affected Barents Sea region, probably the switch between cold and warm states could be the cause of the temperature fluctuations (Ådlandsvik and Loeng, 1991).

In the late Holocene in the Northern Hemisphere reduction of summer insolation at high latitudes (Fig. 1.11 C) and cooling at the sea surface related to this orbital forcing occur (Wanner et al., 2008). In Storfjorden during last c. 3.7 ka BP Atlantic Water was only sporadically present at the surface (Rasmussen et al., 2014). In Kongsfjorden, during the last 4700 years an increase in glacial influence was recorded and the environment became colder (Skirbekk et al., 2010). In northern Svalbard (Hinlopen Trough) dominance of *E. excavatum* over *C. reniforme* was observed, this indicates the presence of cold and low-salinity bottom waters between 4500 and 1100 cal years BP (Ślubowska et al., 2005). The last 1100 cal years BP increase in relative abundance of *M. barleeanus*, *I. norcrossi* and *C. neoteretis*, indicate increased inflow of chilled Atlantic intermediate water to the area, and at the same time low concentration of planktonic foraminifera suggests polar conditions at the surface (Ślubowska et al., 2005).

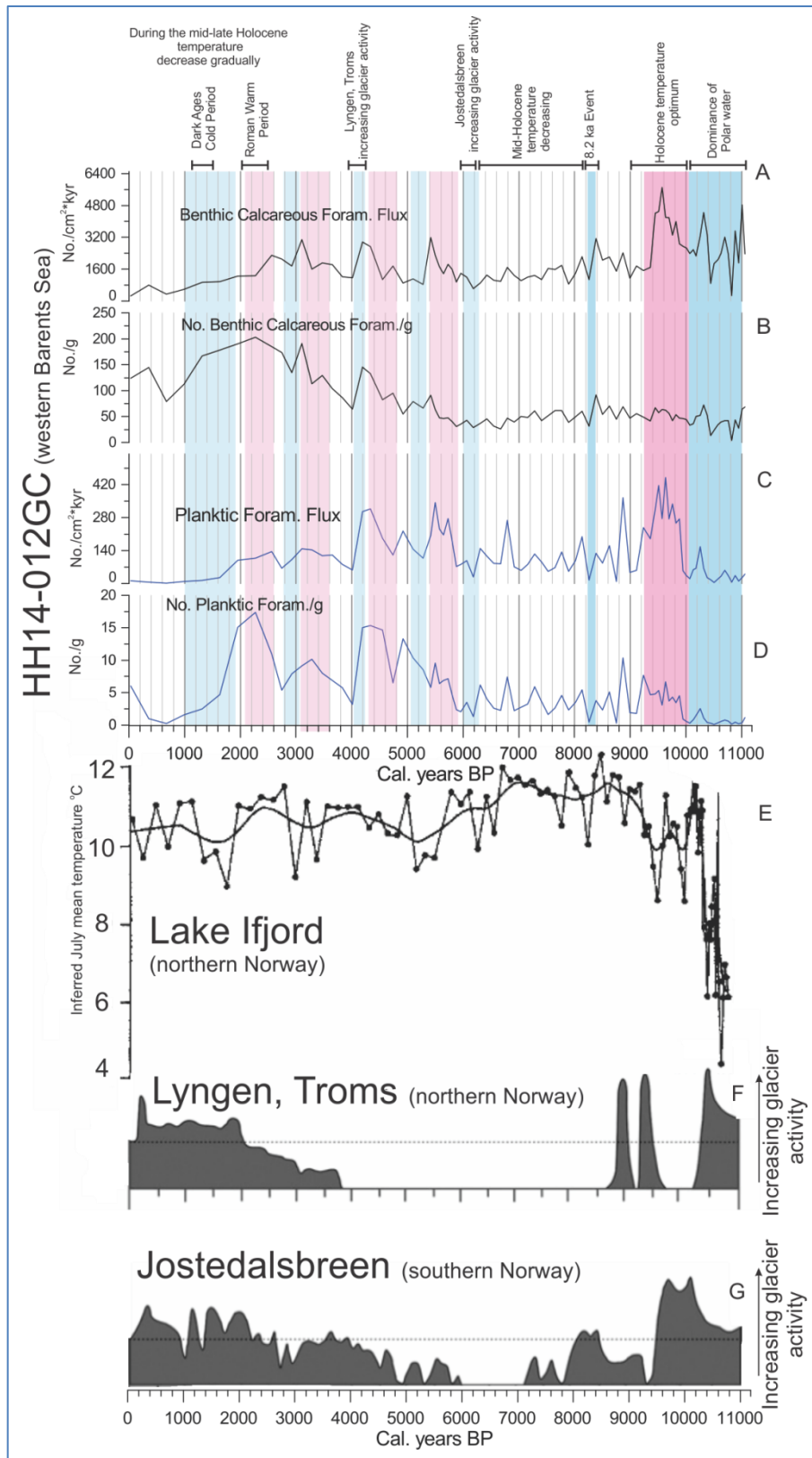


Figure 5.1. A) Benthic calcareous foraminifera and C) planktonic foraminifera flux (No./cm² *kyr), B) benthic calcareous foraminifera and D) planktonic foraminifera concentration (No./g) plotted versus age; E) July mean temperature reconstruction of the Lake Ifjord core (A LOESS smoother with span 0.10 highlights the general pattern of July temperature) from (Seppä et al., 2002); Holocene glacier variations (horizontal scale is schematic, not to scale) of Norwegian glaciers from Nesje et al., (2008) based on data from F) Jostedalbreen glacier (Nesje et al., 2001) and G) Lyngen glacier, Troms (Bakke et al., 2005).

5.2 Stable isotopes and ice rafted debris

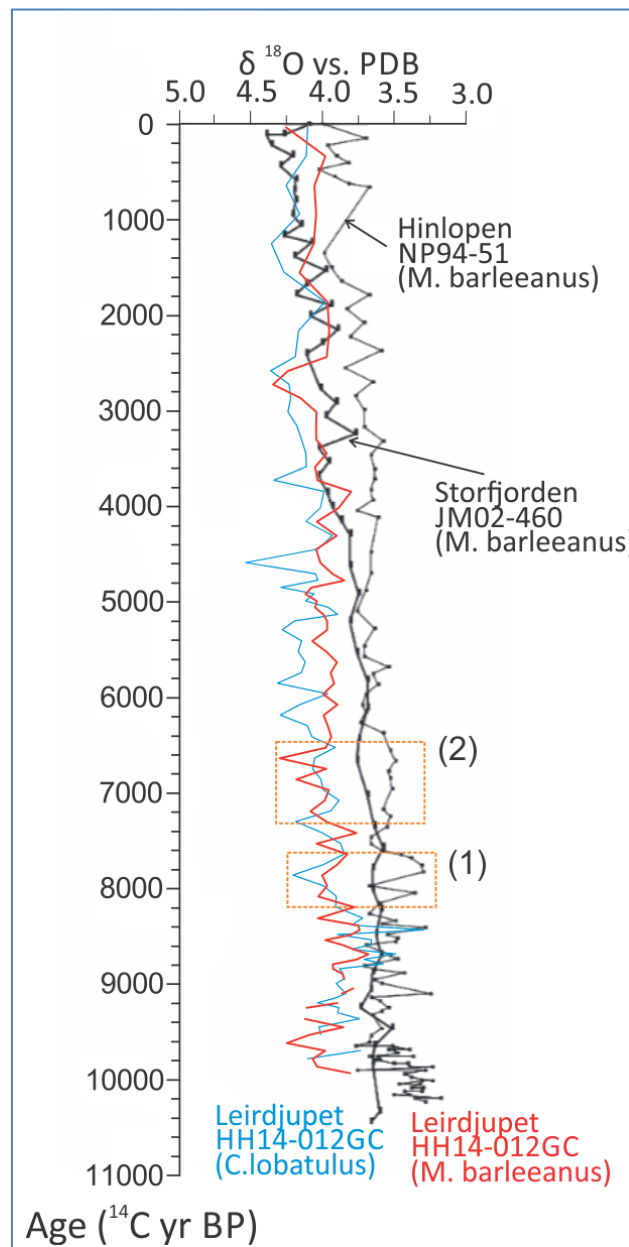


Figure 5.2. $\delta^{18}\text{O}$ records corrected for ice volume changes and 'vital' effects plotted versus ^{14}C yr BP (corrected for reservoir effect -440 years (Mangerud and Gulliksen, 1975) from core HH14-012GC (this study), core NP94-51 (Ślubowska et al., 2005) and core JM02-460 (Rasmussen et al., 2007). Modified after Rasmussen and Thomsen, (2015).

The comparison of benthic foraminiferal $\delta^{18}\text{O}$ values from cores HH14-012GC (this study), JM02-460 from the Storjorden shelf (Rasmussen et al., 2007) and NP94-51 from the northern shelf of Svalbard (Ślubowska et al., 2005) is represented in Figure 5.2. Orange squares highlight several features in the $\delta^{18}\text{O}$ values that are discussed below (Fig. 5.2 (1) and (2)). During the early Holocene temperature optimum from c. 9000 to 8200 ^{14}C yr BP the $\delta^{18}\text{O}$ values of the different records are close to one another. From c. 8200 to c. 7600 ^{14}C yr BP (Fig. 5.2 (1)) the $\delta^{18}\text{O}$ values are higher in Leirdjupet, which indicate colder temperatures compared to Storfjorden and Hinlopen. At this time

the % of *C. reniforme* increases in Leirdjupet, also indicating colder temperatures. The north Svalbard and the southern part of Spitsbergenbanken are under the influence of various currents: the West Spitsbergen current and specially the Svalbard Branch affect the first area and the North Cape current with the Bjørnøya current influence the second area (Introduction chapter). Possibly the climatic conditions, which cause intensification of the Svalbard Branch also caused an increase in polar water in Leirdjupet. This situation is repeated in the time interval (2) (Fig. 5.2). Later at c. 4300 ¹⁴C yr BP values measured on *M. barleeanus* in cores HH14-012GC (study area) and JM02-460 are generally within the same range. At this time interval increase in % of *E. excavatum* and *C. reniforme* is observed in Leirdjupet.

Figure 5.3 (D) represent the scatter plots of $\delta^{13}\text{C}$ versus $\delta^{18}\text{O}$ values and are compared with data from Storfjordrenna (Łącka et al., 2015). The result shows the general decreasing trend of the $\delta^{18}\text{O}$ values and the increasing trend of the $\delta^{13}\text{C}$. The shift from the Arctic Water domain to the Atlantic Water domain during the early Holocene is clearly visible in Figure 5.3 (results in left oval indicate Arctic water domination (Fig. 5.3 (D))).

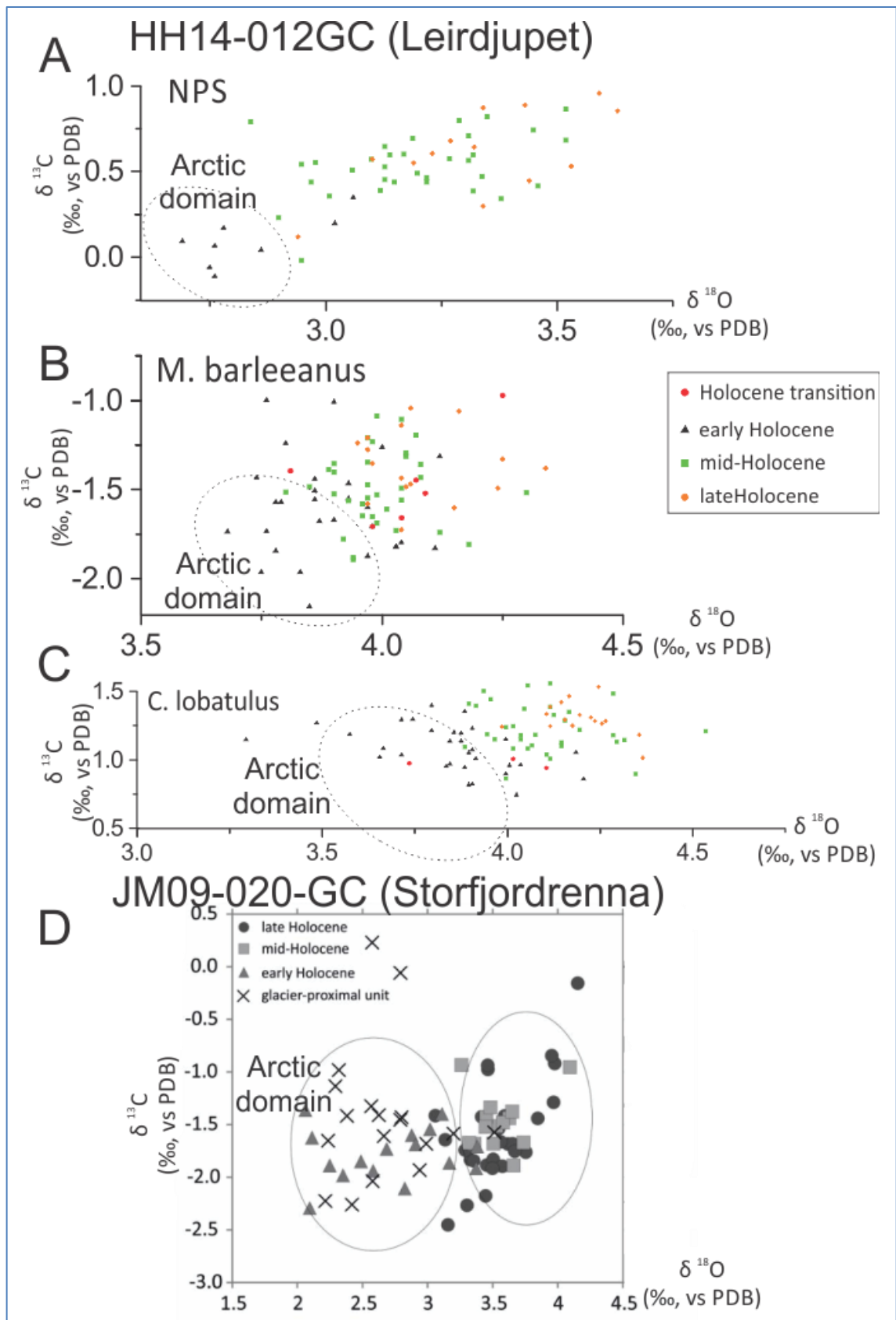


Figure 5.3. Scatter plots showing $\delta^{13}\text{C}$ versus $\delta^{18}\text{O}$ values from core HH14-012GC (A,B,C) (this study) and JM09-020-GC measured on *E. excavatum* (D) (Łączka et al., 2015). NPS= *Neogloboquadrina pachyderma* sinistral.

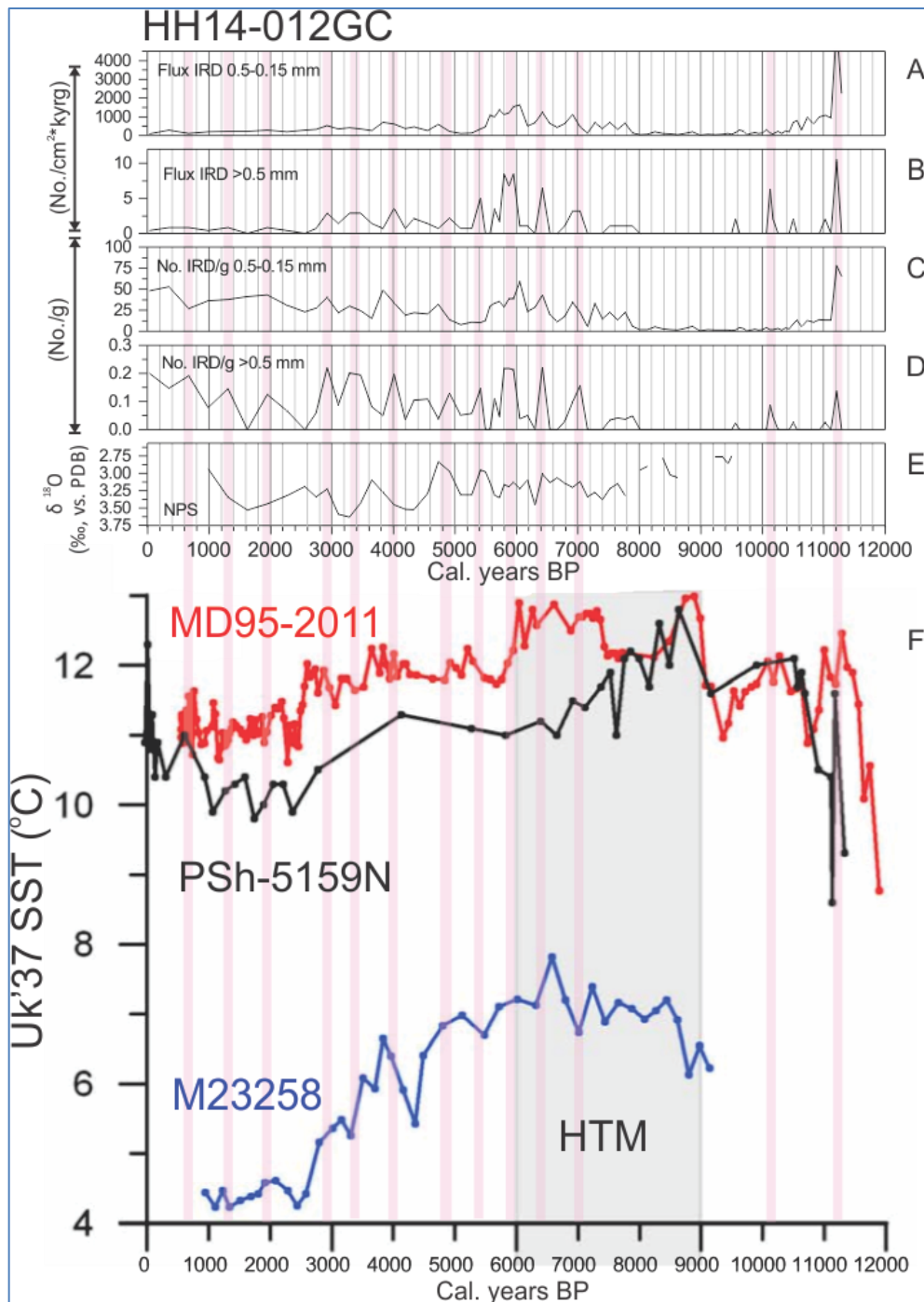


Figure 5.4. The comparison of IRD and oxygen isotope data from core HH14-012GC (this study) and alkenone SSTs from MD695-2011 (Calvo et al., 2002), PSh-5159N (Risebrobakken et al., 2010) and M23258 (Marchal et al., 2002). Modified after Risebrobakken et al., (2011). NPS= *Neoglobogeria pachyderma* sinistral. HTM=Holocene temperature maximum, based on alkenone SST data.

The period of largest IRD flux in HH14-012GC (Fig. 5.4 A and B) occurs at 7.2 – 5.2 ka BP and is mostly linked to the Holocene temperature maximum (based on alkenone SSTs data). The flux of IRD begins to increase towards the end of the temperature maximum. In the Holocene transition c. 11.2 ka BP the peaks of IRD correlate with the temperature increase in Ingøydjupet (core PSh-5159N). Plot also shows increasing concentration of IRD with decreasing SST after c 6 ka BP.

5.3 Regional correlation of foraminiferal records

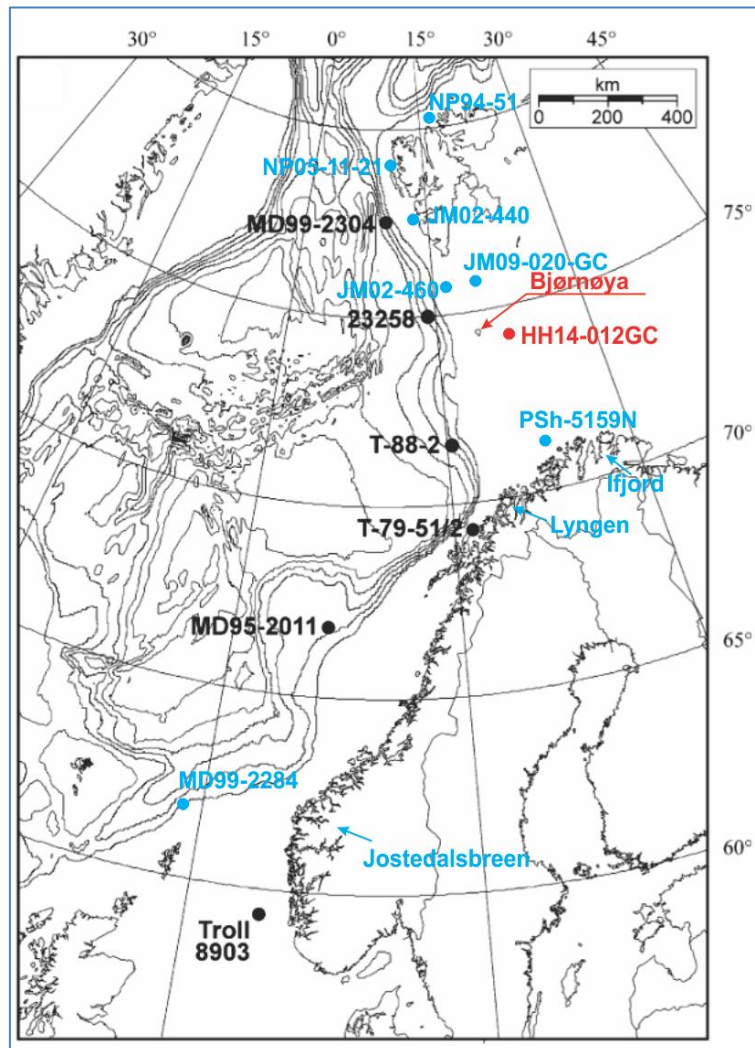


Figure 5.5. Bathymetric map showing the location of sediment cores. Modified from Hald et al., (2007).

Figures 5.6 and 5.7 show correlation between the investigated core HH14-012GC and cores along the Norwegian-Svalbard margin. The most thermophilic species in the present dataset is *G. bulloides* (Hald et al., 2007). The surface water temperature between 11 and 16 °C is most favorable for this species (Bé and Tolderlund, 1971; Sautter and Thunell, 1991). The distribution of *G. bulloides* in the study area correlates well with core 23258. Its reaches a maximum at c. 10 – 9 ka BP and is sporadically present in the mid- late Holocene (Fig. 5.6 A). During the Holocene temperature optimum (10 – 9 ka BP) this species reaches approximately 4 % in Leirdjupet, which is ten times lower compared with the Troll core 8903/28-03 from the Norwegian Channel (c. 40 %). The presence of *G. bulloides* in Leirdjupet is connected to the strong flow of Norwegian Atlantic Current northward, and the large difference in percentage between north and south reflects a strong surface water temperatures contrast (Fig. 5.7 C). In Leirdjupet the environmental conditions was unfavorable for warm water species like *G. bulloides* and *N. pachyderma* dextral (d).

N. pachyderma dextral (d) (Fig. 5.6 B) is a warm water indicator on the Norwegian-Barents Svalbard margin (Hald et al., 2007). Its distribution pattern is linked to the influx of temperate Atlantic Water into the south-eastern part of the northern North Atlantic (Pflaumann et al., 2003; Johannessen et al., 1994). In the northernmost cores the species is rare during the mid- and late Holocene. The distribution of this species at 10 – 9 ka BP in the study area is close to core 23258, but after c. 5.5 ka BP the pattern (largest peaks) is similar to the core T88-2.

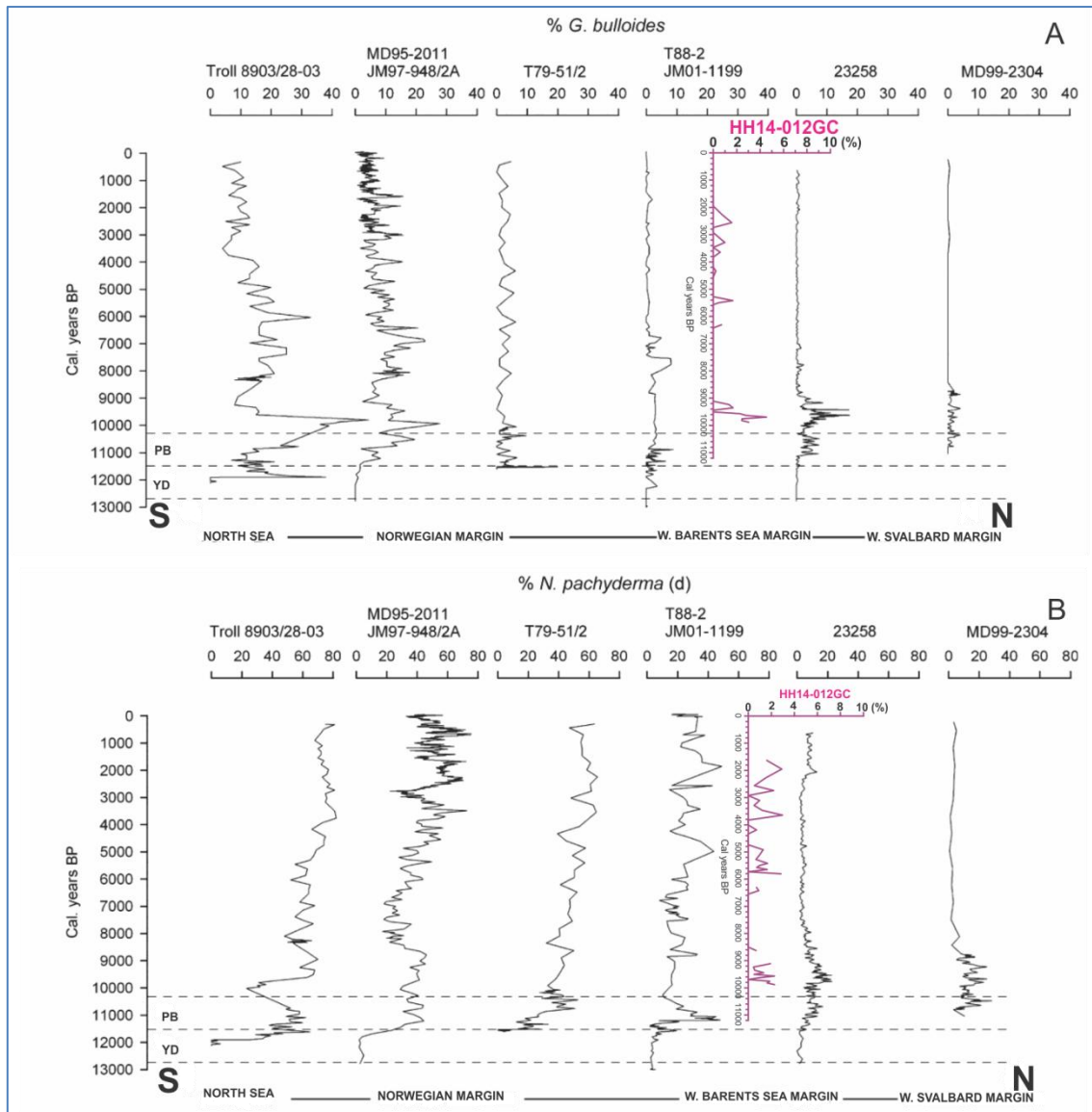


Figure 5.6. Percent distribution of *G. bulloides* (A) and *N. pachyderma* dextral (B) of total planktonic foraminiferal fauna vs. age (cal. years BP) in the sediment cores. Modified after Hald et al., (2007). Core locations are shown in Fig. 5.5.

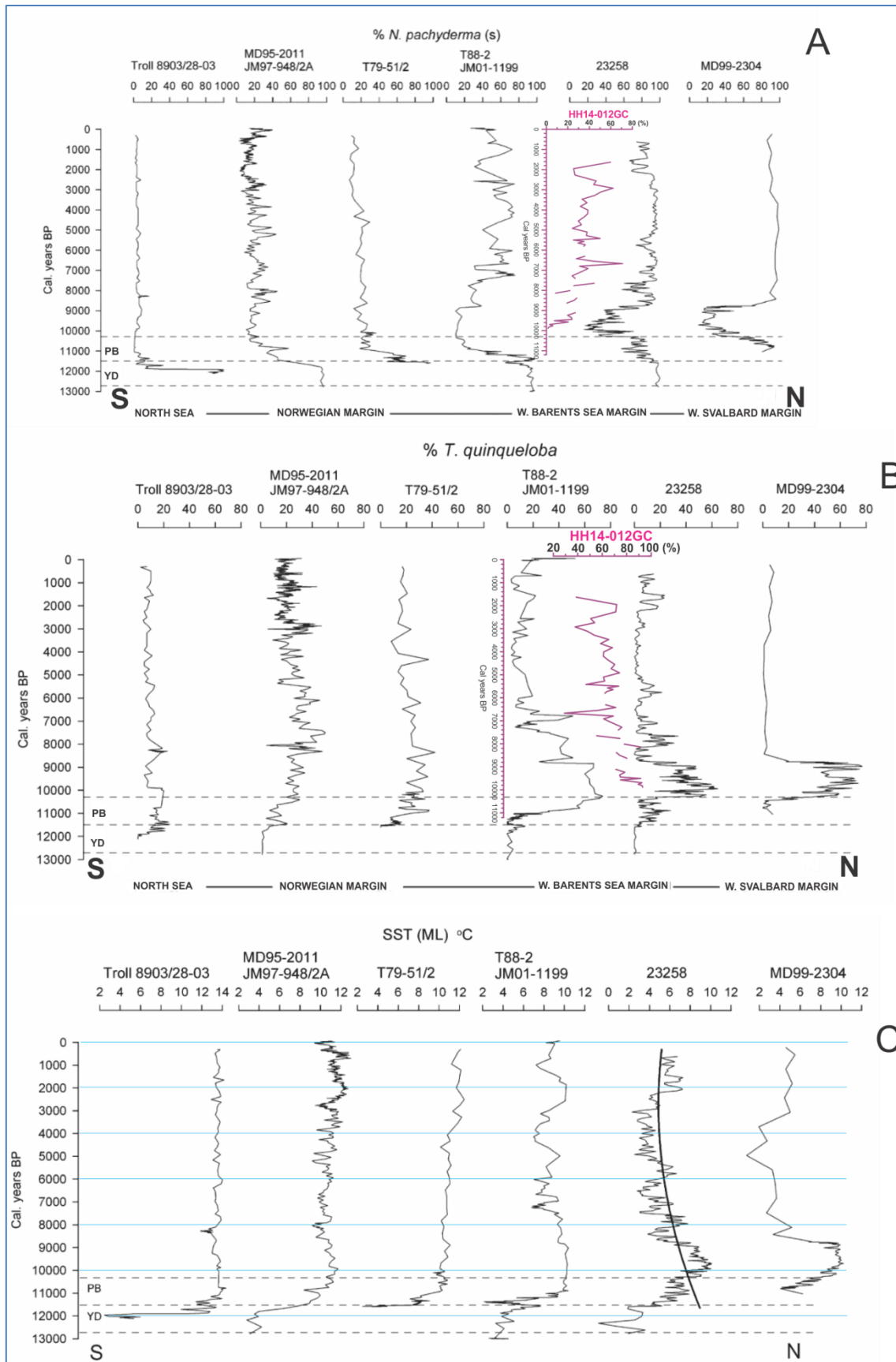


Figure 5.7. Percent distribution of *T. quinqueloba* (A) and *N. pachyderma* sinistral (B) of total planktonic foraminiferal fauna vs. age (cal. years BP) in the sediment cores. C) Reconstructed seasurface temperatures (SST) vs. age. Modified after Hald et al., (2007). Core locations are shown in Fig. 5.5.

T. quinqueloba (Fig. 5.7 A) is a subpolar species and connected to the front separating the Atlantic and Arctic Water masses in the central northern North Atlantic (Johannessen et al., 1994; Pflaumann et al., 2003). In the western Barents Sea this species is also associated with the oceanic fronts (Burhol, 1994). The four northern cores show similar trends: maximum relative abundance at 10 – 9 ka BP and decreasing toward the present. Hald et al., (2007) discuss a south to north time transgressive increase in *T. quinqueloba* from 12 to 11.5 ka BP and following a north to south decline from 9.4 to 4 ka BP. At c. 10.7 ka BP the Polar front was close to the location of core HH14-012GC as seen by high relative abundance of *N. labradorica*. This shift occurs from an east-south to north direction (Fig. 5.8 B). The environmental conditions at the surface were probably severe, as indicated by the low concentration and flux of planktic foraminifera and dominance of *N. pachyderma* (s) (Fig. 5.17). Later, at c. 9.9 ka BP the percent of *T. quinqueloba* increase in together with an increase in relative abundance of *C. neoteretis*, and the environmental conditions probably improved. In Leirdjupet *N. pachyderma* (s) was the dominant planktic species (c. 10.7 – 10.2 ka BP) indicating dominance of Polar water and changes in the position of the Polar front (Fig. 5.8 B).

N. pachyderma sinistral (s) (Fig. 5.7 B) is a cold-water indicator, in the North Atlantic it is dominant in Arctic and Polar Water (Bé and Tolderlund, 1971; Johannessen et al., 1994; Pflaumann et al., 2003). This species is dominant in the Younger Dryas and decline during the Younger Dryas – Preboreal transition (YD-PB) (Hald et al., 2007). At c. 10 ka BP the minimum percentages are observed. The distribution of *N. pachyderma* (s) in the study area is close to the pattern seen in core T88-2. The percentage of this species is lower than in more the northern cores. During early to late Holocene it shows an increasing trend.

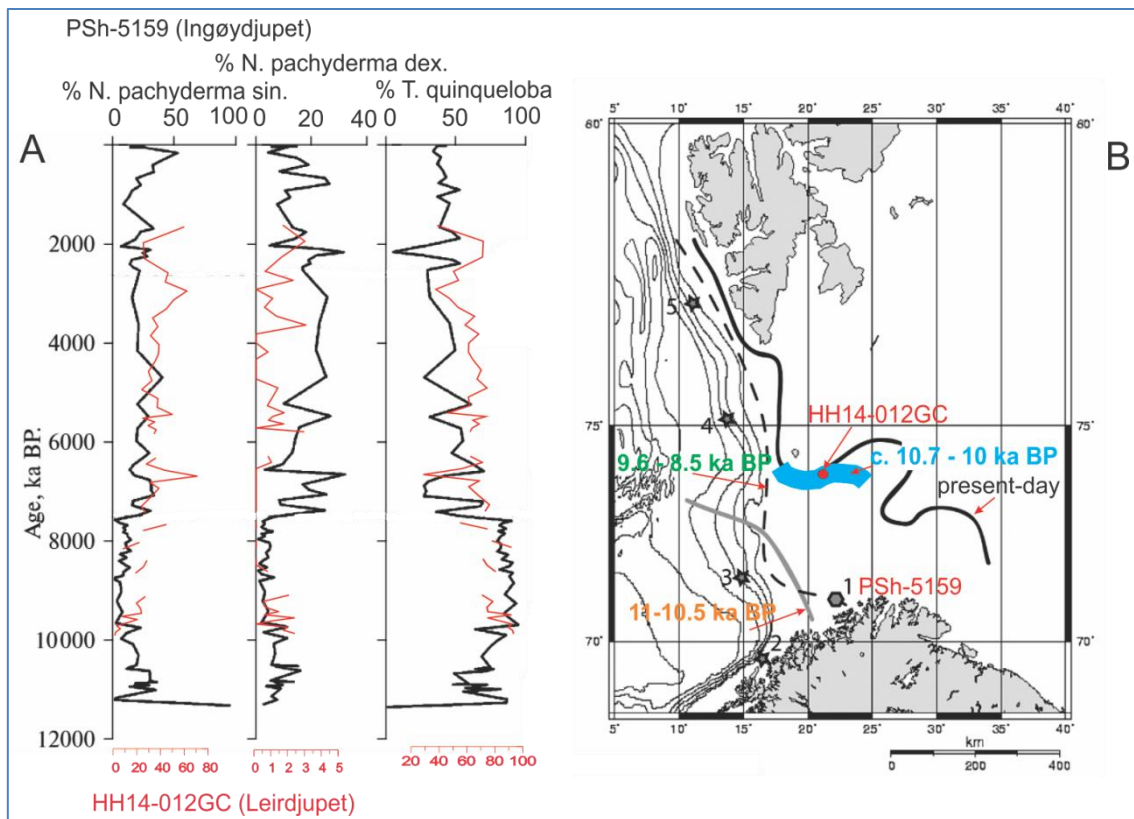


Figure 5.8. Comparison of dominant planktonic foraminifera (A) in the study core HH14-012GC (red lines) and core PSh-5159 from Ingøydjupet Chistyakova et al., (2010) and map (B) with approximate location of the Polar front. Modified from Risebrobakken et al., (2010). Data 11-10.5 and 9.6-8.5 ka BP are from Risebrobakken et al., (2010).

Figure 5.8 (A) shows a comparison of dominant planktic foraminifera species from the study area (red lines) and the southwestern Barents Sea (core PSh-5159). As seen the general trend is an increase in % of *N. pachyderma* (s) and decrease in % *T. quinqueloba*. The percentage of *N. pachyderma* (d) in the northern core HH14-012GC is very rare. The present measurements of temperature and salinity in Ingøydjupet (August 2004) show temperature variation in the range of 4 – 6 °C at water depth 400 to 50 m with salinity close to 32.5 psu (Risebrobakken et al., 2010), this area are affected by the North Cape Current. Probably the small amount of *N. pachyderma* (d) in the Leirdjupet can be related to the Bjørnøya Current. This current transport Arctic water towards the Leirdjupet, along southern flank of Spitsbergenbanken (Loeng, 1991).

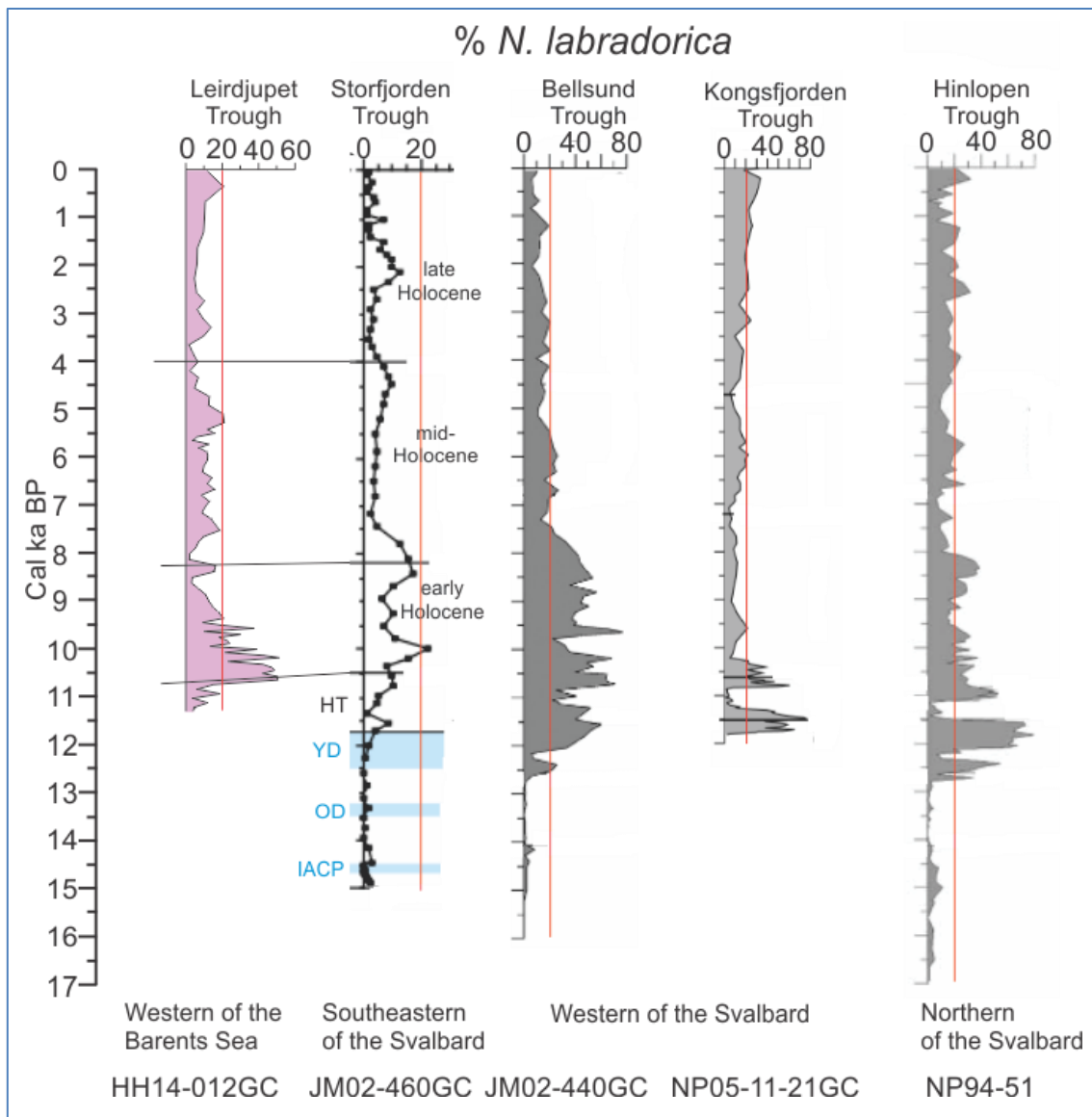


Figure 5.9. Comparison of the distribution pattern of *N. labradorica* in core HH14-012GC (study core) and cores from Storfjorden (Rasmussen and Thomsen, 2015), Bellsund (Ślubowska-Woldengen et al., 2007), Kongsfjorden (Skirbekk et al., 2010) and Hinlopen Trough (Ślubowska et al., 2005). Core locations are shown in Fig. 5.5. Vertical red lines represent 20 %. HT-Holocene transition, YD - Younger Dryas, OD - Older Dryas and IACP - Intra-Allerød cold period from Rasmussen and Thomsen, (2015).

During the early Holocene the most important benthic foraminiferal species is *N. labradorica* (Fig. 5.9). In Storfjorden the sea ice cover was less extensive and more seasonal than during the Holocene transition (Rasmussen and Thomsen, 2015). The strong development of the Arctic Coastal Front in the Bellsund Trough leads to increase in % of *N. labradorica* and *C. reniforme*, which indicate higher salinity and bottom water temperature than during the Younger Dryas (Ślubowska-Woldengen et al., 2007). They decrease at c. 8 ka BP probably related to the Arctic Coastal Front movement away from the site. In Kongsfjorden the dominance of *N. labradorica* at 11.8 ka BP indicates increased inflow of Atlantic bottom water (Skirbekk et al., 2010). In Hinlopen a rapid decrease in % of *N.*

labradorica at 11.5 ka and re-increase between 11.1 – 10.8 ka BP indicate the passage of the Polar front (Ślubowska et al., 2005).

In all cores during the Holocene transition and the early Holocene a high abundance of *N. labradorica* is observed. This may indicate distinct changes in water masses along the west and north Svalbard margin and the western Barents Sea, which occur almost synchronous with changes in location of the Polar front. Increased inflow of Atlantic water affected the entire area and must have been strong. During the mid- late Holocene a decrease in % of *N. labradorica* with some small peaks at c. 0.3 ka BP are observed. This may indicate a retreat of the Polar front to the core site in Leirdjupet.

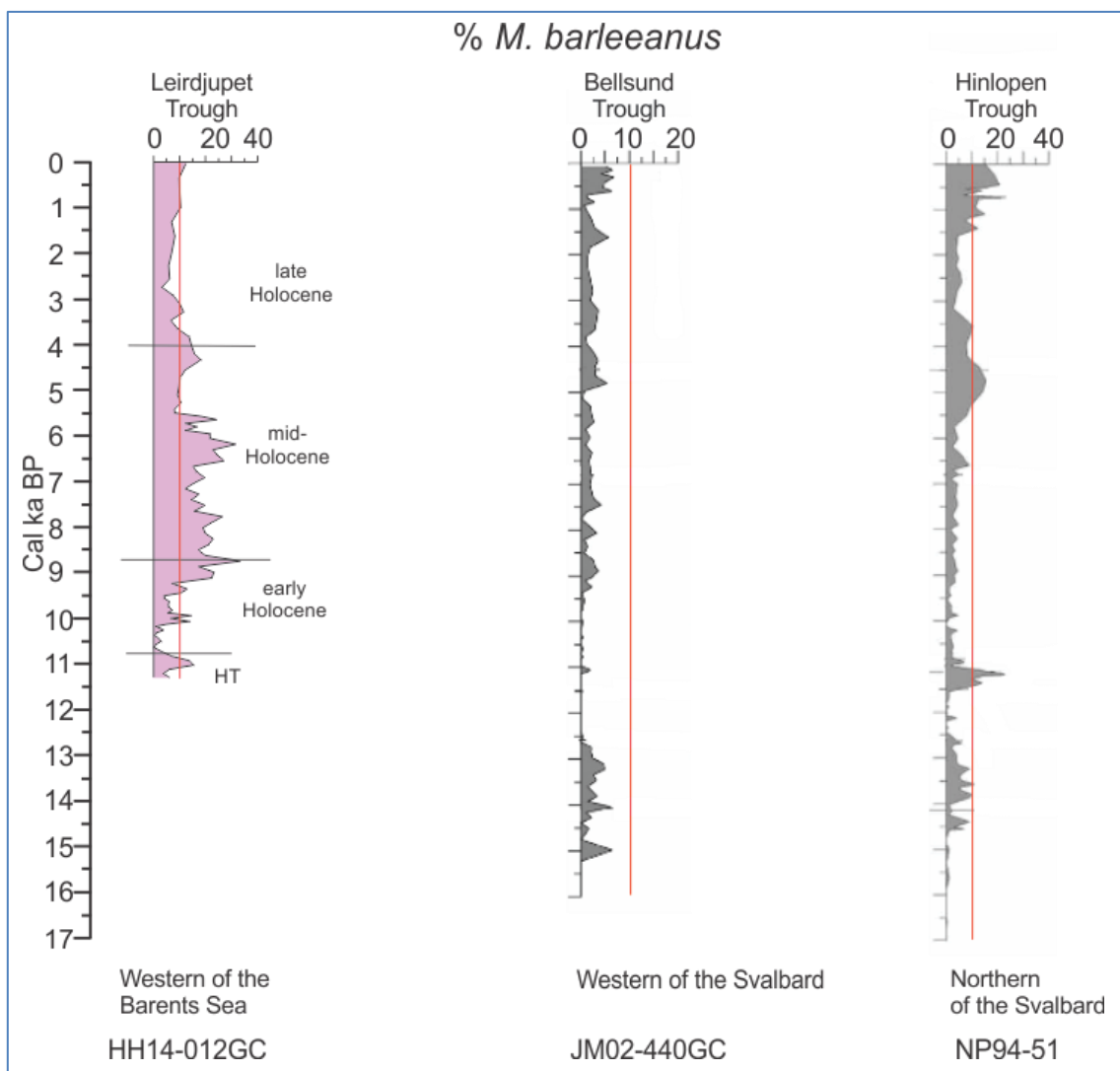


Figure 5.10. Comparison of the distribution pattern of *M. barleeanus* in core HH14-012GC (study core) and cores from Bellsund (Ślubowska-Woldengen et al., 2007) and Hinlopen Trough (Ślubowska et al., 2005). Core locations are shown in Fig. 5.5. Vertical red lines represent 10 %.

The high distribution of *M. barleeanus* is linked to enhanced inflow of Atlantic water to the Arctic Ocean (Korsun and Polyak, 1989; Polyak and Sulheim, 1994; Steinsund, 1994) and a high fluxes of organic matter to the sea bottom (Jennings et al., 2004) (Fig. 5.10). *M. barleeanus* can be found in the western Barents Sea at water temperature 3 – 4 °C and salinities above 32 ‰ (Hald and Steinsund, 1992). During the mid-Holocene in Leirdjupet high abundance of *M. barleeanus* is observed. Peak in % of *M. barleeanus* correlate well in three cores at c. 5 – 3.5 ka BP. The increase of this species occurred earlier in Hinlopen and Bellsund and later in Leirdjupet. The environmental deterioration at c. 3.2 ka BP is marked by decrease in this species. The last 1 ka BP in the % of *M. barleeanus* increases probably as a response to the increase in food supply.

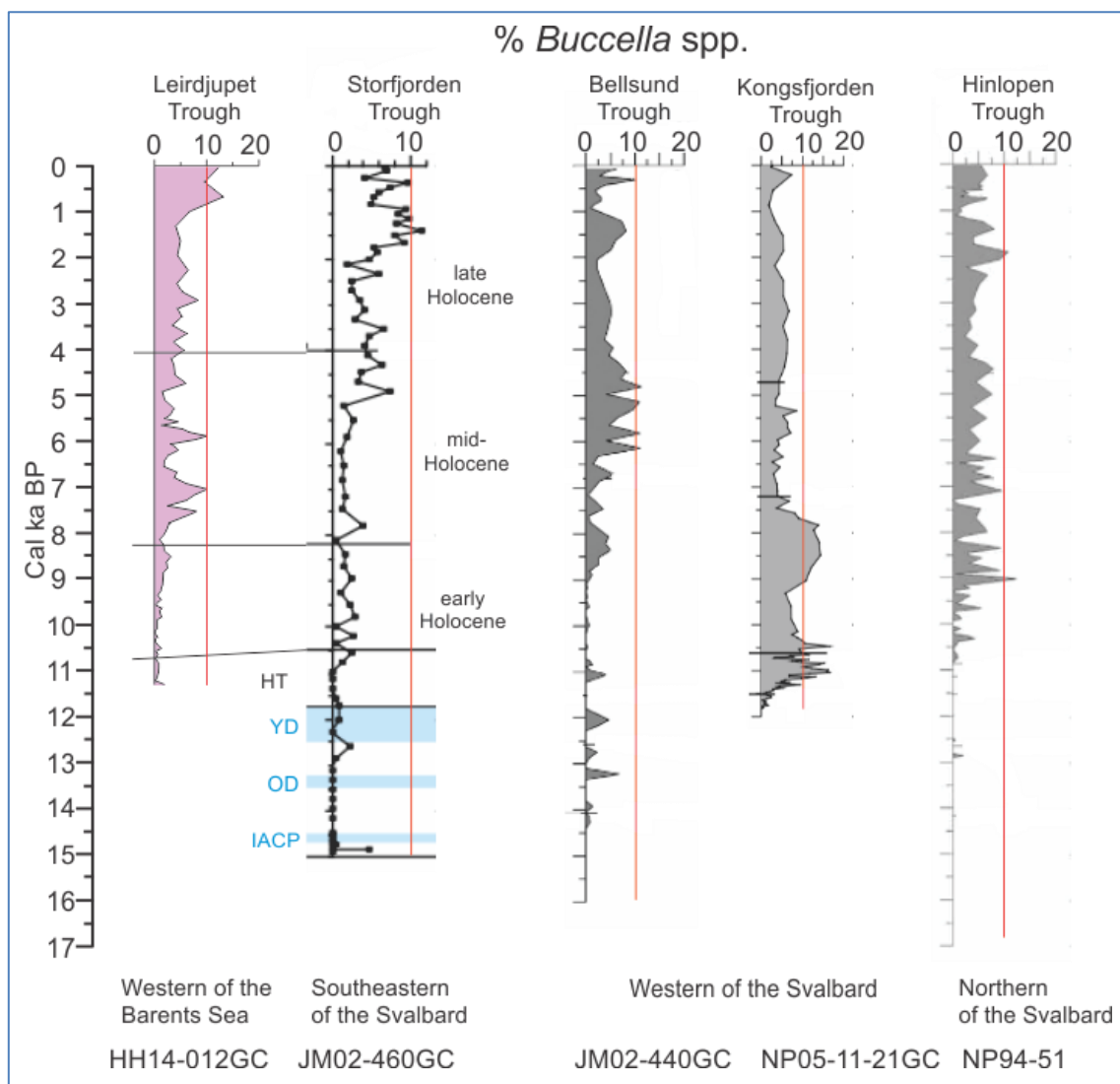


Figure 5.11. Comparison of the distribution pattern of *Buccella spp* in core HH14-012GC (study core) and cores from Storfjorden (Rasmussen and Thomsen, 2015), Bellsund (Ślubowska-Woldengen et al., 2007), Kongsfjorden (Skirbekk et al., 2010) and Hinlopen Trough (Ślubowska et al., 2005). Core locations are shown in Fig. 5.5. Vertical red lines represent 10 %.

Buccella spp is linked to the high productivity zone near ice fronts, living on fresh phytodetritus (Steinsund 1994; Hald and Korsun 1997; Polyak et al., 2002) (Fig. 5.11). *Buccella spp* species prefer temperatures in the range 0 – 1 °C and salinities around 33 – 34 ‰ (Steinsund 1994). The high percentage of *Buccella spp* in Kongsfjorden is linked to the high productivity in these areas, and indicates improved climatic conditions (Skirbekk et al., 2010). Increase in relative abundance of this species during the last c. 2 – 3 ka BP indicates expanded sea ice distribution. The increased abundance of *Buccella spp* in Bellsund during the mid-Holocene (together with *E. excavatum*) suggests increase in sea ice cover, and decreasing in temperatures and salinities of the bottom waters (Ślubowska-Woldengen et al., 2007). The trend in Leirdjupet and Storfjorden is similar. The rise in % of *Buccella spp* reflects enhanced sea ice cover enhanced during the late Holocene. In Hinlopen the same and relative stable abundance of this species suggests presence of sea ice during a longer time period; this core site position is more northward. The lowest percentage is observed at c. 11 – 9 ka BP and can be related to the stronger inflow of Atlantic water and changes in surface water temperatures.

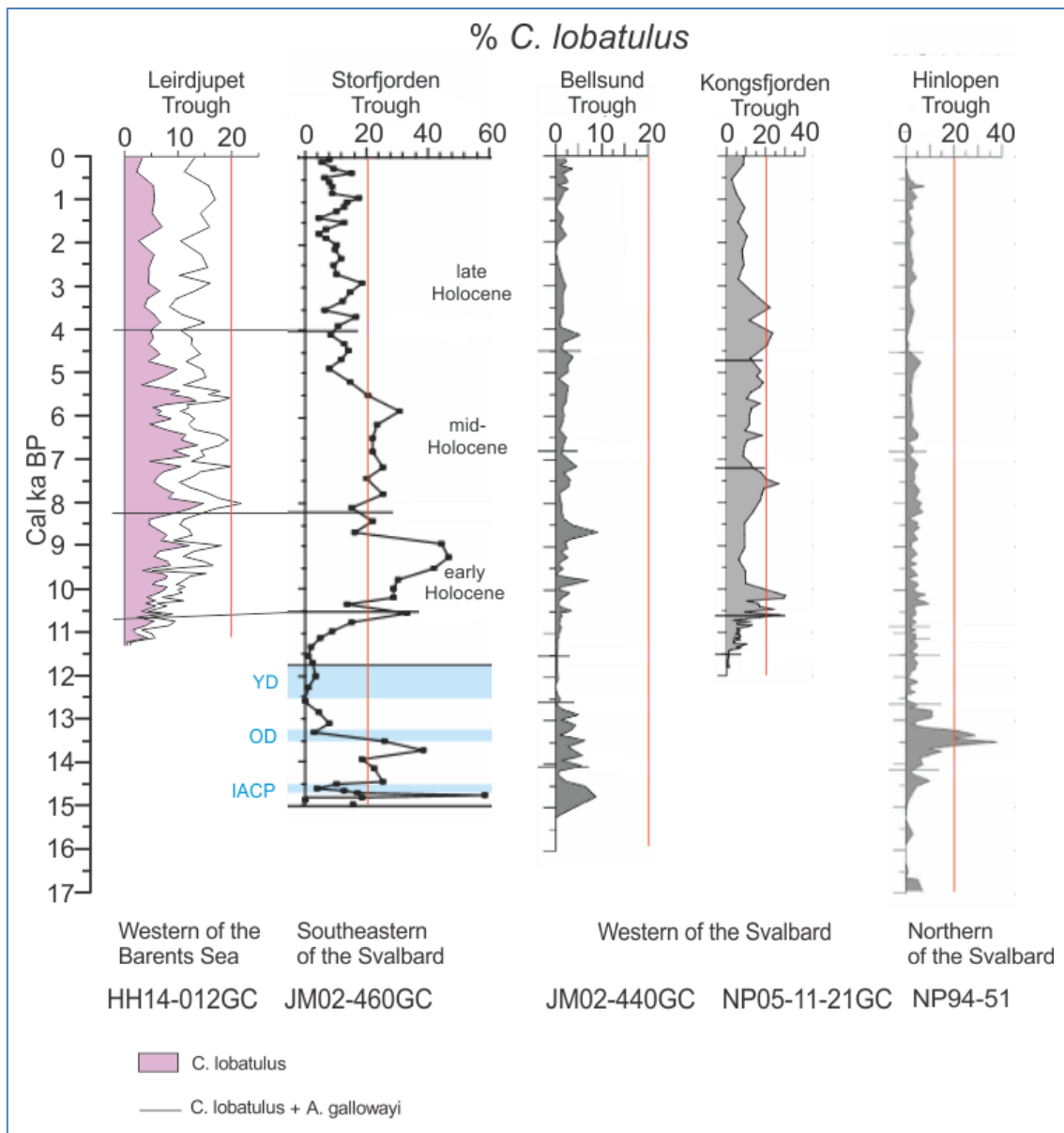


Figure 5.12. Comparison of the distribution pattern of *C. lobatulus* in core HH14-012GC (study core) and cores from Storfjorden (Rasmussen and Thomsen, 2015), Bellsund (Ślubowska-Woldengen et al., 2007), Kongsfjorden (Skirbekk et al., 2010) and Hinlopen Trough (Ślubowska et al., 2005). Core locations are shown in Fig. 5.5. Vertical red lines represent 20 %.

C. lobatulus is associated with strong bottom currents (Sejrup et al., 1981; Mackensen et al., 1985; Hald and Korsun 1997) (Fig. 5.12). Together with *A. gallowayi* these two species indicate enhanced current activity in the bottom waters (Murray 1991). The high brine formation resulted in the stronger overflow over the sill and caused increase in the % of *C. lobatulus* in the mid- Holocene in the Storfjorden (Rasmussen and Thomsen, 2015). An important observation shows that the warmer intervals contain *C. lobatulus* at 14.6 – 11.7 ka BP. The Polar front shift northward at c. 10.7 – 10.0 ka BP affected the increase in % of *C. lobatulus* in Leirdjupet. Predominantly the largest percentage of *C.*

lobatulus during the Holocene is observed in the early-mid time interval. The enhanced water circulation in the Barents Sea – Svalbard area probably has a regional character.

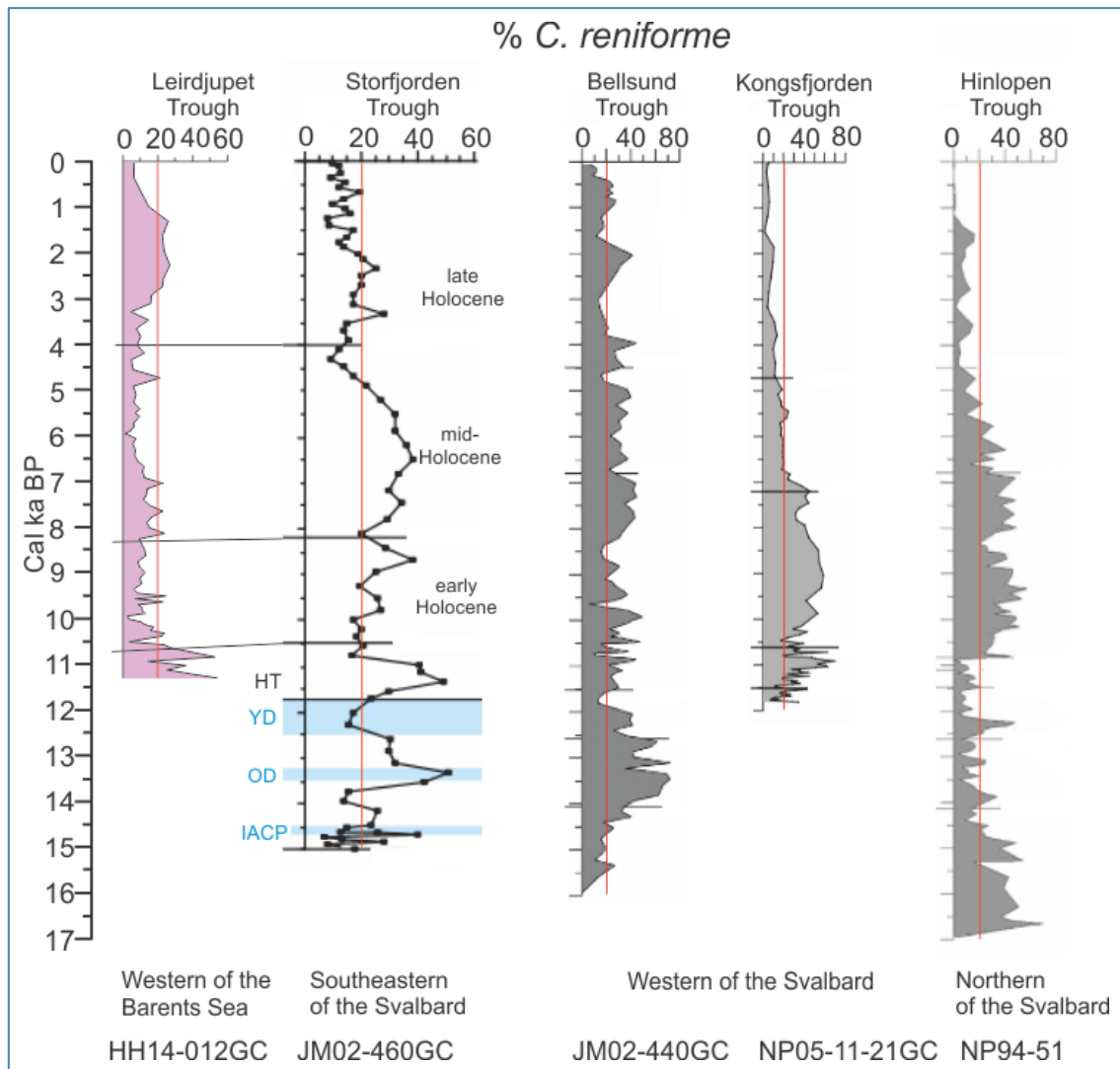


Figure 5.13. Comparison of the distribution pattern of *C. reniforme* in core HH14-012GC (study core) and cores from Storfjorden (Rasmussen and Thomsen, 2015), Bellsund (Ślubowska-Woldengen et al., 2007), Kongsfjorden (Skirbekk et al., 2010) and Hinlopen Trough (Ślubowska et al., 2005). Core locations are shown in Fig. 5.5. Vertical red lines represent 20 %.

The present day distribution of *C. reniforme* and *E. excavatum* are related to front of glaciers and termed ‘ice-proximal’ faunas (Hald and Korsun, 1997) (Fig. 5.13). The dominance of *C. reniforme* over *E. excavatum* is observed in less stressed environments, with increased food supply and reduced influence of glaciers (Korsun and Hald, 1998). *C. reniforme* indicate cold bottom water with lower salinity (>30 ‰) (Hald and Korsun, 1997). The dominance of *C. reniforme* during the early Holocene in Bellsund, Kongsfjorden and Hinlopen with absence of *E. excavatum*, low IRD flux and high concentration of benthic foraminifera indicates a strong influence of Atlantic water masses at the core site and a significant climatic improvement. In Leirdjupet during the early Holocene, the

abundance of *C. reniforme* decreases, while *N. labradorica* increases (close proximity to the sea-ice margin (Hald and Steinsund, 1996)), followed by increase the subpolar species *C. neoteretis*, which is associated with chilled Atlantic water in the Arctic region (Mackensen and Hald, 1988) and is observed at temperatures in the range 0 – 4 °C (Rytter et al., 2002). The last event is increase in *M. barleeanus*, an arctic-boreal species that prefers higher salinities (Hald and Steinsund, 1992). Replacement of one species with another is clearly seen in Leirdjupet during the early Holocene. The dominant species changes in succession and reflect the strength of Atlantic water influence in Leirdjupet (Fig. 4.4). The definitive contrast of Leirdjupet from other records is an increase of *C. neoteretis* and *M. barleeanus* during the early Holocene. It suggests better conditions in Leirdjupet than in northwestern and northern Svalbard, where an increase in percentage of *C. reniforme* occurs.

The presence of *E. excavatum* more likely indicate more extensive sea-ice cover, high turbidity and lowered and fluctuating salinities (Steinsund, 1994; Hald et al., 1994; Hald and Korsun, 1997) (Fig. 5.14). The abundance of *E. subarcticum* is higher in environments with lowered salinities (Lutze, 1965; Feyling-Hanssen et al., 1971; Polyak et al., 2002). A high proportion of small-sized and juvenile specimens indicates stressed conditions in glaciomarine environments (Korsun et al., 1995). In Storfjorden 15 – 11.7 ka BP in cold intervals (Younger Dryas, Older Dryas and Intra-Allerød cold period) the dominant species are *E. excavatum* and *C. reniforme*, these indicate polar conditions. The increase in *E. excavatum* during the late Holocene indicates harsh conditions in Storfjorden, which was caused probably by extensive seasonal sea ice cover (Rasmussen and Thomsen, 2015). Paleorecords from Hinlopen (17.5 – 14.5 ka BP) show high percentages of *E. excavatum* and *C. reniforme* and low flux of benthic and planktic foraminifera with high $\delta^{18}\text{O}$ values, this all indicate harsh conditions with cold bottom waters temperatures and lowered salinities and probably extensive sea ice cover (Ślubowska-Woldengen et al., 2007). In Kongsfjorden during the late Holocene the dominant species is *E. excavatum*, which together with increased IRD flux and sufficient decreasing in productivity indicate a colder environment with enhanced glacial influence and in addition a decline in the influence of Atlantic water (Skirbekk et al., 2010). In Leirdjupet increase in % of *E. excavatum* during the late Holocene at c. 2.7 and 1.3 ka BP correlate well with the decreasing abundance of planktic foraminifera. In all cores the percentage of *E. excavatum* increases, indicating the deterioration of environmental conditions in all records and over the Barents Sea region.

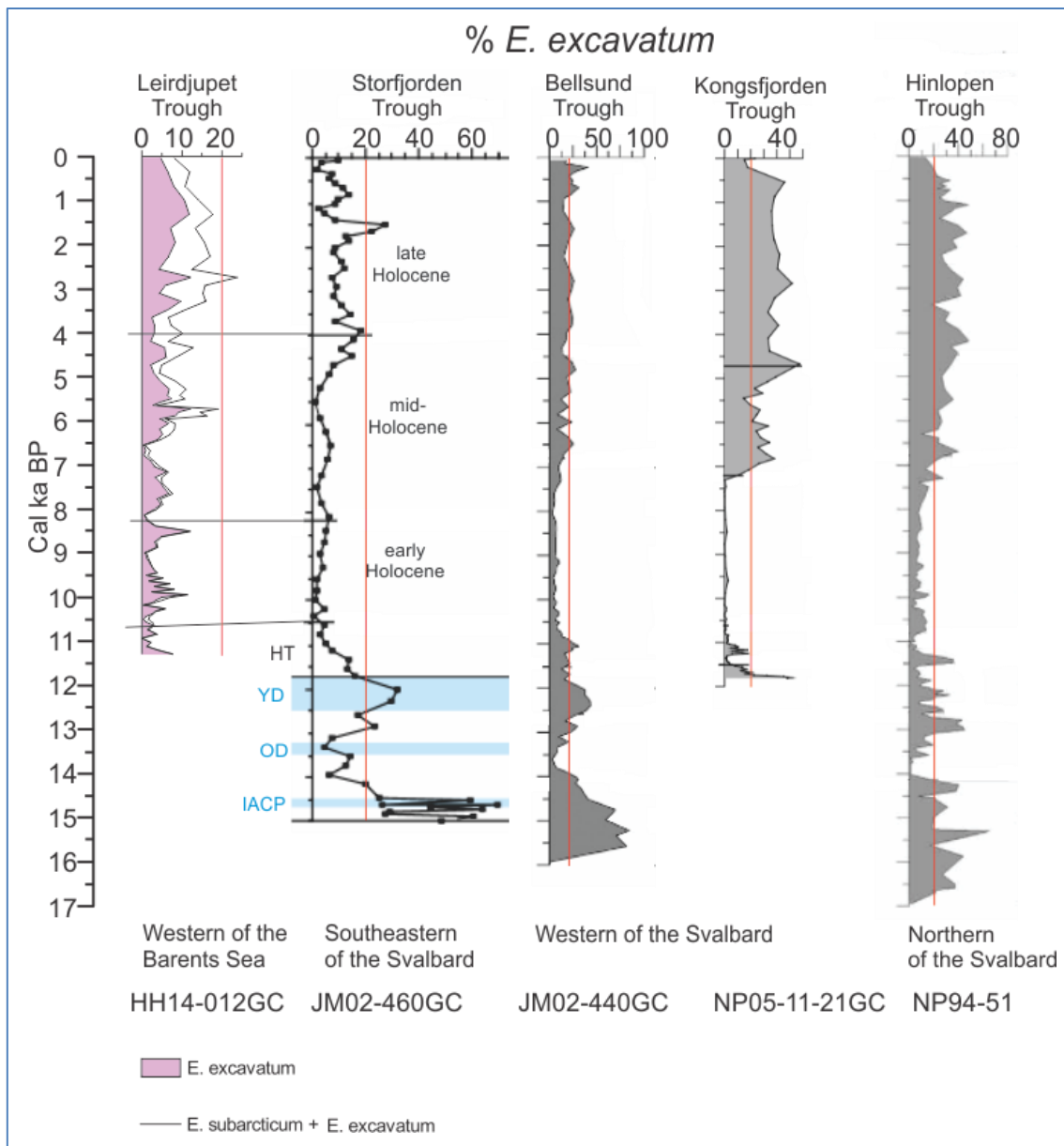


Figure 5.14. Comparison of the distribution pattern of *E. excavatum* in core HH14-012GC (study core) and cores from Storfjorden (Rasmussen and Thomsen, 2015), Bellsund (Ślubowska-Woldengen et al., 2007), Kongsfjorden (Skirbekk et al., 2010) and Hinlopen Trough (Ślubowska et al., 2005). Core locations are shown in Fig. 5.5. Vertical red lines represent 20 %.

S. loeblichii is associated with seasonal sea ice cover and is sensitive to the seasonal high productivity (Steinsund, 1994; Polyak et al., 2002) (Fig. 5.15). This species show rapid growth during the winter months (Korsun and Hald, 2000).

I. norcrossi/helena as well as *Buccella* spp are linked to the high productivity zone near ice edges, living on fresh phytodetritus. The former species also prefers relatively high and stable bottom water salinities (Steinsund 1994; Hald and Korsun, 1997; Polyak et al., 2002) (Fig. 5.16). *I. norcrossi/helena* prefers fresh organic matter, whereas *M. barleeanus* prefers partly degraded organic matter (Caralp, 1989; Korsun and Polyak, 1989). *I. norcrossi/helena*, *M. barleeanus* and *N.*

labradorica are controlled more by food supply than by water temperature (Lloyd, 2006; Ivanova et al., 2008). In Kongsfjorden during the final stage of the Younger Dryas period increase in *I. norcrossi/helenae* indicates a more glacier-distal environment (Osterman and Nelson, 1989). In Bellsund during the late Holocene *I. norcrossi/helenae* indicate lower salinities, wider sea ice cover and proximal position of the sea ice edge (Ślubowska-Woldengen et al., 2007). In Hinlopen and Kongsfjorden growth in % of *I. norcrossi/helenae* arise at c. 4.0 ka BP and is in accordance with the Leirdjupet. The general pattern is similar for all records and shows a peak in the Holocene transition and gradually increases in the late Holocene.

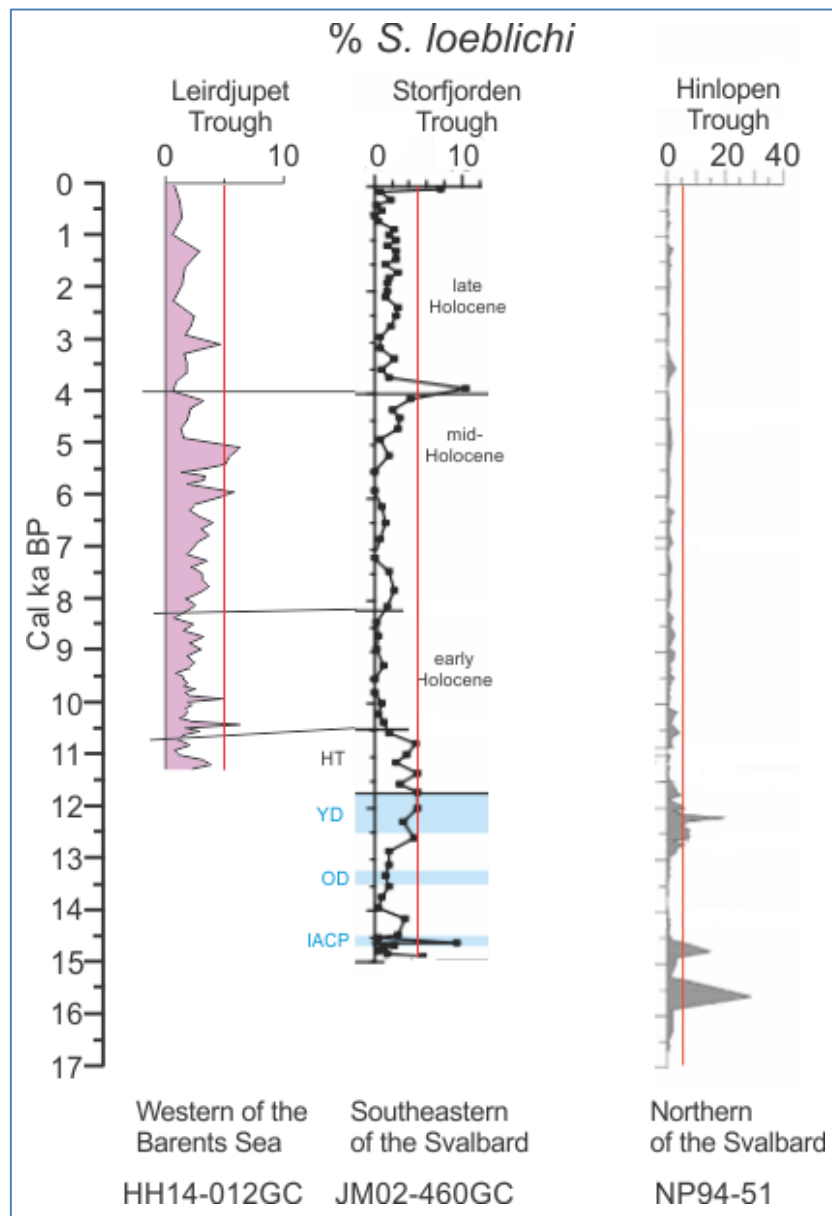


Figure 5.15. Comparison of the distribution pattern of *S. loeblichii* in core HH14-012GC (study core) and cores from Storfjorden (Rasmussen and Thomsen, 2015) and Hinlopen Trough (Ślubowska et al., 2005). Core locations are shown in Fig. 5.5. Vertical red lines represent 5 %.

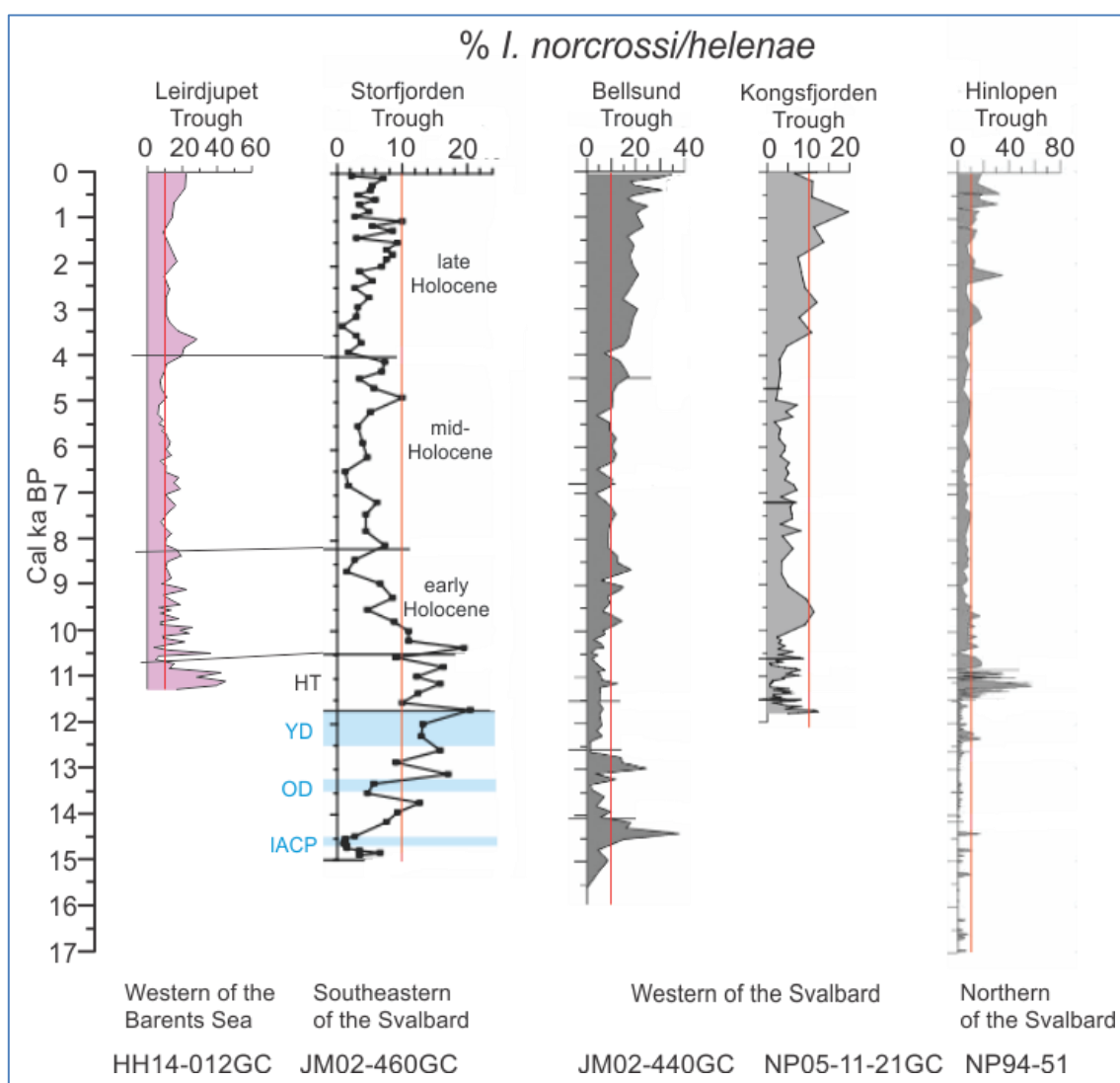


Figure 5.16. . Comparison of the distribution pattern of *I. norcrossi/helenae* in core HH14-012GC (study core) and cores from Storffjorden (Rasmussen and Thomsen, 2015), Bellsund (Ślubowska-Woldengen et al., 2007), Kongsfjorden (Skirbekk et al., 2010) and Hinlopen Trough (Ślubowska et al., 2005). Core locations are shown in Fig. 5.5. Vertical red lines represent 10 %.

5.4 The Polar front observation

The high percentages of the polar benthic and planktic species *C. reniforme* and *N. pachyderma* (s), respectively in combination with a low concentration of planktic and benthic foraminifera describes a period of Polar water spreading over Leirdjupet (Fig. 5.17). The flux of *C. reniforme* follows the moderate inflow of Atlantic water, which brings a food into the area. Carstens et al., (1997) found that the planktic foraminiferal amounts in areas covered by sea ice are low, probably the expansion of sea ice can explain the low concentration of planktic foraminifera during the Holocene transition. A stronger inflow of Atlantic water results in rapid changes in the dominant species of benthic foraminifera (Fig. 5.17 green line (1)) than in the planktic fauna (Fig. 5.17 green

dashed line (2)). Atlantic water inflow below the Polar water apparently first affect the bottom fauna (increase *I. norcrossi*) and only thereafter changes in the planktic fauna (increase *T. quinqueloba*) occur. This inflow may be strong enough to cause this change in the upper part of the water column.

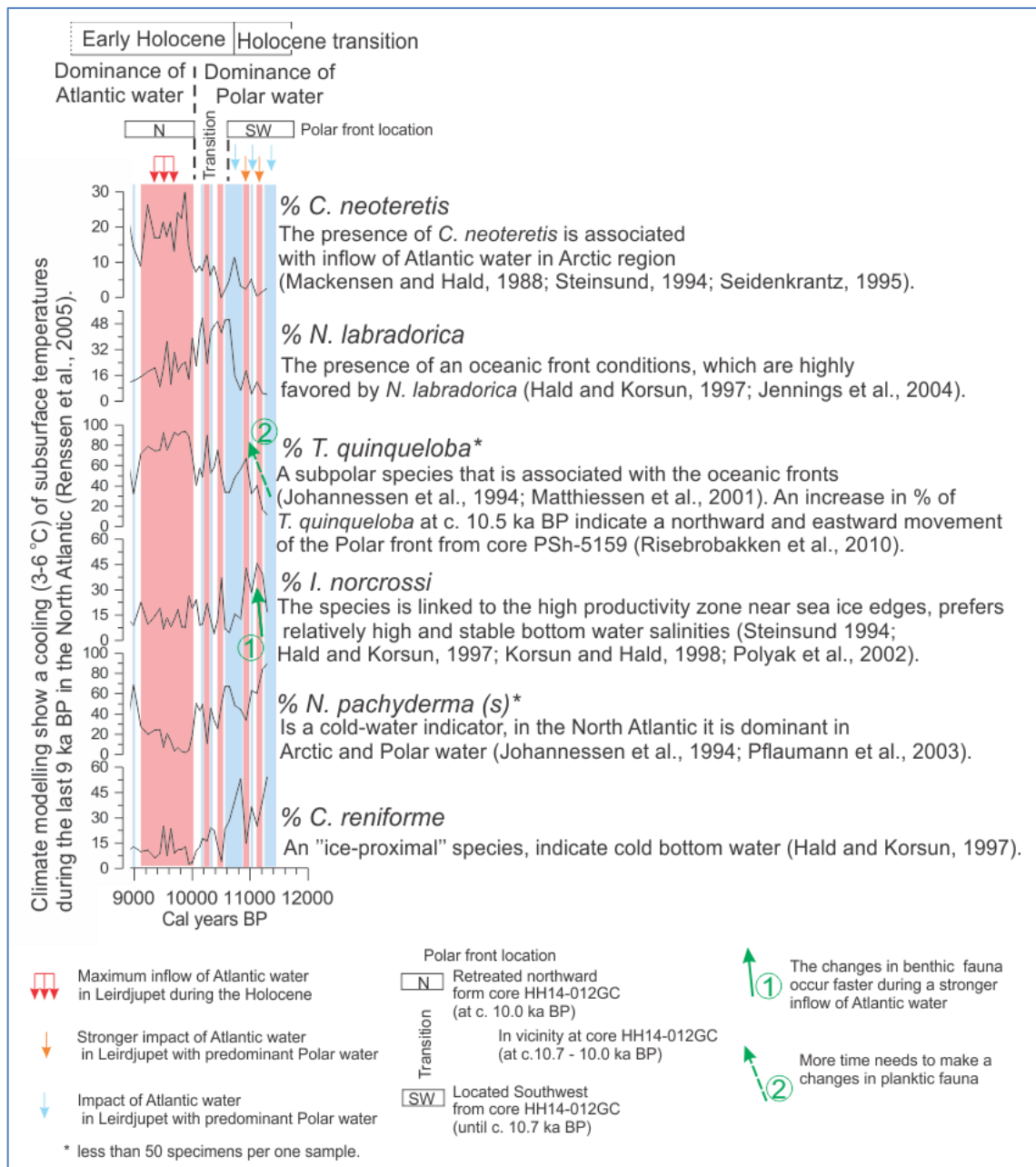


Figure 5.17. Benthic and planktic foraminifera percent distribution in core HH14-012GC plotted versus age.

In the time interval c. 10.7 – 10.0 ka BP high percentages of *N. labradorica* and presence of the subdominant species *C. reniforme* and *I. norcrossi* as well as low $\delta^{18}\text{O}$ values suggest severe conditions and lower temperatures. The dominant planktic species is *N. pachyderma* (s). The environmental conditions show high variability (when *N. labradorica* increases in relative abundance, both *C. reniforme* and *I. norcrossi* decreases). An improvement occurs after c. 10.4 ka BP probably due to changes in the location of the Polar front. The time of migration of the Polar front correlates well with the timing obtained from core PSh-5159 in the southern Barents Sea (Fig. 5.8 B). Here, at c.

10.5 ka BP a pronounced change in the position of the front was recorded (Risebrobakken et al., 2010). After c. 10.0 ka BP *C. neoteretis* and *T. quinqueloba* rapidly increase in percentages. The largest flux of planktic and benthic foraminifera occurs during c. 10 – 9 ka BP and is probably related to the maximum inflow of Atlantic water into Leirdjupet. The lowest $\delta^{18}\text{O}$ values supports this and indicates the Holocene temperature optimum and the dominance of Atlantic water after c. 10 ka BP in Leirdjupet.

6 Summary and conclusions

The study of multi-proxy data from core HH14-012GC has provided new information on the environmental development of the western Barents Sea in the Leirdjupet Trough since the early Holocene.

Analyses of sediment core HH14-012GC show that Atlantic water has continuously been present in the study area during the last 11,000 years. In the Holocene transition until c. 10.7 ka BP, Atlantic water was present as a subsurface water mass below colder Polar water at the surface and extensive sea ice cover. *Cassidulina reniforme* and *Islandiella norcrossi* were the dominant species in the Holocene transition period indicating glaciomarine environmental conditions. Low concentration and flux of planktic foraminifera are typical for this interval. With increasing percentages of *C. reniforme* at the beginning of the Holocene transition dominance of Polar water indicator *Neogloboquadrina pachyderma* sinistral (s) over the subpolar species *Turborotalia quinqueloba* (which is associated with the oceanic fronts in the central northern North Atlantic) is observed. The percent of these species is 85 and 15, respectively. The area was affected by less saline, but cold Atlantic-derived water; the effect of the reduced salinity of the water is related to strong influence of cold and low salinity polar water and meltwater input. The later rise in percent of *I. norcrossi* at c. 11 ka BP is linked to the change in proportion of the two dominant planktic species to 60 and 40 %, respectively. The inflow of more saline and slightly warmer Atlantic-derived water occur during this period, at the same time a low percentage of *Cassidulina neoteretis* indicates that this inflow was fairly weak. The dominance of cold water planktic species together with its minimum concentration and flux show severe environmental conditions at the surface. Fluctuations in benthic foraminiferal concentrations correlates closely with the changes in the planktic faunas and show synchronous episodic coolings corresponding to a rise in % of *C. reniforme* and *N. pachyderma* (s).

At c. 10.7 ka BP the Polar Front changed position close to the core site, which resulted in an increase of both seasonal productivity as well as sea ice cover, as shown by a rapid increase in % of *Nonionellina labradorica*. In particular, the changes in the location of the Polar Front is seen by the dominance of *N. pachyderma* (s) until c. 10 ka BP and prevailing of cold conditions at the surface. During the early Holocene a significant increase of Atlantic Water inflow into Leirdjupet Trough occurred. In the interval c. 10 – 9 ka BP a rapidly increasing flux of benthic and planktic foraminifera, dominance of the benthic foraminiferal species *C. neoteretis*, and low of $\delta^{18}\text{O}$ values represent the Holocene temperature optimum at the study area and the strongest warm Atlantic water inflow for the Holocene. In response to changes in the environment, the species composition of planktic foraminiferal faunas also changes. During the Holocene temperature optimum the relative

abundance of *T. quinqueloba* increases to 90 %. In addition, *N. pachyderma* dextral (d) a warm water indicator of the Norwegian-Barents margin shows its highest abundance (percentage varies in range 1-10%). One more thermophilic species *Globigerina bulloides* was found in the record (2-6%). Based on the planktic foraminiferal $\delta^{18}\text{O}$ data subsurface water temperature probably was c. 2 °C higher than today.

The mid-Holocene (8.3 – 4 ka BP) represents a transition period with relative stable environmental conditions. Increasing deposition of IRD indicates sea ice and icebergs arriving at the core site and is probably related to decrease in sea surface temperature. Planktic foraminiferal data show dominance of *T. quinqueloba* with gradually increasing % of *N. pachyderma* (s). In the periods with higher IRD flux and lower planktic foraminifera concentration, *N. pachyderma* (s) becomes the dominant species. The dominant benthic foraminiferal species are *C. neoteretis* and *Melonis barleanus* which are linked to chilled Atlantic Water and indicate continuous inflow of Atlantic water. Increasing *C. lobatulus* and *A. gallowayi* indicates enhanced bottom water currents during the mid-Holocene.

In the late Holocene climatic conditions became cooler. The dominant benthic species *C. reniforme* and *I. norcrossi* indicate cooling of the bottom water. The dominance of *N. pachyderma* (s) and *T. quinqueloba* with increasing trend of *N. pachyderma* (s) is related to the continuous decreasing of surface water temperature in the area. The decreasing trend in temperature continues during the late Holocene and the influence of Atlantic water in the area diminished further.

The difference between the benthic faunas in the Leirdjupet Trough record and in records from the western and northern Svalbard region during the mid-late Holocene is prominent. The main features of environmental changes around Svalbard are rapid and high increase *E. excavatum* and the corresponding decrease in *C. reniforme* (clearly seen in Storfjorden, Kongsfjorden and Hinlopen Trough records) In Leirdjupet, *E. excavatum* also show an increasing trend during the mid-late Holocene, but to a much more moderate degree, and more importantly, *C. reniforme* increases instead of decreasing as elsewhere around Svalbard. This fact may indicate a less stressed environment in the Leirdjupet Trough than in comparison with western and especially north-western and northern Svalbard, probably because of its more southerly location south of Spitsbergenbanken.

7 References

1. Aagaard-Sørensen, S., Husum, K., Hald, M. & Knies, J. Paleoceanographic development in the SW Barents Sea during the late Weichselian--Early Holocene transition. *Quat. Sci. Rev.* **29**, 3442–3456 (2010).
2. Andreassen, K. & Winsborrow, M. Signature of ice streaming in Bjørnøya, Polar North Atlantic, through the Pleistocene and implications for ice-stream dynamics. *Ann. Glaciol.* **50**, 17–26 (2009).
3. Asplin, L., Ingvaldsen, R., Loeng, H. & Ådlandsvik, B. *Description and validation of a three-dimensional numerical model of the Nordic and Barents Seas.* (1998).
4. Bakke, J., Dahl, S. O., Paasche, Ø., Løvlie, R. & Nesje, A. Glacier fluctuations, equilibrium-line altitudes and palaeoclimate in Lyngen, northern Norway, during the Lateglacial and Holocene. *The Holocene* **15**, 518–540 (2005).
5. Barber, D. C. *et al.* Forcing of the cold event of 8,200 years ago by catastrophic drainage of Laurentide lakes. *Nature* **400**, 344–348 (1999).
6. Berger, A. L. Astronomical theory of paleoclimates and the last glacial-interglacial cycle. *Quat. Sci. Rev.* **11**, 571–581 (1992).
7. Berger, a. & Loutre, M. F. Insolation values for the climate of the last 10 million years. *Quat. Sci. Rev.* **10**, 297–317 (1991).
8. Bjarnadóttir, L. R., Rütger, D. C., Winsborrow, M. & Andreassen, K. Grounding-line dynamics during the last deglaciation of Kveithola, W Barents Sea, as revealed by seabed geomorphology and shallow seismic stratigraphy. *Boreas* **42**, 84–107 (2013).
9. Bjørlykke, K., Bue, B. & ELVERHØT, A. Quaternary sediments in the northwestern part of the Barents Sea and their relation to the underlying Mesozoic bedrock. *Sedimentology* **25**, 227–246 (1978).
10. Broecker, W. The Great Ocean Conveyor. *Oceanography* **4**, 79–89 (1991).
11. Carstens, J., Hebbeln, D. & Wefer, G. Distribution of planktic foraminifera at the ice margin in the Arctic (Fram Strait). *Mar. Micropaleontol.* **29**, 257–269 (1997).
12. Chistyakova, N. O., Ivanova, E. V., Risebrobakken, B., Ovsepyan, E. a. & Ovsepyan, Y. S. Reconstruction of the postglacial environments in the southwestern Barents Sea based on foraminiferal assemblages. *Oceanology* **50**, 573–581 (2010).
13. Clarke, G. K. C., Leverington, D. W., Teller, J. T. & Dyke, A. S. Paleohydraulics of the last outburst flood from glacial Lake Agassiz and the 8200BP cold event. *Quat. Sci. Rev.* **23**, 389–407 (2004).
14. Cofaigh, C. Ó. & Dowdeswell, J. A. Laminated sediments in glacial marine environments: diagnostic criteria for their interpretation. *Quat. Sci. Rev.* **20**, 1411–1436 (2001).
15. Dickson, R. R., Midttun, L. & Mukhin, A. I. The hydrographic conditions in the Barents Sea in August--September 1965--1968. *Int. O-gr. fish Surv. Barents Sea* **1968**, 3–24 (1965).
16. Douglas, R. G. Benthic foraminiferal ecology and paleoecology: a review of concepts and methods. (1979).

17. Dowdeswell, J. a. Glacimarine sedimentary processes and facies on the polar north atlantic Margins. *Quat. Sci. Rev.* **17**, 243–272 (1998).
18. Duplessy, J., Ivanova, E. & Murdmaa, I. Holocene paleoceanography of the northern Barents Sea and variations of the northward heat transport by the Atlantic Ocean. *Boreas* **2001**, 2–16 (2001).
19. Duplessy, J. C. *et al.* Paleoceanography of the Barents Sea during the Holocene. *Paleoceanography* **20**, (2005).
20. Duplessy, J.-C., Moyes, J. & Pujol, C. Deep water formation in the North Atlantic Ocean during the last ice age. *Nature* **286**, 479–482 (1980).
21. Ehrmann, W. U. & Thiede, J. Correlation of terrigenous and biogenic sediment fluxes in the North Atlantic Ocean during the past 150 my. *Geol. Rundschau* **75**, 43–55 (1986).
22. Elverhøi, A. & Solheim, A. The Barents Sea ice sheet-a sedimentological. (1983).
23. Elverhøi, A., Pfirman, S. L., Solheim, A. & Larssen, B. B. Glaciomarine sedimentation in epicontinental seas exemplified by the northern Barents Sea. *Mar. Geol.* **85**, 225–250 (1989).
24. Elverhøi, A., Vinje, T., Solheim, A., Kristoffersen, Y. & others. *Physical Environment, Western Barents Sea: Drift, Composition, Morphology and Distribution of the Sea Ice Fields in the Barents Sea.* (Norsk Polarinstitutt, 1985).
25. Fairbanks, R. G. A 17,000-year glacio-eustatic sea level record: influence of glacial melting rates on the Younger Dryas event and deep-ocean circulation. *Nature* **342**, 637–642 (1989).
26. Faleide, J. I., Gudlaugsson, S. T. & Jacquart, G. Evolution of the western Barents Sea. *Mar. Pet. Geol.* **1**, 123–150 (1984).
27. Faleide, J. I. *et al.* Late Cenozoic evolution of the western Barents Sea-Svalbard continental margin. *Glob. Planet. Change* **12**, 53–74 (1996).
28. Feyling-Hanssen, R. W. The foraminifer *Elphidium excavatum* (Terquem) and its variant forms. *Micropaleontology* **18**, 337–354 (1972).
29. Feyling-Hanssen, R. W. Mikropaleontologiens teknikk. *Nor. Geotech. Inst.* **29**, 1–14 (1958).
30. Gibson, T. G. Planktonic benthonic foraminiferal ratios: modern patterns and Tertiary applicability. *Mar. Micropaleontol.* **15**, 29–52 (1989).
31. Gibson, T. G. & Buzas, M. A. Species diversity: patterns in modern and Miocene foraminifera of the eastern margin of North America. *Geol. Soc. Am. Bull.* **84**, 217–238 (1973).
32. Gilbert, R. Rafting in glacimarine environments. *Geol. Soc. London, Spec. Publ.* **53**, 105–120 (1990).
33. Goodman, W. K. *et al.* The Yale-Brown obsessive compulsive scale: I. Development, use, and reliability. *Arch. Gen. Psychiatry* **46**, 1006–1011 (1989).
34. Gornitz, V. *Rising seas: past, present, future.* (Columbia University Press, 2013).
35. Groot, D. E., Aagaard-Sørensen, S. & Husum, K. Reconstruction of Atlantic water variability during the Holocene in the western Barents Sea. *Clim. Past* **10**, 51–62 (2014).

36. Hagen, J. O., Melvold, K., Pinglot, F. & Dowdeswell, J. A. On the net mass balance of the glaciers and ice caps in Svalbard, Norwegian Arctic. *Arctic, Antarct. Alp. Res.* **35**, 264–270 (2003).
37. Hald, M. & Korsun, S. Distribution of modern benthic foraminifera from fjords of Svalbard, European Arctic. *J. Foraminifer. Res.* **27**, 101–122 (1997).
38. Hald, M. & Steinsund, P. I. Distribution of surface sediment benthic Foraminifera in the southwestern Barents Sea. *J. Foraminifer. Res.* **22**, 347–362 (1992).
39. Hald, M. *et al.* Variations in temperature and extent of Atlantic Water in the northern North Atlantic during the Holocene. *Quat. Sci. Rev.* **26**, 3423–3440 (2007).
40. HALD, M., DANIELSEN, T. O. R. K. & LORENTZEN, S. Late Pleistocene-Holocene benthic foraminiferal distribution in the southwestern Barents Sea: Paleoenviromental implications. *Boreas* **18**, 367–388 (1989).
41. Hald, M., Dokken, T. & Hagen, S. Palaeoceanography on the European arctic margin during the last deglaciation. *Geol. Soc. London, Spec. Publ.* **111**, 275–287 (1996).
42. Hald, M. *et al.* Holocene paleoceanography and glacial history of the West Spitsbergen area, Euro-Arctic margin. *Quat. Sci. Rev.* **23**, 2075–2088 (2004).
43. Hald, M. *et al.* Late-glacial and Holocene paleoceanography and sedimentary environments in the St. Anna Trough, Eurasian Arctic Ocean margin. *Palaeogeogr. Palaeoclimatol. Palaeoecol.* **146**, 229–249 (1999).
44. Hald, M. & Korsun, S. The 8200 cal. yr BP event reflected in the Arctic fjord, Van Mijenfjorden, Svalbard. *The Holocene* **18**, 981–990 (2008).
45. Hald, M. & Steinsund, P. I. Benthic foraminifera and carbonate dissolution in the surface sediments of the Barents and Kara Seas. *Surface-sediment Compos. Sediment. Process. Cent. Arct. Ocean along Eurasian Cont. Margin. Berichte zur Polarforsch.* **212**, 285–307 (1996).
46. Harris, C. L., Plueddemann, A. J. & Gawarkiewicz, G. G. Water mass distribution and polar front structure in the western Barents Sea. *J. Geophys. Res. Ocean.* **103**, 2905–2917 (1998).
47. Hart, J. K. & Roberts, D. H. Criteria to distinguish between subglacial glaciotectionic and glaciomarine sedimentation, I. Deformation styles and sedimentology. *Sediment. Geol.* **91**, 191–213 (1994).
48. Hass, H. C. A method to reduce the influence of ice-rafted debris on a grain size record from northern Fram Strait, Arctic Ocean. *Polar Res.* **21**, 299–306 (2002).
49. Hebbeln, D. Flux of ice-rafted detritus from sea ice in the Fram Strait. *Deep. Res. Part II Top. Stud. Oceanogr.* **47**, 1773–1790 (2000).
50. Holzhauser, H., Magny, M. & Zumbuühl, H. J. Glacier and lake-level variations in west-central Europe over the last 3500 years. *The Holocene* **15**, 789–801 (2005).
51. Hop, H. *et al.* Progress in Oceanography Physical and biological characteristics of the pelagic system across Fram Strait to Kongsfjorden. *Current* **71**, 182–231 (2006).
52. Hopkins, T. S. The GIN Sea—A synthesis of its physical oceanography and literature review 1972–1985. *Earth-Science Rev.* **30**, 175–318 (1991).

53. Horn, G. & Orvin, A. K. Geology of Bear Island: with special reference to the coal deposits, and with an account of the history of the island. (1928).
54. Husum, K. & Hald, M. A continuous marine record 8000–1600 cal. yr BP from the Malangenfjord, north Norway: foraminiferal and isotopic evidence. *The Holocene* **14**, 877–887 (2004).
55. Imbrie, J., Berger, A. & Shackleton, N. J. Role of orbital forcing: a two-million-year perspective. *Glob. Chang. Perspect. Past* 263–277 (1993).
56. Ingvaldsen, R. B. Width of the North Cape Current and location of the Polar Front in the western Barents Sea. *Geophys. Res. Lett.* **32**, 1–4 (2005).
57. Ingvaldsen, R., Loeng, H. & Asplin, L. Variability in the Atlantic inflow to the Barents Sea based on a one-year time series from moored current meters. *Cont. Shelf Res.* **22**, 505–519 (2002).
58. Ivanova, E. V., Ovsepyan, E. a., Risebrobakken, B. & Vetrov, a. a. Downcore Distribution of Living Calcareous Foraminifera and Stable Isotopes in the Western Barents Sea. *J. Foraminifer. Res.* **38**, 337–356 (2008).
59. Jarke, J. Beitrag zur Kenntnis der Foraminiferenfauna der mittleren und westlichen Barents-See. *Int. Rev. Ges. Hydrobiol* **45**, 581–654 (1960).
60. Jennings, A. E. & Helgadottir, G. Foraminiferal assemblages from the fjords and shelf of eastern Greenland. *J. Foraminifer. Res.* **24**, 123–144 (1994).
61. Jennings, A. E., Weiner, N. J., Helgadottir, G. & Andrews, J. T. Modern foraminiferal faunas of the southwestern to northern Iceland shelf: oceanographic and environmental controls. *J. Foraminifer. Res.* **34**, 180–207 (2004).
62. Jernas, P., Klitgaard Kristensen, D., Husum, K., Wilson, L. & Koç, N. Palaeoenvironmental changes of the last two millennia on the western and northern Svalbard shelf. *Boreas* **42**, 236–255 (2013).
63. Johannessen, O. M. & Foster, L. A. A note on the topographically controlled oceanic polar front in the Barents Sea. *J. Geophys. Res. Ocean.* **83**, 4567–4571 (1978).
64. Johannessen, T., Jansen, E., Flatøy, A. & Ravelo, A. C. in *Carbon cycling in the glacial ocean: constraints on the ocean's role in global change* 61–85 (Springer, 1994).
65. Juggings, S. C2 Version 1.7. 2 User Guide. *Softw. Ecol. Paleoecol. data Anal. Vis. Newcastle Univ. Newcastle upon Tyne UK* (2010).
66. Junttila, J., Aagaard-Sørensen, S., Husum, K. & Hald, M. Late Glacial–Holocene clay minerals elucidating glacial history in the SW Barents Sea. *Mar. Geol.* **276**, 71–85 (2010).
67. Khusid, T. A. & Polyak, L. V. Biogeography of Benthic Foraminifera of the Arctic Ocean. *Neogene-Quaternary Paleoceanology from Micropaleontol. Data* 42–50 (1989).
68. Klitgaard-Kristensen, D., Sejrup, H. P. & Haflidason, H. The last 18 kyr fluctuations in Norwegian Sea surface conditions and implications for the magnitude of climatic change: Evidence from the North Sea. *Paleoceanography* **16**, 455–467 (2001).
69. Knies, J., Vogt, C. & Stein, R. Growth and decay patterns of the Svalbard/Barents Sea-ice sheet and palaeoceanographic evolution during Saalian and Weichselian glaciations. *Geo Mar. Lett* **18**, 195–202 (1999).

70. Knudsen, K. L. *LATE QUATERNARY FORAMINIFERA FROM VENDSYSSEL , DENMARK AND SANDNES , NORWAY Systematic part. Late Quaternary Foraminifera From Vendsyssel , Denmark and Sandnes , Norway* (Geological Society of Denmark., 1969).
71. Koç, N., Jansen, E. & Hafliðason, H. Paleoceanographic reconstructions of surface ocean conditions in the Greenland, Iceland and Norwegian seas through the last 14 ka based on diatoms. *Quat. Sci. Rev.* **12**, 115–140 (1993).
72. Koç, N., Klitgaard-Kristensen, D., Hasle, K., Forsberg, C. F. & Solheim, A. Late glacial palaeoceanography of Hinlopen Strait, northern Svalbard. *Polar Res.* **21**, 307–314 (2002).
73. Kohler, J. *et al.* Acceleration in thinning rate on western Svalbard glaciers. *Geophys. Res. Lett.* **34**, (2007).
74. Korsun, S. & Hald, M. Modern benthic foraminifera off Novaya Zemlya tidewater glaciers, Russian Arctic. *Arct. Alp. Res.* **30**, 61–77 (1998).
75. Kristensen, D. K., Rasmussen, T. L. & Koç, N. Palaeoceanographic changes in the northern Barents Sea during the last 16 000 years - new constraints on the last deglaciation of the Svalbard-Barents Sea Ice Sheet: Palaeoceanographic changes in the northern Barents Sea during the last 16 000 years. *Boreas* **42**, 798–813 (2013).
76. Landvik, J. Y. *et al.* The last glacial maximum of Svalbard and the Barents Sea area: ice sheet extent and configuration. *Quat. Sci. Rev.* **17**, 43–75 (1998).
77. Loeng, H. Features of the physical oceanographic conditions of the Barents Sea. *Polar Res.* **10**, 5–18 (1991).
78. Loeng, H. & Sætre, R. *Features of the Barents Sea circulation.* (2001).
79. Lowe, J. J. & Walker, M. J. C. *Reconstructing Quaternary Environments.* (1984).
80. Lubinski, D. J., Polyak, L. & Forman, S. L. Freshwater and Atlantic Water inflows to the deep northern Barents and Kara seas since ca 13 14C ka: Foraminifera and stable isotopes. *Quat. Sci. Rev.* **20**, 1851–1879 (2001).
81. Mackensen, a. & Hald, M. *Cassidulina teretis* Tappan and *C. laevigata* d’Orbigny; their modern and late Quaternary distribution in northern seas. *J. Foraminifer. Res.* **18**, 16–24 (1988).
82. Mangerud, J. A. N. & Landvik, J. Y. Younger Dryas cirque glaciers in western Spitsbergen: smaller than during the Little Ice Age. *Boreas-International J. Quat. Res.* **36**, 278–285 (2007).
83. Mangerud, J., Andersen, S. T., BERGLUND, B. E. & Donner, J. J. Quaternary stratigraphy of Norden, a proposal for terminology and classification. *Boreas* **3**, 109–126 (1974).
84. Mangerud, J., Bondevik, S., Gulliksen, S., Hufthammer, A. K. & Høisæter, T. Marine 14 C reservoir ages for 19th century whales and molluscs from the North Atlantic. *Quat. Sci. Rev.* **25**, 3228–3245 (2006).
85. Mangerud, J. & Gulliksen, S. Apparent radiocarbon ages of recent marine shells from Norway, Spitsbergen, and Arctic Canada. *Quat. Res.* **5**, 263–273 (1975).
86. Manley, T. O. Branching of Atlantic Water within the Greenland-Spitsbergen Passage: An estimate of recirculation. *J. Geophys. Res.* **100**, 20627 (1995).
87. Matishov, G. *et al.* Global International Waters Assessment Barents Sea, GIWA Regional

- assessment 11. *GIWA Reg. Assess. reports* 118 (2004).
88. Meldgaard, S. & Knudsen, K. L. Metoder til indsamling og oparbejdning af prøver til foraminifer-analyser. *Dansk natur Dansk Sk.* 48–57 (1979).
 89. Midttun, L. Formation of dense bottom water in the Barents Sea. *Deep Sea Res. Part A. Oceanogr. Res. Pap.* **32**, 1233–1241 (1985).
 90. Mudie, P. J., Keen, C. E., Hardy, I. A. & Vilks, G. Multivariate analysis and quantitative paleoecology of benthic foraminifera in surface and Late Quaternary shelf sediments, northern Canada. *Mar. Micropaleontol.* **8**, 283–313 (1984).
 91. Munsell. Munsell Color Chart. *New Wind. United States Macbeth* 1–29 (1994).
 92. Munsell Colour Company & Munsell Colour Company. Munsell Soil Colour Charts. *Geoderma* **48**, 199 (1975).
 93. Nathorst, A. G. The Swedish arctic expedition of 1898. *Geogr. J.* **14**, 51–76 (1899).
 94. Nesje, A., Bakke, J., Dahl, S. O., Lie, Ø. & Matthews, J. A. Norwegian mountain glaciers in the past, present and future. *Glob. Planet. Change* **60**, 10–27 (2008).
 95. Nesje, A., Matthews, J. A., Dahl, S. O., Berrisford, M. S. & Andersson, C. Holocene glacier fluctuations of Flatebreen and winter-precipitation changes in the Jostedalsgreen region, western Norway, based on glaciolacustrine sediment records. *The Holocene* **11**, 267–280 (2001).
 96. Nichols, G. *Sedimentology and stratigraphy*. (John Wiley & Sons, 2009).
 97. Ottesen, D. & Rise, L. Submarine landforms and the reconstruction of fast-flowing ice streams within a large Quaternary ice sheet : The 2500-km-long Norwegian- Svalbard margin (57 ° – 80 ° N). *America (NY)*. **117**, 1033–1050 (2005).
 98. Parsons, A. R. *et al.* The Barents Sea polar front in summer. *J. Geophys. Res. Ocean.* **101**, 14201–14221 (1996).
 99. Pfirman, S. L., Bauch, D. & Gammelsrød, T. The Northern Barents Sea: Water Mass Distribution and Modification. *Polar Ocean. Their Role Shap. Glob. Environ. Geophys. Monogr.* **85** 77–94 (1994).
 100. Polyak, L. Benthic Foraminiferal Assemblages From the Southern Kara Sea, a River-Influenced Arctic Marine Environment. *J. Foraminifer. Res.* **32**, 252–273 (2002).
 101. Polyak, L. & Solheim, a. Late- and postglacial environments in the northern Barents Sea west of Franz Josef Land. *Polar Res.* **13**, 197–207 (1994).
 102. Polyak, L. & Mikhailov, V. Post-glacial environments of the southeastern Barents Sea: foraminiferal evidence. *Geol. Soc. London, Spec. Publ.* **111**, 323–337 (1996).
 103. Powell, R. D. Glacimarine processes and inductive lithofacies modelling of ice shelf and tidewater glacier sediments based on Quaternary examples. *Mar. Geol.* **57**, 1–52 (1984).
 104. Rasmussen, T. L. *et al.* Holocene temperature variability in the northern Nordic Seas: Interplay of Atlantic-, Arctic-and Polar water masses. *Quat. Sci. Rev.*, *doi* **10**, (2014).
 105. Rasmussen, T. L., Forwick, M. & Mackensen, a. Reprint of: Reconstruction of inflow of Atlantic

- Water to Isfjorden, Svalbard during the Holocene: Correlation to climate and seasonality. *Mar. Micropaleontol.* **99**, 18–28 (2013).
106. Rasmussen, T. L., Thomsen, E., Labeyrie, L. & van Weering, T. C. E. Circulation changes in the Faeroe-Shetland Channel correlating with cold events during the last glacial period (58–10 ka). *Geology* **24**, 937–940 (1996).
 107. Rasmussen, T. L. *et al.* Paleoceanographic evolution of the SW Svalbard margin (76 ° N) since 20 , 000 14 C yr BP. *Quat. Res.* **67**, 100–114 (2007).
 108. Rasmussen, T. L., Thomsen, E., Weering, T. C. E. & Labeyrie, L. Rapid changes in surface and deep water conditions at the Faeroe Margin during the last 58,000 years. *Paleoceanography* **11**, 757–771 (1996).
 109. Reading, H. G. *Sedimentary Environments and Facies.* (1986).
 110. Reimer, P. J. *et al.* IntCal13 and Marine13 radiocarbon age calibration curves 0-50,000 years cal BP. (2013).
 111. Rey, F. & Loeng, H. The influence of ice and hydrographic conditions on the development of phytoplankton in the Barents Sea. *Mar. Biol. polar Reg. Eff. Stress Mar. Org.* 49–63 (1985).
 112. Reynolds, L. & Thunell, R. C. Seasonal succession of planktonic foraminifera in the subpolar North Pacific. *J. Foraminifer. Res.* **15**, 282–301 (1985).
 113. Risebrobakken, B., Moros, M., Ivanova, E. V., Chistyakova, N. & Rosenberg, R. Climate and oceanographic variability in the SW Barents Sea during the Holocene. *The Holocene* **20**, 609–621 (2010).
 114. Risebrobakken, B. *et al.* Early Holocene temperature variability in the Nordic Seas: The role of oceanic heat advection versus changes in orbital forcing. *Paleoceanography* **26**, (2011).
 115. Risebrobakken, B., Jansen, E., Andersson, C., Mjelde, E. & Hevrøy, K. A high-resolution study of Holocene paleoclimatic and paleoceanographic changes in the Nordic Seas. *Paleoceanography* **18**, (2003).
 116. Robinson, S. G. The late Pleistocene palaeoclimatic record of North Atlantic deep-sea sediments revealed by mineral-magnetic measurements. *Phys. Earth Planet. Inter.* **42**, 22–47 (1986).
 117. Robinson, S. G., Maslin, M. A. & McCave, I. N. Magnetic susceptibility variations in Upper Pleistocene deep-sea sediments of the NE Atlantic: Implications for ice rafting and paleocirculation at the last glacial maximum. *Paleoceanography* **10**, 221–250 (1995).
 118. ROKOENGEN, K. & BUGGE, T. O. M. Quaternary geology and deglaciation of the continental shelf off Troms, north Norway. *Boreas* **8**, 217–227 (1979).
 119. Rütther, D. C. *et al.* Pattern and timing of the northwestern Barents Sea Ice Sheet deglaciation and indications of episodic Holocene deposition. *Boreas* **41**, 494–512 (2012).
 120. Salvigsen, O., Forman, S. L. & Miller, G. H. Thermophilous molluscs on Svalbard during the Holocene and their paleoclimatic implications. *Polar Res.* **11**, 1–10 (1992).
 121. Sarynina, R. N. Conditions of origin of cold deep-sea waters in the Bear Island Channel. in *Council Meeting, International Council for the Exploration of the Sea 1969 (Symp: 28)* 1–8 (1969).

122. Seidenkrantz, M.-S. *Cassidulina teretis* Tappan and *Cassidulina neoteretis* new species (Foraminifera): stratigraphic markers for deep sea and outer shelf areas. *J. Micropalaeontology* **14**, 145–157 (1995).
123. Seppä, H., Birks, H. H. & Birks, H. J. B. Rapid climatic changes during the Greenland stadial 1 (Younger Dryas) to early Holocene transition on the Norwegian Barents Sea coast. *Boreas* **31**, 215–225 (2002).
124. Shackleton, N. J. Attainment of isotopic equilibrium between ocean water and the benthonic foraminifera genus *Uvigerina*: isotopic changes in the ocean during the last glacial. (1974).
125. Shackleton, N. J. Attainment of isotopic equilibrium between ocean water and the benthonic foraminifera genus *Uvigerina*: Isotopic changes in the ocean during the last glacial. *Les Méthodes Quant. d'étude des Var. du Clim. au cours du pléistocène, Colloq. Int. du CRNS. Gif-sur-Yvette*. **219**, 203–210 (1974).
126. Skirbekk, K., Kristensen, D. K., Rasmussen, T. L., Koc, N. & Forwick, M. Holocene climate variations at the entrance to a warm Arctic fjord: evidence from Kongsfjorden trough, Svalbard. *Geol. Soc. London, Spec. Publ.* **344**, 289–304 (2010).
127. Ślubowska, M. a., Koç, N., Rasmussen, T. L. & Klitgaard-Kristensen, D. Changes in the flow of Atlantic water into the Arctic Ocean since the last deglaciation: Evidence from the northern Svalbard continental margin, 80°N. *Paleoceanography* **20**, (2005).
128. Ślubowska-Woldengen, M. *et al.* Time-slice reconstructions of ocean circulation changes on the continental shelf in the Nordic and Barents Seas during the last 16,000 cal yr B.P. *Quat. Sci. Rev.* **27**, 1476–1492 (2008).
129. Ślubowska-Woldengen, M. *et al.* Advection of Atlantic Water to the western and northern Svalbard shelf since 17,500 cal yr BP. *Quat. Sci. Rev.* **26**, 463–478 (2007).
130. Smelror, M., Petrov, O. V., Larssen, G. B. & Werner, S. Geological history of the Barents Sea. *Norges Geol. undersøkelse* 1–135 (2009). at <http://www.ngu.no/upload/Publikasjoner/B?ker/Brosjyre-ATLAS-Barents.pdf>
131. Solheim, A. & Kristoffersen, Y. *Sediments above the upper regional unconformity: thickness, seismic stratigraphy and outline of the glacial history*. (Norsk Polarinstitutt, 1984).
132. Steinsund, P. I. & Hald, M. Recent calcium carbonate dissolution in the Barents Sea: paleoceanographic applications. *Mar. Geol.* **117**, 303–316 (1994).
133. Stuiver, M., Reimer, P. J. & Reimer, R. CALIB Radiocarbon calibration version 5.0.2. *Available from calib. qub. ac. uk/calib/[accessed Sept. 2008]* **5**, (2005).
134. Svendsen, J. I. & Mangerud, J. Holocene glacial and climatic variations on Spitsbergen, Svalbard. *The Holocene* **7**, 45–57 (1997).
135. Vogt, C. & Knies, J. Sediment pathways in the western Barents Sea inferred from clay mineral assemblages in surface sediments. *Nor. J. Geol.* **89**, 41–55 (2009).
136. Vorren, T. O., Hald, M. & Thomsen, E. Quaternary sediments and environments on the continental shelf off northern Norway. *Mar. Geol.* **57**, 229–257 (1984).
137. Vorren, T. O., Kristoffersen, Y. & Andreassen, K. Geology of the inner shelf west of North Cape, Norway. *Nor. Geol. Tidsskr* **66**, (1986).

138. Vorren, T. O. *et al.* the Norwegian – Greenland Sea Continental Margins : Morphology and Late Quaternary Sedimentary Processes and Environment. *Quat. Sci. Rev.* **17**, 273–302 (1998).
139. Vorren, T. O. & Laberg, J. S. Trough mouth fans—palaeoclimate and ice-sheet monitors. *Quat. Sci. Rev.* **16**, 865–881 (1997).
140. Vorren, T. O., Landvik, J. Y., Andreassen, K. & Laberg, J. S. Glacial History of the Barents Sea Region. *Quat. Glaciat. Chronol. Closer Look, Dev. Quat. Sci* **15**, 361–372 (2011).
141. Winsborrow, M. C. M., Andreassen, K., Corner, G. D. & Laberg, J. S. Deglaciation of a marine-based ice sheet: Late Weichselian palaeo-ice dynamics and retreat in the southern Barents Sea reconstructed from onshore and offshore glacial geomorphology. *Quat. Sci. Rev.* **29**, 424–442 (2010).
142. Wohlfarth, B. *et al.* Early Holocene environment on Bjornoya (Svalbard) inferred from multidisciplinary lake sediment studies. *Polar Res.* **14**, 253–275 (1995).
143. Zubov, N. N. Arctic Ice. Moscow 1943. (1943).
144. Østby, K. L. & Nagy, J. Foraminiferal distribution in the western Barents Sea, Recent and Quaternary. *Polar Res.* **1982**, 53–87 (1982).
145. Ådlandsvik, B. & Loeng, H. A study of the climatic system in the Barents Sea. *Polar Res.* **10**, 45–50 (1991).